Revealing the drivers of space use patterns in a bird population using mechanistic modelling

The University Of Sheffield.

Natasha Ellison

School of Mathematics and Statistics

Faculty of Science

The University of Sheffield

This dissertation is submitted for the degree of

Doctor of Philosophy

February 2021

Declaration

I hereby declare that except where specific reference is made to the work of others, the contents of this thesis are original and have not been submitted in whole or in part for consideration for any other degree or qualification in this, or any other university. This thesis is my own work and contains nothing which is the outcome of work done in collaboration with others, except as specified in the text and the following acknowledgements.

Natasha Ellison

February 2021

Acknowledgements

I would first like to thank my supervisor Jonathan. His guidance, advice and research skills have not only developed me as a researcher, but changed me as a person. Throughout the last four years Jonathan has been very generous with his time, provided me with feedback and discussed ideas. I am grateful for the supervision Jonathan has given me, for all his inspirational research and for taking me on as a PhD student.

I thank my co-supervisor Ben who introduced me to ornithology and field work. Ben has been an extremely beneficial influence on my research by providing me with ecological discussions that have inspired models and helped me understand results. I am also thankful for Ben for ensuring I am involved within his wider research group.

I also thank my advisor Alex for always being interested in my well-being and providing me with excellent advice and positivity.

My research would not have been possible without the incredible and precise field work of Sarah, Clare and Tobit. Following long-tailed tits around for several months requires incredible patience and I am very grateful to collaborate with them.

I've been lucky to be part of two active research groups within the University: the mathematical biology group and the life history behaviour group. Both groups have influenced my work, introduced me to new and interesting parts of science and been extremely supportive.

I'd like to thank all the staff and students in the School of Mathematics and Statistics who have encouraged me throughout the last four years both academically and personally. The Hicks building has felt like a second home and I am extremely thankful to everyone who has given me their time.

Thank you to my examiners Natalia Petrovskaya and Alexander Fletcher for reading this thesis, for being interested in my work and for making my viva an enjoyable experience.

I am certain that without all of the good times and emotional support from my friends, this thesis would not have been possible. Particular thanks go to the friends I have spent evenings and weekends with, those who I regularly meet for coffee and Luca.

Lastly I'd like to thank Ian, Jim and Kevin whose positive greetings and chats often changed a bad day into a good one.

Abstract

As wild animals advance through their available habitat, interactions with other organisms and their environment occur. These interactions influence movement decisions, giving rise to complex space use patterns across landscapes. Untangling the behavioural drivers of movement is therefore critical in understanding animal space use and ultimately in managing the conservation of ecosystems. Some animals restrict their movement to a limited area of their available habitat, known as a home range. This thesis uses mechanistic modelling to uncover the behavioural drivers behind home range formation in of a population of long-tailed tits.

Long-tailed tits (*Aegithalos caudatus*) are small, non-territorial passerines, commonly found in Europe. Flocks live in partly-exclusive home ranges, patterns which are unusual amongst non-territorial animals. This thesis shows that a combination of memory-mediated conspecific avoidance and a response to the deciduous woodland can adequately explain the observed home range patterns. Furthermore, I show that the avoidance mechanism depends upon kin-relatedness and flock size. Finally, I investigate the birds' fine-scale selection for different types of trees whilst foraging within their breeding home ranges. I reveal a set of preferred foraging trees and how the population of birds are selecting them.

Overall, the conclusions and methods throughout this thesis advance not only our knowledge of long-tailed tits but exemplify the application of mathematics to understand ecological processes.

Table of contents

List of figures

List of tables

Symbols

Chapter 1 .

i an index representing either a flock or a pair of long-tailed tits.

t time.

Ω_i the domain available to flock or pair i.

$\partial\Omega_i$ the boundary of the domain Ω_i.

$\mathbf{x}$ a location in the landscape Ω_i where $\mathbf{x} = (x, y)$.

$u_i(\mathbf{x}, t)$ the utilisation distribution for flock or pair i.

$D_i(\mathbf{x}, t)$ a function for the diffusion at location $\mathbf{x}$ at time t.

$\mathbf{A}_i(\mathbf{x}, t)$ a function for the taxis at location $\mathbf{x}$ at time t.

$\nabla = \left(\frac{\partial}{\partial x}, \frac{\partial}{\partial y} \dots\right)$, the differential operator.

$\mathbf{n}_\mathbf{x}$ the vector normal to the boundary at $\mathbf{x}$.

$u_i^*(\mathbf{x})$ the steady-state solution of a system describing $u_i(\mathbf{x}, t)$.

$\mathbf{x}_j$ the spatial location for the end of a step j.

$\mathbf{x}_{j-1}$ the spatial location for the start of a step j.

$\Psi_i(\mathbf{B} \cdot \mathbf{Z}_i)$ a habitat-selection function for pair i with covariates $\mathbf{Z}_i(\mathbf{x}_j)$ and corresponding parameters $\mathbf{B}$.

$\phi_\tau(\mathbf{x}_j|\mathbf{x}_{j-1}, \mathbf{x}_{j-2})$ a movement kernel.

$f_{i,\tau}(\mathbf{x}_j|\mathbf{x}_{j-1}, \mathbf{x}_{j-2})$ a step-selection function for pair i.

Chapter 2 .

$\mathbf{n} = (n, m)$ discrete space.

s discrete time.

$U_i(n, m, s)$ the probability density of flock i being in $\mathbf{n}$ at s.

$K_i(n, m, s)$ the probability of $\mathbf{n}$ being in the interaction zone of flock i at s.

τ the length of a discrete time step in real time.

l the length of a discrete square cell.

μ the reduction of the interaction zone due to finite memory.

$\rho_{\tau,l}$ the probability of an interaction occurring.

β_l the reduction of the interaction zone due to safe visits.

q the strength of the tendency to move away from the interaction zone.

e the probability of not staying in the same place in the IBM model.

d the discrete perceptual radius of a flock.

$k_i(\mathbf{x}, t)$ the probability of location $\mathbf{x}$ at time t being in the interaction zone.

$\bar{k_i}(\mathbf{x}, t|\delta)$ an average of $k_i(\mathbf{x}, t)$ over the disc with radius, δ, centre $\mathbf{x}$.

δ the perceptual radius of a flock.

L the length of the domain.

Ω the domain to be solved over, where $\Omega = [0, L] \times [0, L]$.

D the diffusion parameter.

c the parameter describing taxis away from the interaction zone.

ρ the rate at which an interaction happens when two flocks meet.

β the rate of decay of the IZ due to i visiting without encountering other flocks.

$\partial\Omega$ the boundary of the domain to be solved over.

$a = \frac{D}{\rho}$, controlling the speed of the rate of change of k_i.

$b = \frac{\beta l}{\rho}$, controlling the decay of the interaction zone for safe visits.

$m = \frac{\mu L^2}{\rho}$, controlling the decay of the interaction zone to time passing.

$\gamma = \frac{c}{D}$, controlling the taxis away from the interaction zone.

$E(u_i)$ the energy of the function $u_i(\mathbf{x}, t)$.

$\kappa_i(t)$ the threshold for stopping the evolution of $k_i(\mathbf{x}, t)$.

Chapter 3 .

M the model number.

$\mathbf{v}_M(\mathbf{x})$ a vector field of unit vectors directing towards woodland, different for each model M, visualized in Fig. 3.3.

ζ the magnitude of taxis along the vector field $\mathbf{v}_M(\mathbf{x})$.

ω_M a parameter related to the rate of attraction towards larger woodland areas.

Chapter 4 .

s a tree type.

S_{22} the set of twenty-two different tree types collected at habitat locations.

τ_j the step time of step j.

l_j the step length of step j.

α_j the step heading of step j.

$\phi(\mathbf{x}_j, \tau_j | \mathbf{x}_{j-1}, \mathbf{x}_{j-2})$ an availability kernel for the population.

$\tilde{\phi}(\mathbf{x}_j, \tau_j | \mathbf{x}_{j-1}, \mathbf{x}_{j-2})$ an availability kernel for the population.

$\mathbf{Z}_i$ the vector of covariates describing attributes of the habitat at $\mathbf{x}_j$ and may also depend on $\mathbf{x}_{j-1}$ and $\mathbf{x}_{\text{nest},i}$.

$\mathbf{B}$ the vector of selection parameters β_n for covariates $\mathbf{Z}(\mathbf{x}_j)$.

$\mathbf{x}_{\mathbf{nest},i}$ the spatial location of the nest for pair i.

$f_i(\mathbf{x}_j, \tau_j | \mathbf{x}_{j-1}, \mathbf{x}_{j-2})$ a step-selection function for pair i which describes the probability of moving to $\mathbf{x}_j$ in step time τ_j given previous locations $\mathbf{x}_{j-1}$ and $\mathbf{x}_{j-2}$.

$C_n(\tau_j, \mathbf{x}_j, \mathbf{x}_{j-1})$ a function of $\mathbf{x}_{j-1}$, $\mathbf{x}_j$ and τ_j to correct the availability kernel parametrisation to derive a movement kernel ϕ in a weighting function W_i.

S_r a subset of preferred tree types in S_{22} used in model selection.

$T_s(\mathbf{x})$ the percentage estimate of tree type s at location $\mathbf{x}$.

$P_S(\mathbf{x})$ a binary variable which equals 1 if any tree type $s \in S$ is present at location $\mathbf{x}$.

$V_S(\mathbf{x})$ the number of tree types $s \in S$ at location $\mathbf{x}$.

Abbreviations

BIC bayesian information criterion.

CLR conditional logistic regression.

IBM individual-based model.

iSSA integrated step-selection analysis.

KDE kernel density estimation.

LSA linear stability analysis.

MLE maximum likelihood estimation.

MSD mean square displacement.

MHRA mechanistic home range analysis.

MCP minimum convex polygon.

ODE ordinary differential equation.

PDE partial differential equation.

RSA resource-selection analysis.

SSA step-selection analysis.

SSF step-selection function.

Chapter 1

Background

1.1 Mathematical patterns in ecological systems

Nature exhibits an abundance of diverse patterns across multiple scales (Liu et al., 2014). The biological mechanisms driving some of these patterns, such as the pigment pattern of an adult jaguar (*Panthera onca*), are unable to be studied experimentally, but are observed in mathematical equations (Liu et al., 2006; Xu et al., 1983). Biological insight can be obtained from these mathematical patterns, if the equations that produce the patterns are built from some understanding of biological mechanisms (Murray, 1993; Pielou, 1969; Turchin, 1998).

Nature has a part in revealing mathematical methods too. For instance, the motion of pollen particles in water observed by the botanist Brown (1828), now known as Brownian Motion, influenced the work of Einstein (1905) who described the random movement of the particles as a diffusive process. Einstein's

work provided an alternative to the phenomenological approach of deriving the diffusion equation using Fick's laws (Fick, 1855); work influenced by the experiments of Graham (1833). Moreover, Einstein (1905) derived an equation for the mean squared displacement of a particle, which was later evidenced experimentally by Perrin (1909); work that subsequently convinced many scientists of the existence of the atom (Bernstein, 2006). Today, the diffusion equation is a fundamental equation in ecology and studied across the sciences (Okubo, 1980; Philibert, 2005).

Patterns in life are not necessarily visual, for instance, the changes in a population through time (Bulmer, 1974; Elton and Nicholson, 1942) and the movement of animals through space and time (Turchin, 1998) reveal patterns that are only identified by collecting data (Kays et al., 2015). The cyclic temporal patterns of the population densities of lynx (*Lynx canadensis*) and hare (*Lepus americanus*) were famously noticed by fur vendors in 1881 (Krebs et al., 2001). These temporal patterns were modelled by Lotka (1924) and Volterra (1926) and have a rich literature of analyses (Wangersky, 1978).

In reality, ecological systems change through both space and time. Introducing diffusion into a temporal model, such as the Lotka-Volterra equations, describes the population density spreading out though space (Fisher, 1937; Kolmogorov et al., 1937). Mathematical descriptions of predator-prey interactions are similar to chemical reactions and analogous equations are used to describe the reaction and diffusion of chemical densities in biological systems (Volpert and Petrovskii, 2009), such as the pigment patterns of a jaguar. The emergence of patterns in reaction-diffusion systems was predicted in the seminal work of Turing (1952). Though overlooked at the time (Ball, 2015), recent biological experiments have revealed that the mechanisms described by Turing (1952)

are driving the patterns of mammalian hair growth (Sick et al., 2006) and teeth-like shark scales (Cooper et al., 2018).

Analysing ecological processes requires not only understanding the abundance of organisms in space and time, such as the lynx and hare populations but also the predicted location of individual organisms (Turchin, 1998). Rather than modelling the population density of a species, one can model the probability density of the occurrence of an individual (Moorcroft and Lewis, 2006). In this thesis, I explore models for the spatio-temporal change of the probability density of animal occurrence and uncover the behavioural mechanisms driving space use patterns.

1.1.1 Movement and space use in ecology

Space use patterns emerge as wild animals move around their landscape (Kernohana et al., 2001). These patterns are driven by the behaviours that influence an animal's movement decisions (Börger et al., 2008). The fundamental movement behaviours that shape an animal's space use pattern can be revealed by modelling the animal's behavioural decisions as mathematical mechanisms (Moorcroft and Lewis, 2006; Turchin, 1998). Throughout this thesis, I explore ways of modelling animal space use mechanistically, meaning that space use patterns are derived from the process of underlying movement behaviours.

Motivation for studying movement behaviour comes from the effect that moving organisms have on entire ecosystems. For example, the behavioural decisions of one animal may drive the movement of other animals by altering the environment (Riotte-Lambert and Matthiopoulos, 2020). Furthermore, direct and indirect

interactions between animals can drive the space use of a population (Bateman et al., 2015; Giuggioli et al., 2011; Potts et al., 2014a).

Further motivation for animal movement research is driven by the impact that humans have on habitats. Anthropogenic stresses on wildlife influence space use across the world and continue to be a problem for preserving ecological integrity in ecosystems. Human disturbance has been shown to reduce movement distances (Tucker et al., 2018), affect energy expenditure (Houston et al., 2012), increase disease transmission from animals to humans (Daszak et al., 2000) and impact patterns of space use temporally (Gaynor et al., 2018). Human effects can be managed using the predictions achieved from mathematical modelling and models have previously influenced important conservation decisions (Morris et al., 2016).

1.1.2 Modelling across scales

In this thesis, I study animal movement mechanisms on two scales, leading to the following two modelling types;

(1) Individual-based models, where the *location* of an individual varies through time. Successive locations in a time series are modelled as a stochastic path. An example of a path of successive locations is shown in Fig. 1.1a.

(2) Utilisation distribution models, describing the *probability* of finding an individual at a given region in space and time. Here space use patterns are modelled as a *utilisation distribution*; a spatio-temporal probability density of animal occurrence. An example of a utilisation distribution, at one point in time, is shown in Fig. 1.1b.

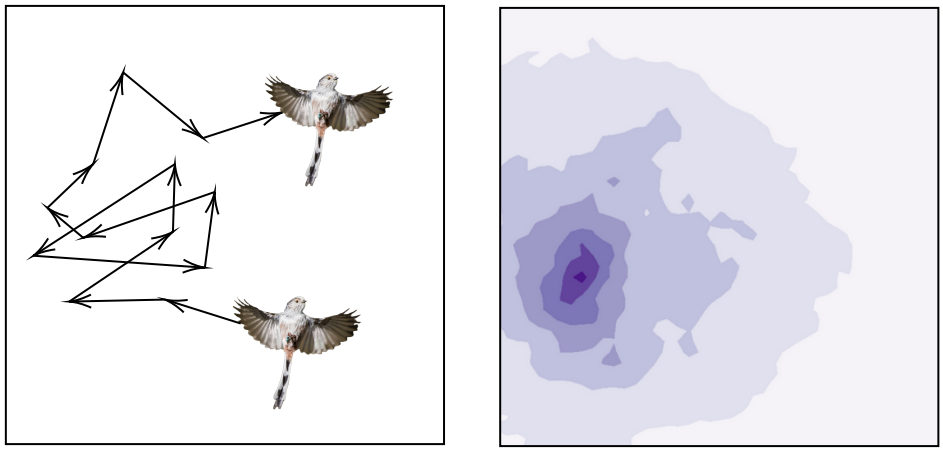

(a) (b)

Fig. 1.1. The output from two types of movement mechanisms. Panel (a) shows a stochastic path drawn from an individual-based movement model. Panel (b) shows a utilisation distribution model. A utilisation distribution is a probability density function for an animal's location at a given time. Darker shades in Panel (b) indicate higher densities. Space use (Panel b) can be estimated from a individual-based model (Panel a) using simulations or mathematical derivations.

Individual-based models (Modelling type 1) define movement mechanisms using the speed and direction of movement. These individual-based descriptions range from movement on a discrete grid, governed by transition probabilities (Hooten et al., 2010), to movement in continuous space, structured using a probability density function (Ellis et al., 2019; Thurfjell et al., 2014). In this thesis, I focus on a specific individual-based framework; step-selection analysis (SSA). This analysis is used to understand a time series of animal locations, by comparing recorded relocations to other possible relocations to fit a mechanistic movement model. I review SSA in §1.5, in preparation for applying it to data in Chapter 4.

A utilisation distribution (Modelling type 2) represents the space use of an animal. Space use can be estimated from a set of animal locations using statistical methods to determine areas that are frequently used by the animal

(Worton, 1989). However, describing a utilisation distribution without dynamic origins gives little insight into the underlying behaviours of the space use pattern. Individual-based movement models (Modelling type 1) can estimate space use by simulations, or mathematical approximations to produce a utilisation distribution model (Modelling type 2).

The mathematical bridge between a utilisation distribution and an individual-based model arises from defining a master equation. A master equation is an iterative equation describing the utilisation distribution at one point in time, given the utilisation distribution at a previous point in time and the individual-based description of movement (Okubo, 1980; Turchin, 1998; van Kampen, 1981). A master equation can be used to derive a partial differential equation (PDE), a description of the spatio-temporal change of the utilisation distribution that has the advantage of a rich literature of analysis and numerical methods (Fritz, 1982). The technique of encapsulating individual-based motion as a master equation and forming a PDE was introduced by Einstein (1905) and further advanced by statistical physicists in the early part of the 20th century to incorporate movement with a bias (Chandrasekhar, 1943; Fokker, 1914; Planck, 1917).

Using ideas from statistical physics, the emergence of animal space use patterns from individual-based behaviours can be analysed by approximating a master equation as a diffusion-taxis equation; a type of PDE (Moorcroft, 2012; Moorcroft and Lewis, 2006). An advantage of using diffusion-taxis equations is that one can relate the underlying movement decisions to the emergent spatio-temporal patterns. The diffusion-taxis equation can be analysed to predict space use patterns and solved numerically to a *steady-state* to give

a temporally constant utilisation distribution. I show the derivation of a diffusion-taxis equation from an individual-based model in Appendix A.1.

Some animals live in restricted areas of space for a long time, known as the animal's *home range* (Börger et al., 2008; Burt, 1943). Home ranges are a particular type of space use, so are a consequence of dynamic movement processes (Moorcroft, 2012), however they are often modelled using descriptive techniques (Fieberg and Börger, 2012). Particular behavioural mechanisms in diffusion-taxis equations restrict space use to give a home range model (Moorcroft and Lewis 2006). This method of modelling home ranges is termed mechanistic home range analysis (MHRA) and is outlined in §1.4. I study these utilisation distribution models further in Chapter 2 and apply them to data in Chapter 3.

Prior to detailing the general form of the modelling techniques used in this thesis, typical animal movement behaviours for understanding space use are discussed in the next section.

1.2 Why does an animal move?

With appropriate models, patterns of space use resulting from movement decisions can be calculated (Turchin, 1998). To derive models that answer ecological questions, one must first develop and test reasonable empirical hypotheses. Prior to reviewing possible hypotheses for movement, I discuss differences that may arise in behaviour between individuals and over space and time.

Life history needs can shift as the seasons change (Birkett et al., 2012; Ferguson and Elkie, 2004) or throughout the day (Rockhill et al., 2013) so behaviours

may depend on time. Some types of modelling processes account for this shift by allowing movement mechanisms to switch as the needs of the animal vary through time (Parton and Blackwell, 2017; Patterson et al., 2008). Behaviours may also depend on the habitat. Physical movement may be restricted in some places as the physiology of an animal affects its ability to explore its landscape (Kerr and Bull, 2006). There may be places which are unavailable to the animal, due to the topology of the landscape or fragmentation (Fischer and Lindenmayer, 2007). An animal may be slower or faster in certain environments, depending on their individual condition, locomotive or navigation capabilities (Nathan et al., 2008). Lastly, behaviours may vary between individuals. Animals within a species may exhibit quite different behaviour (Spiegel et al., 2017). Differences such as personality traits (Spiegel et al., 2017) or body size (Adams and Plowes, 2019; Jetz et al., 2004; Nilsson et al., 2014) have an effect on the movement and behaviour of some species (Leclerc et al., 2016).

Before formulating hypotheses, one should consider if temporal, spatial or individual differences should be accounted for within models, or whether the differences are insignificant enough to be ignored, to reveal more significant behaviours driving the pattern of space use.

1.2.1 Movement Mechanisms

Throughout the rest of §1.2, I discuss typical animal behaviours that have been used to drive movement in previous studies. It can be argued that these behaviours affect the movement decisions of any animal species, but mathematical modelling aims to untangle the most important mechanisms. I discuss behaviours and give examples of previous studies in the following four subsections.

Memory

Modelling an individual that moves in response to spatial memory has been shown to improve foraging success (Bracis et al., 2015; Riotte-Lambert et al., 2015). For many species, a realistic assumption is that an animal's spatial memory develops and decays as it moves around its environment (Fagan et al. 2013; Potts and Lewis 2016a, Chapter 3). A dynamic memory leads to the the concept of *umwelt*, meaning that each individual has a different perception of the world (Kull, 1998).

An animal's spatial memory can be modelled using a *cognitive map*, a density map taking the same shape and size of the available environment. The dynamic change of the map is driven by events as they occur, for example, finding a desirable resource or an interaction with another individual (Potts and Lewis 2016a; Riotte-Lambert et al. 2015, Chapter 3). A cognitive map could be made up of many layers which each describe a different behaviour and these layers could be constantly changing (Avgar et al., 2015; Potts and Lewis, 2016a).

Indeed, all of the reasons for movement mentioned within this section can be modelled as layers of a dynamic cognitive map, changing as an animal moves through time and space. Still, one must decide whether or not it is sufficient to assume the knowledge of the animal is not changing through time to unlock more interesting mechanisms of movement.

Environmental attributes

Most species move around their environment to use resources which are essential to their survival. Therefore the structure of the environment is an important part of animal movement models. The simplest assumption (other than a

homogeneous environment) is to assume that animals are moving within a unchanging spatially heterogeneous landscape, for example, if resource depletion is very low then a modeller may consider resource change to be negligible (Avgar et al. 2015, Chapter 3). However, for some species, modelling a changing environment is necessary due to extensive resource depletion or seasonal change (Birkett et al., 2012; Riotte-Lambert et al., 2015).

Location fidelity

Some species of animal have a localizing tendency to a particular place (Okubo, 1980) or places (Benhamou and Riotte-Lambert, 2012), for instance, a watering hole or den (Moorcroft et al., 2006). The fidelity of a location (Bateman et al., 2015), or alternatively, the strength of the attraction to a location could change with time, as with birds provisioning nests (Hatchwell and Russell, 1996). As attraction to particular places restricts space use, site fidelity gives rise to a home range, a finite area that an animal chooses to live in, despite having access to a much larger area (Börger et al. 2008; Moorcroft and Lewis 2006, §1.4).

In response to other individuals

Animals are likely to move in response to the movements of other individuals (Avgar et al., 2015). The reaction to this knowledge of other individuals can be categorised in three ways (Potts and Lewis, 2019): mutual attraction, mutual avoidance or pursue-and-avoid. Mutually attracting individuals may benefit from each other such as with large carnivores (Vanak et al., 2013) and birds (Mönkkönen and Forsman, 2002). Mutual avoidance occurs with interactions which are either direct (Potts and Lewis, 2016a) such as aggressive displays

(King, 1973) or indirect such as scent marking (Lewis and Murray, 1993) or the risk of depleted resources (Ford, 1983). These avoidance mechanisms could be territorial (Bateman et al., 2015; Potts and Lewis, 2014) or non territorial (Knapp 2000, Chapter 3). Lastly, an animal being pursued by another animal can be seen in predator-prey systems (Berryman, 1992).

1.2.2 Data collection

Data collected in field studies can restrain the type of useful models, therefore restricting the questions which can be answered. Furthermore, data collection may be impeded by the study species or their habitat. Wild animals are masters of eluding danger and it is difficult to track and observe them in locations with challenging topography, particularly ensuring that the animal's behaviour is not influenced by the observer.

Modern Global Positioning System (GPS) devices in the form of radio tags can be fitted to animals as small as some birds and bats (Kays et al., 2015). GPS devices are capable of producing accurate descriptions of fine scale linear movements and turning angles with a best expected accuracy of 5m (Bridge et al., 2011). Still, studies on the majority of species of bats and birds cannot take advantage of the most recent GPS tagging devices due to the requirement of tags being less than 5% of the animal's body weight. The restriction is to ensure behaviour is minimally affected (Bridge et al., 2011). Some geolocators are able to be fit to small passerine birds, however the spatial resolution is very low and unsuitable for tracking fine scale movements that are less than 100m (Thorup et al., 2014). Alternatively, animals can be tracked on foot with locations recorded using handheld GPS devices, but this relies on the species

being easily detectable. Moreover, there must be minimal behavioural effects from the observer and suitable terrain (Wikelski et al. 2007, Chapters 3 and 4).

Technological advances in the past twenty years (Hays et al., 2016; Signer et al., 2017; Williams et al., 2020) mean that animal tracking data can produce spatial relocations of very fine temporal resolution. With the correct mathematical tools (Potts et al., 2018) researchers are able to estimate when decisions to change movement direction have been made. Alternatively, when tracking animals on foot observers may be able to recognise and record when decisions to move have occurred (Chapter 4).

1.2.3 Uncovering movement drivers of animal space use

Understanding the movement drivers behind the space use of animals requires developing useful questions, establishing hypotheses and building models. Detailed processes of model development are discussed in Turchin (1998), who suggests a reiterative modelling process. Turchin (1998) proposes an initial round of simple model development, where the model and its parameters are formulated using empirical knowledge of the animal, such as previous observations or studies. Collecting initial data and observations in the field can reveal how the model and perhaps the entire question of the study can be modified and improved. Following this process repeatedly, whilst redesigning the model and the fieldwork, ensures rigorous systematic data collection and model fitting.

Realistically, due to time and financial limitations, the repetitive interplay of model formulation and fieldwork is not always practical. I summarise ideas

for modelling animal space use mechanistically in the Model Design Process section of Fig. 1.2.

1.3 The long-tailed tit: a home ranging passerine

The home range patterns of flocks of my study species, the long-tailed tit (*Aegithalos caudatus*), are intriguing since they are stationary, without fidelity to a location and partly exclusive, yet they are not defending a territory. Furthermore, the birds are too small to be GPS tagged, therefore direct observations are necessary to collect movement data that is accurate enough to examine behavioural decisions.

The long-tailed tit is a small, predominantly insectivorous passerine weighing only 7-8g, primarily residing in woodland and scrub habitats (Hatchwell, 2016). Long-tailed tits live in home ranging flocks in the non-breeding season and are not territorial at any time of the year. The population of long-tailed tits in a 3km^2 site of the the Rivelin Valley in Sheffield (52 23°N, 1 34°W), has been studied since 1994.

Outside of the breeding season, flocks of long-tailed tits are comprised of 10-20 individuals that forage and roost together. A flock sometimes uses the same perch over successive nights, but changes over the season. Immigration between flocks happens at the start of the non-breeding season as flocks are forming, but is uncommon later in the season. Locational data shows that each flock's home range is mostly comprised of an area exclusive to that flock, with some overlap with other flock's home ranges (Hatchwell et al., 2001a; Napper and

Hatchwell, 2016). In the Rivelin Valley, the abundance of food is plentiful and the birds are not sharing any finite resources (Hatchwell, 2016). Exclusive home ranges in other animal species are often due to territory defence or resource competition, however these behaviours are not observed in this population of birds.

Whilst nest building, pairs of long-tailed tits forage together. Since the birds have site fidelity to the nest location, their fine scale movements are easier to study than the flocks in the non-breeding season. The Rivelin Valley consists of a complex woodland structure and the location and abundance of different trees can be estimated with careful fieldwork throughout home range areas. It is thought that the birds move in response to different tree species, but it is not known which tree species are preferred.

Field workers in the Rivelin Valley locate birds by listening for birdsong and locating nests in the breeding season. Once birds are located, they can be identified by coloured rings on their legs, where $> 95\%$ of the population are ringed each year. Located and identified birds are followed and their location is recorded on a handheld GPS device at certain time intervals. Since the birds within a flock (in the non-breeding season) or pair (within the breeding season) forage together, locations are recorded for the flock or pair, rather than for individual birds. The data used in this thesis was collected for flocks over five non-breeding seasons from 2010 to 2019 and for nest building pairs in 2019. Due to the substantial time consumption and the specific skills required for this field work, the locations of different pairs or flocks were not recorded simultaneously.

Understanding the behavioural mechanisms that lead to the emergence of stationary home ranges in the long-tailed tit system is interesting both ecologically and mathematically (Börger et al., 2008; Moorcroft, 2012; Napper and Hatchwell, 2016). Revealing the drivers using mechanistic techniques discloses behaviours not easily found by an experimental approach. Furthermore, the home range patterns of the non-breeding flocks require movement mechanisms that produce restricted space use patterns in a limitless area without an attractive point.

I answer two overall questions in this thesis: (1) what are the behaviours driving the space use patterns of flocks of long-tailed tits and (2) how are pairs of long-tailed tits moving in response to the complex woodland structure of the Rivelin Valley. I explore question (1) using a utilisation distribution approach and question (2) using an individual-based approach. The general ideas of both methods are introduced in the next two sections.

1.4 Diffusion-taxis models: a utilisation distribution approach

Non-breeding flocks of long-tailed tits live in home ranges which are largely exclusive. Since each flock is using a different part of the Rivelin Valley, it is likely that the space use of one flock depends on the space use of other flocks. Locations of flocks were not able to be recorded at the same time, so fitting an individual-based model of movement, based on the movements of other flocks would not be suitable. Instead, I fit a diffusion-taxis model of space use, built from underlying behaviours, to locational data. Here I describe the structure of diffusion-taxis equation models for animal space use, where specific behaviours are defined in Chapter 3.

A diffusion-taxis equation is built by approximating an individual-based model as a spatio-temporal description of space use. The derivation of a diffusion-taxis equation requires one to form a master equation as described in §1.1.1. These methods are standard (e.g. van Kampen 1981) and I show the derivation in Appendix A.1. Diffusion-taxis equations consist of a *diffusion* and a *taxis* term. The diffusion term models movement processes that do not have any directional bias and drives the speed of diffusion, $D(\mathbf{x}, t)$, at location $\mathbf{x}= (x, y)$ and time t. The taxis term models movement in the direction of the vector field $\mathbf{A}(\mathbf{x}, t)$. Different behaviours can be included into the terms by including these in the functions $D(\mathbf{x}, t)$ and $\mathbf{A}(\mathbf{x}, t)$. The diffusion and taxis terms drive the space use of flock i, defined as the utilisation distribution, $u_i(\mathbf{x}, t)$ which describes the probability density of finding flock i at location $\mathbf{x}$ at time t.

Each flock of birds, i, requires a different equation to describe their space use. The diffusion and taxis functions may also depend on i and are denoted here as $D_i(\mathbf{x}, t)$ and $\mathbf{A}_i(\mathbf{x}, t)$ respectively. It may be noted that the diffusion and taxis functions can also depend on other flocks (e.g. j, Chapters 2 and 3), however I omit this dependence here for notational purposes. Therefore, a diffusion-taxis equation for flock i has the general form

$$\frac{\partial u_i}{\partial t} = \underbrace{\nabla^2 \left[D_i(\mathbf{x}, t)u_i(\mathbf{x}, t)\right]}_{\substack{\text{Diffusion: aspects of movement} \\ \text{that do not have a directional bias}}} - \underbrace{\nabla \cdot \left[\mathbf{A}_i(\mathbf{x}, t)u_i(\mathbf{x}, t)\right]}_{\substack{\text{Taxis: directional} \\ \text{bias in movement}}}, \tag{1.1}$$

where $\nabla= \left(\frac{\partial}{\partial x}, \frac{\partial}{\partial y}\right)$. To describe space use completely, Equation (1.1) requires both an initial description of space use and conditions on the boundaries to be

included in the system. I use zero-flux boundary conditions, defined as follows

$$\left|\mathbf{n}_{\mathbf{x}} \cdot \left[\nabla \left(D_i(\mathbf{x},t)u_i(\mathbf{x},t)\right) - \mathbf{A}_i(\mathbf{x},t)u_i(\mathbf{x},t)\right]\right|_{\mathbf{x}\in\partial\Omega_i} = 0, \tag{1.2}$$

where $\mathbf{n}_{\mathbf{x}}$ is the normal to the boundary $\partial\Omega_i$ at $\mathbf{x}$ and Ω_i is the landscape available to flock i. The space use of flock i is determined by the solution to Equation (1.1) which is a probability distribution if the following condition is imposed

$$\int_{\Omega_i} u_i(\mathbf{x},t)\mathrm{d}\mathbf{x} = 1. \tag{1.3}$$

Notice that, with boundary conditions (1.2), $\int_{\Omega_i} u_i(\mathbf{x},t)\mathrm{d}\mathbf{x}$ does not change over time. Therefore if the initial condition $\int_{\Omega_i} u_i(\mathbf{x},0)\mathrm{d}\mathbf{x} = 1$ then Equation (1.3) holds. For modelling animal space, the initial conditions of space use should relate to the ecology of the species being modelled, I consider different ways of describing initial space use in Chapter 3.

The form of the diffusion term in Equation (1.1) differs from that of a general convection-diffusion equation with diffusion term $\nabla[D(\mathbf{x},t)\nabla u(\mathbf{x},t)]$. One may obtain a diffusion term of the form $\nabla[D(\mathbf{x},t)\nabla u(\mathbf{x},t)]$ by deriving a partial differential equation using diffusive flux described by Fick's first law (Fick, 1855). Instead, I obtained a diffusion term of the form $\nabla^2[D(\mathbf{x},t)u(\mathbf{x},t)]$ following the derivation in Appendix A.1, which is more suitable for modelling animal movement as it is approximated from a stochastic model of movement, similar to the diffusion equation derivation of Einstein (1905) from Brownian motion.

In animal movement studies, the diffusion function is often set to be a constant, $D_i(\mathbf{x}, t) = D$ (Moorcroft and Lewis, 2006). In Chapter 3, I trial models for each flock using either a constant or a spatio-temporally varying $D_i(\mathbf{x}, t)$.

A steady-state solution to Equation (1.1), $u_i^*(\mathbf{x})$, is found when $\frac{\partial u_i}{\partial t} = 0$. Whether Equation (1.1) settles to a steady-state distribution that results in home range patterns depends on the movement mechanisms that built the diffusion-taxis equation. Parameter schemes which give rise to home range patterns can be analysed without solving the diffusion-taxis equation to a steady-state (Murray 1993; Turing 1952, Chapter 2), which is useful to find initial values for fitting to data. For a set of locations $\mathbf{x}_d \in S_i$ for flock i, the steady-state of a diffusion-taxis equation can be fit to the locations by maximising the following likelihood (Moorcroft and Lewis, 2006)

$$L_i(P|\mathrm{X}) = \prod_{\mathbf{x}_d \in S_i} u_i^*(\mathbf{x}_d), \tag{1.4}$$

where P is the set of parameters in the model and X is the data set. One can then fit these distributions to data and test between various hypothesised movement mechanisms to find which set of mechanisms best fits the observed home range patterns. Such a process is often termed mechanistic home range analysis (MHRA; Moorcroft and Lewis 2006).

Previous studies of MHRA fit a diffusion-taxis equation to location data by including an attraction towards a known central place. Including this site fidelity in a diffusion-taxis equation restricts the movement that drives the steady-state solution, to give rise to a home range (Okubo, 1980). Furthermore, many MHRA studies aim to model territorial animals (Moorcroft et al., 2006) using mechanisms describing scent marking or territorial conflicts (Bateman et al.,

2015; Moorcroft et al., 2006). However, individual based models of home ranges show that patterns can arise from environmentally driven mechanisms such as optimal foraging and memory (Mitchell and Powell, 2004; Riotte-Lambert et al., 2015).

Non-breeding flocks of long-tailed tits do not have site fidelity or display territorial behaviour (Napper and Hatchwell, 2016). Recent studies describing mechanisms of direct conflicts (Potts and Lewis, 2016a) and scent marking (Potts and Lewis, 2016b) show that it is possible to form stable home ranges from one-dimensional diffusion-taxis equations, without an attraction towards a central place.

In Chapter 2, I use the methods of Potts and Lewis (2016a) to derive a diffusion-taxis equation in two dimensions, with a memory mechanism to model conspecific interactions. Furthermore, I detail numerical procedures to solve the diffusion-taxis equation to a steady-state. In Chapter 3, I use the methods defined in Chapter 2, alongside a habitat taxis mechanism to model the space use patterns of flocks of long-tailed tits.

1.5 Step-selection analysis: an individual-based modelling approach

To understand more about the woodland foraging preferences of long-tailed tits, the movement of pairs whilst nest building was observed. The recorded movements in response to the distribution of tree species in the Rivelin Valley can be analysed by fitting the data to an individual-based model. Step-selection

analysis (SSA) parametrises an individual-based model by comparing recorded movements to those which were available (Thurfjell et al., 2014).

SSA began as a way to include movement in resource-selection analysis (RSA), a method of comparing independent locations and the habitat of an individual (Manly et al., 2002). Analysing autocorrelated locations produces a more realistic model than independent locations, as animals are likely to make movement decisions based on their current and previous locations (Forester et al., 2009; Rhodes et al., 2005). SSA analyses the straight-line segment between successive locations, termed a *step*. One of the first studies to introduce SSA models the movements of elk in response to the risk of encountering wolves (Fortin et al., 2005). The study incorporated successive movement in their analyses to include movement characteristics in the model, such as the average energy cost and the average wolf density of the steps. SSA has since been used to uncover the movement drivers of many species of birds and mammals (Potts et al., 2014b; Thurfjell et al., 2014; Zeller et al., 2016). Furthermore, it has helped to understand influences on movement such as memory (Oliveira-Santos et al., 2016), responses to roads (Prokopenko et al., 2017), energy benefits (Merkle et al., 2017) and it was recently used to inform conservation decisions (Osipova et al., 2019). In Chapter 4 I use SSA to analyse the fine scale woodland foraging movements of pairs of long-tailed tits.

SSA consists of forming two functions, describing movement and habitat-selection, respectively. Behaviours are included in SSA using a *habitat-selection function*, which often has the log-linear form

$$\Psi(\mathbf{x}_j, t) = \exp\left(\mathbf{B} \cdot \mathbf{Z}(\mathbf{x}_j, t)\right), \tag{1.5}$$

where $\mathbf{Z}(\mathbf{x}_j, t) = \Big(Z_1(\mathbf{x}_j, t), \ldots, Z_n(\mathbf{x}_j, t)\Big)$ is a vector of covariate functions describing behaviours in response to attributes of the habitat at the end of the step $\mathbf{x}_j$ at time t. The parameter vector $\mathbf{B} = (\beta_1, \ldots, \beta_n)$ control each covariate. The value of each parameter describes how movement is affected by the covariate function. Covariate functions may also depend on the individual, for the long-tailed tits they depend on the pair i, giving a habitat-selection function, $\Psi_i(\mathbf{B} \cdot \mathbf{Z}_i)$.

Usually steps are recorded over constant intervals in time, τ. A *movement kernel*, $\phi_\tau(\mathbf{x}_j|\mathbf{x}_{j-1}, \mathbf{x}_{j-2})$ is used to define movement by calculating attributes from the data such as speeds and turning angles and fitting them to models. The movement kernel depends on two previous locations, $\mathbf{x}_{j-1}$ and $\mathbf{x}_{j-2}$, so that the angle turned through from one step to the next can be included in the model.

Realistically, animals make movement decisions by simultaneously evaluating habitat information and the distance and turning angle required to get there. However, in many SSA studies the movement kernel is not parametrised concurrently with the habitat-selection function. Avgar et al. (2016) introduced integrated step-selection analysis (iSSA) to express a general framework for a SSA that defines a movement kernel within the mechanistic model and simultaneously parametrises the movement kernel and the habitat-selection function. The model in iSSA is denoted the step-selection function (SSF) and defines the probability density of moving from $\mathbf{x}_{j-1}$ to $\mathbf{x}_j$ at time t. For a pair i, this would have the form

$$f_{\tau,i}(\mathbf{x}_j|\mathbf{x}_{j-1}, \mathbf{x}_{j-2}, t) = K^{-1} \underbrace{\phi_\tau(\mathbf{x}_j|\mathbf{x}_{j-1}, \mathbf{x}_{j-2})}_{\text{Movement}} \underbrace{\Psi_i(\mathbf{x}_j, t)}_{\substack{\text{Habitat} \\ \text{Selection}}}, \tag{1.6}$$

where K normalises the function to ensure it is a probability density function.

Space use can be estimated from behaviours by first defining an individual-based model of movement and simulating the model thousands of times until the stochasticity is smoothed out (Fieberg et al., 2018; Signer et al., 2019). Simulations result in a utilisation distribution, but are computationally costly. Instead a diffusion-taxis equation can be derived from the parametrised individual-based SSA model (Potts and Schlägel, 2020).

In Chapter 4, I introduce specific forms of Equation (1.6) using iSSA to represent the movement of nest-building long-tailed tits and calculate a utilisation distribution by approximating the SSF as a PDE.

1.6 Thesis outline

I derive a two-dimensional diffusion-taxis system to model conspecific avoidance in flocks of long-tailed tits in Chapter 2. The PDE formalism was previously introduced in one dimension by Potts and Lewis (2016a).

In Chapter 3, I examine drivers of space use patterns of flocks of long-tailed tits using mechanistic home range analysis (MHRA). Specifically, I look at the effects of conspecific avoidance, the response to the woodland environment and the effect on conspecific avoidance of group size and kinship. Much of this Chapter has been published in Ellison et al. (2020).

In Chapter 4, I use SSA to understand the foraging decisions of long-tailed tits within their home ranges, specifically focussing on their response to the woodland habitat. I use the resulting models to estimate the birds' home ranges via a diffusion-taxis approximation.

Lastly, in Chapter 5 I give some discussion and conclusions.

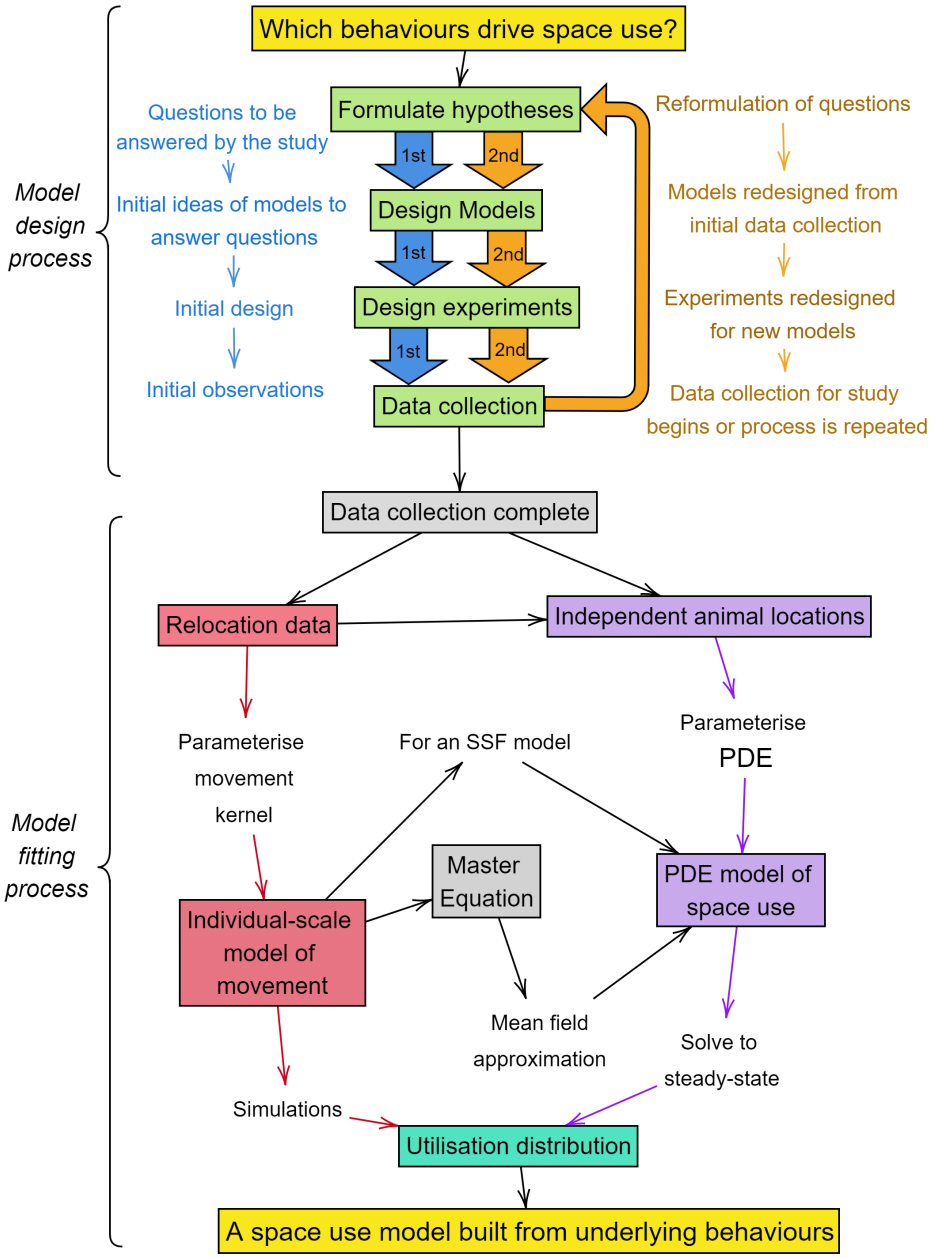

Fig. 1.2. A flow chart to model the space use of an animal mechanistically using the methods in this thesis. The top half (§1.2.3) indicates a framework to re-iteratively design experiments and models, where the blue route would be followed before the orange route. Once the data collection is complete, the model fitting process (shown in the lower half of the diagram) can begin. The model fitting process is discussed in §1.5-§1.4. These ideas summarise those in Turchin (1998).

Chapter 2

A diffusion-taxis model for direct interactions

2.1 Introduction

Flocks of long-tailed tits in the Rivelin Valley live in home ranges that are partly exclusive to each flock and partly overlapping with other flocks (Napper and Hatchwell, 2016). Despite being a well studied population (Hatchwell, 2016), the behaviours driving these space use patterns are not known (Hatchwell et al., 2001a; Napper and Hatchwell, 2016). In other home ranging animal species, territoriality, site fidelity and resource depletion are all thought to be common mechanisms driving home range space use patterns (Moorcroft and Lewis, 2006; Riotte-Lambert et al., 2015). However, these behaviours are not present in this population of long-tailed tits (Hatchwell, 2016). In this Chapter, I introduce methods to model home ranges arising from a memory mechanism that records conspecific interactions between flocks of long-tailed tits.

Potts and Lewis (2016a) introduced a one-dimensional diffusion-taxis model for two hypothetical territorial animals, where space use is driven by the animal's memory of direct conflicts. I extend the model of Potts and Lewis (2016a) into two dimensions to model multiple interacting flocks of birds. I denote this model as the *interaction model*, and build it to describe conspecific interactions that are not necessarily conflicts, broadening this mechanism to be applied to non-territorial, home ranging animal species.

I introduce the interaction model by deriving a system of partial differential equations (PDEs) in two dimensions, for multiple flocks. Space use in the interaction model is described using a diffusion-taxis equation, built from underlying movement rules. The system is solved through time to a point where its stops changing and this is the system's *steady-state*. I show that in two spatial dimensions, steady-states corresponding to home ranges are possible. Furthermore, when the PDEs are solved numerically, the steady-states may never be reached, as numerical approximations can cause the system to move between nearby steady-states, without settling on one. I detail a numerical procedure to determine when the system first becomes sufficiently close to a steady-state solution to gain a good numerical estimate of that solution, but before it begins to move towards nearby steady-states. Lastly, I give examples of possible home ranges that can emerge from the interaction model. The objective of this Chapter is to introduce and analyse the interaction model, so that it may be used to understand long-tailed tit ecology in Chapter 3.

2.2 A diffusion-taxis model for direct interactions

In the Rivelin Valley, it is thought that flocks of long-tailed tits are avoiding other flocks (Hatchwell et al., 2001a). I introduce a diffusion-taxis model that gives rise to home range patterns, built from these observed behaviours of long-tailed tits. I hypothesise that when two flocks are close enough, they are able to detect each other via birdsong or sight. I denote this detection generally as an *interaction*. I further hypothesise that the birds are recording these interactions in their memory and avoiding locations where the interactions occurred. I introduce data, revisit and test these hypotheses with the models proposed here in Chapter 3.

To understand the behaviours driving the movement of the birds, the spatial data we model in Chapter 3 is from direct observations, where observing one flock interacting with another is rare. Approximating an individual based model as a PDE (see Moorcroft and Lewis 2006) is chosen here to be a computationally efficient way of modelling the flocks, as extensive simulations would be required to parametrise individual based mechanisms of interactions. Other individual based methods such as using an off-lattice model (e.g. Ellis et al. 2019; Patterson et al. 2008; Thurfjell et al. 2014) would be equivalently costly to parametrise, discussed further in Chapter 5. The PDE model defined in Potts and Lewis (2016a) indicates that individual-level interactions can drive home range formation, without the usually required central place seen in the literature (Moorcroft and Lewis, 2006).

2.2.1 The individual-based movement model

The individual-based model (IBM) defined by Potts and Lewis (2016a) was introduced in two dimensions, here I detail their model specifically for multiple flocks of long-tailed tits. The IBM describes flocks moving on a grid of square cells, $\mathbf{n} = (n, m)$, of length l. Since the birds within a flock forage together and have the same home range, I model each flock as one entity, i and I do not consider inter-flock dynamics. At each point in discrete time, s, each flock moves either up, down, left, right or stays in the same cell. The probability of moving in each direction depends on a dynamic *cognitive map* of interactions, which has the same size and shape as the grid. Places that these interactions are likely to happen are denoted as the flock's *interaction zone*.

Each flock has a different cognitive map, $K_i(n, m, s)$, and the map describes the probability of location (n, m) being in the flock's interaction zone at time s. The probability, $K_i(n, m, s)$, changes as locations are visited. $K_i(n, m, s)$ increases in places that direct interactions happen and decreases in places without interactions. The probability that space (n, m) is in the interaction zone of flock i in response to other flocks j at time step $s + 1$ is

$$K_i(n, m, s{+}1) = \begin{cases} 1 - \mu\tau & \text{if } i \text{ and any } j \text{ are in } (n, m) \text{ at } s \text{ and an interaction occurs with probability } \rho_{\tau l} \\ [1 - (\mu + \beta_l)\tau]\, K_i(n, m, s) & \text{if } i \text{ has no interaction in } (n, m) \text{ at } s, \\ (1 - \mu\tau)\, K_i(n, m, s) & \text{if } i \text{ is not in } (n, m) \text{ at } s, \end{cases} \tag{2.1}$$

where μ represents the decay of the interaction zone due to finite memory, β_l is the represents the decay of the interaction zone due to flock i visiting alone and

τ is the interval in time. Interactions between flocks occur with probability $\rho_{\tau,l}$. Equation (2.1) can be explained as follows; $K_i(n, m, s)$ is at its highest value when i and any other flock j are in (n, m) at s *and* an interaction happens. If flock i visits (n, m) at s and no interaction occurs, $K_i(n, m, s)$ is reduced by β_l. Regardless of the event, $K_i(n, m, s)$ is reduced at each time step due to memory decay, represented by μ.

When making a decision to move, flock i averages over grid spaces in its *perceptual range*, d, and moves in response to this average in each direction. The average is defined as

$$\bar{K}_i(n, m, s) = \frac{1}{N(P)} \sum_{(n',m')\in P} K_i(n', m', s) \tag{2.2}$$

where P is the set of all spaces (n', m') which are within a radius, d, of (n, m) and $N(P)$ is the number of elements in the set P. The probability of flock i moving to discrete space (n, m) at time step $s + 1$, given that the flock was at (n', m') at s can be described as $f_i(n, m|n', m') =$

$$\begin{cases} \frac{e}{4}\left[1 + q\bar{K}_i(n' + d, m, s) - q\bar{K}_i(n' - d, m, s)\right], & \text{if } (n, m) = (n' - 1, m'), \\ \frac{e}{4}\left[1 - q\bar{K}_i(n' + d, m, s) + q\bar{K}_i(n' - d, m, s)\right], & \text{if } (n, m) = (n' + 1, m'), \\ \frac{e}{4}\left[1 + q\bar{K}_i(n, m' + d, s) - q\bar{K}_i(n, m' - d, s)\right], & \text{if } (n, m) = (n', m' - 1), \\ \frac{e}{4}\left[1 - q\bar{K}_i(n, m' + d, s) + q\bar{K}_i(n, m' - d, s)\right], & \text{if } (n, m) = (n', m' + 1), \\ 1 - e & \text{if } (n, m) = (n', m'), \end{cases} \tag{2.3}$$

where $q \in (0, 1)$ is the strength of the tendency to move away from the interaction zone. To ensure that the parameters are biologically viable with

the numerical methods used, I have extended the model of Potts and Lewis (2016a) to include the probability of a flock staying in the same place, $1 - e$.

2.2.2 Deriving the Interaction System

The one-dimensional IBM defined by Potts and Lewis (2016a) was approximated and analysed as a PDE system. Throughout the rest of this Chapter I extend their work by deriving a two-dimensional PDE system from their IBM which I defined in §2.2.1. The interaction model is a system of PDEs where a diffusion-taxis equation describes the space use of a flock as a *utilisation distribution*. PDEs are defined in continuous space, $\mathbf{x} = (x, y)$ and time, t. To move to continuous space and time, I make the following redefinitions

$$\begin{aligned} x = nl, \quad y = ml, \quad t = s\tau, \\ k_i(x, y, t) = K_i(n, m, s), \quad l^2 u_i(x, y, t) = U_i(n, m, s), \end{aligned} \tag{2.4}$$

where l is the length of each discrete grid square and τ is the length of the discrete time interval. The multiple of l^2 is required because the utilisation distributions u_i and U_i must both integrate to 1 (explained further in Appendix A.2).

I begin by approximating the probability of a location being in the interaction zone as a PDE in continuous space and time. I first assume that the grid is large enough so that the probability of more than two flocks being present at (n, m) at s is negligible. Then, the probability of an interaction occurring at (n, m) at time s for flock i is

$$\rho_{\tau,l}\, U_i(n, m, s) \sum_{j \neq i} U_j(n, m, s). \tag{2.5}$$

The probability of a location being in the interaction zone is defined using the expected value of $K_i(n, m, s)$ (Equation 2.1). Writing $U_i(n, m, s)$ as U_i, the expected value of $K_i(n, m, s+1)$ is

$$\begin{aligned}\langle K_i(n,m,s+1)\rangle &= (1-\mu\tau)\,\rho_{\tau,l}U_i\sum_{j\neq i}U_j \\ &\quad + (1-(\mu+\beta_l)\,\tau)\,\langle K_i(n,m,s)\rangle\left[1-\rho_{\tau,l}U_i\sum_{j\neq i}U_j\right]U_i \\ &\quad + (1-\mu\tau)\,\langle K_i(n,m,s)\rangle\left[1-\rho_{\tau,l}U_i\sum_{j\neq i}U_j\right](1-U_i)\,, \quad (2.6)\end{aligned}$$

where the angle brackets in Equation (2.6) represent the expected value of $K_i(n, m, s)$. Moving to continuous space and time using the redefinitions (2.4), requires taking a continuum limit and follows a similar process to the one-dimensional derivation in Potts and Lewis (2016a), therefore I omit the full derivation here. Equation (2.6) is approximated as

$$\frac{dk_i}{dt} = \rho u_i \sum_{j\neq i} u_j\,(1-k_i) - k_i\,(\mu+\beta u_i)\,, \quad (2.7)$$

where $\rho = \lim_{l,\tau\to 0}\frac{l^4\rho_{\tau,l}}{\tau}$ and $\beta = \lim_{l\to 0} l^2\beta_l$. Additionally, as I move to continuous space and time, the average over the interaction zone becomes

$$\bar{k}_i(\mathbf{x},t) = \frac{1}{\pi\delta^2}\int_{B_\delta(\mathbf{x})} k_i(\mathbf{x},t)\,\mathrm{d}\mathbf{x}, \quad (2.8)$$

where $\delta = \lim_{\substack{d\to\infty \\ l\to 0}}(dl)$ and $B_\delta(\mathbf{x})$ defines the ball with radius δ around the point $\mathbf{x}$.

The derivation of the diffusion-taxis equation for space use from the IBM shown by Equation (2.3) begins by defining a master equation for moving to space

(n, m) at time $s + 1$:

$$
\begin{aligned}
&U_i(n, m, s+1) = \\
&\quad \frac{e}{4}\left[1 + q\bar{K}_i(n+1+d, m, s) - q\bar{K}_i(n+1-d, m, s)\right] U_i(n+1, m, s) \\
&\quad + \frac{e}{4}\left[1 + q\bar{K}_i(n-1-d, m, s) - q\bar{K}_i(n-1+d, m, s)\right] U_i(n-1, m, s) \\
&\quad + \frac{e}{4}\left[1 + q\bar{K}_i(n, m+1+d, s) - q\bar{K}_i(n, m+1-d, s)\right] U_i(n, m+1, s) \\
&\quad + \frac{e}{4}\left[1 + q\bar{K}_i(n, m-1-d, s) - q\bar{K}_i(n, m-1+d, s)\right] U_i(n, m-1, s) \\
&\quad + (1-e)U_i(n, m, s). \qquad (2.9)
\end{aligned}
$$

Using the redefinitions (2.4) and rearranging I obtain

$$
\begin{aligned}
&\frac{1}{\tau}\left(u_i(x, y, t) - u_i(x, y, t+\tau)\right) = \\
&\qquad \frac{e}{4\tau}\left[u_i(x+l, y, t) + u_i(x-l, y, t)\right] \\
&\qquad + \frac{e}{4\tau}\left[u_i(x, y+l, t) + u_i(x, y-l, t) - 4u_i(x, y, t)\right] \\
&\qquad + \frac{qe}{4\tau}\left[\left(\bar{k}_i(x+(1+d)l, y, t) - \bar{k}_i(x+(1-d)l, y, t)\right) u_i(x+l, y, t)\right] \\
&\qquad - \frac{qe}{4\tau}\left[\left(\bar{k}_i(x-(1+d)l, y, t) - \bar{k}_i(x-(1-d)l, y, t)\right) u_i(x-l, y, t)\right] \\
&\qquad + \frac{qe}{4\tau}\left[\left(\bar{k}_i(x, y+(1+d)l, t) - \bar{k}_i(x, y+(1-d)l, t)\right) u_i(x, y+l, t)\right] \\
&\qquad - \frac{qe}{4\tau}\left[\left(\bar{k}_i(x, y-(1+d)l, t) - \bar{k}_i(x, y-(1-d)l, t)\right) u_i(x, y-l, t)\right]. \\
&\qquad\qquad\qquad\qquad\qquad\qquad\qquad\qquad\qquad\qquad\qquad\qquad (2.10)
\end{aligned}
$$

Each u_i and $\bar{k}_i$ is expanded as an approximation of their Taylor series around (x, y), where any terms of order l^3 or higher are considered to be negligible as l is small. By substituting the Taylor approximations into (2.10) and taking the limit as $\tau, l \to 0$ the diffusion-taxis equation becomes

$$\frac{\partial u_i}{\partial t} = D\nabla^2 u_i + c\nabla \cdot \left[u_i \nabla \bar{k}_i\right], \tag{2.11}$$

where $\nabla = \left(\frac{\partial}{\partial x}, \frac{\partial}{\partial y}\right)$, $c = 4dqD$ and $D = \lim_{\tau,l\to 0}\left(\frac{l^2 e}{4\tau}\right)$.

Non-dimensionalization of Equations (2.11) and (2.7) reduces the amount of parameters, so that analyses of the system and fitting to data are more efficient. I redefine the parameters in Equations (2.7), (2.8) and (2.11) in Appendix A.3. The new parameters have the form

$$\begin{aligned}
&\rho = \lim_{l,\tau\to 0}\frac{\rho_{\tau,l} l^4}{\tau}, \quad \beta = \lim_{l,\tau\to 0} l^2\beta_l, \quad D = \lim_{l,\tau\to 0}\frac{l^2 e}{4\tau}, \quad \delta = \lim_{l\to 0} ld \\
&c = 4dqD, \quad \tilde{x} = \frac{x}{L}, \quad \tilde{y} = \frac{y}{L}, \quad \tilde{\delta} = \frac{\delta}{L}, \quad \tilde{u_i} = Lu_i, \quad \tilde{k_i} = k_i, \quad \tilde{t} = \frac{Dt}{L^2}, \\
&a = \frac{D}{\rho}, \quad b = \frac{\beta L}{\rho}, \quad \gamma = \frac{c}{D}, \quad m = \frac{\mu L^2}{\rho}.
\end{aligned} \tag{2.12}$$

where l is change in space, which is same in both the x and y directions and τ is the change in time. L is the length of the square domain $\Omega = [0, L] \times [0, L]$ that the system is solved over, which is the same for each flock. The continuous perceptual radius of a flock, when averaging $k_i(\mathbf{x}, t)$ is denoted by δ.

The system defined here describes the spatio-temporal change of a probability density function therefore $\int_\Omega u_i \, \mathrm{d}\mathbf{x} = 1$ must always be true, to ensure this I set zero-flux boundary conditions meaning that the amount of density entering the spatial domain is always equal to the amount exiting. These conditions

give the interaction system

$$\frac{\partial u_i}{\partial t} = \nabla^2 u_i + \nabla \cdot \left[\gamma u_i \nabla \bar{k}_i\right], \tag{2.13}$$

$$a\frac{\partial k_i}{\partial t} = u_i \Sigma_{i \neq j} u_j (1 - k_i) - k_i(m + b u_i), \tag{2.14}$$

$$\left| \mathbf{n}_{\mathbf{x}} \cdot \left[\nabla u_i + \gamma u_i \nabla \bar{k}_i\right] \right|_{\mathbf{x} \in \partial\Omega} = 0, \tag{2.15}$$

$$\int_{\Omega} u_i \, \mathrm{d}\mathbf{x} = 1, \tag{2.16}$$

where the tildes from (2.12) are omitted for notational purposes. The boundary of the domain to be solved over is $\partial\Omega$ and $\mathbf{n}_{\mathbf{x}}$ is the normal to the boundary at $\mathbf{x}$. When averaging over $k_i(\mathbf{x}, t)$ using Equation (2.8), the circular area is truncated at the boundaries accordingly.

2.2.3 Initial Numerical Solutions

I solve the system (2.13)-(2.16) using finite difference methods, detailed in Appendix A.4. Numerical solutions for two flocks with initial conditions that are Dirac delta functions (with the mass concentrated at the points (0.25, 0.25) and (0.75, 0.75) in the domain $[0, 1]^2$) and parameter values $a = 0.01$, $b = 5$, $\gamma = 10$, $m = 0$ and $\delta = 0.05$ are shown in Fig. 2.1. Solutions that are biologically relevant consist of home range patterns where each flock's space use is concentrated on either side of the domain, as a result of the avoidance mechanism. As the system evolves through time, different biologically relevant solutions appear. At around $t = 0.5$ the system appears to be close to a stable steady state, changing little from $t = 0.5$ to $t = 2$. However, if we carry on simulating the system, it in fact changes very slowly through time. This suggests the possibility that the numerical system may have a continuum of

stable steady states and the numerics are moving close to this continuum, but never quite settling on one stable state, due to small numerical approximations. In §2.3.2, we demonstrate this continuum of stable steady states in the limit as $\delta \to 0$, giving evidence to support this interpretation of what we are seeing numerically. In the next section, I investigate the conditions in which patterns may form in the system (2.13)-(2.16) and define a method to find the numerical steady-state.

2.3 Pattern formation analysis

The emergence of patterns in non-linear diffusion systems can be predicted using linear stability analysis (LSA, Murray 1993; Turing 1952). LSA allows one to investigate the short-term behaviour of a system to estimate when patterns may occur. Moreover, the asymptotic behaviour of a system can be analysed with energy functional analysis, using Lyapunov's direct method for stability (e.g. Krstic and Smyshlyaev 2008). To analyse when home range patterns may form in the one-dimensional system for two individuals, Potts and Lewis (2016a) used both analyses, finding that (1) patterns form for some parameter regimes and (2) steady-state patterns may depend on the initial conditions. I extend these analyses to understand the conditions in which patterns may form in the two-dimensional system for multiple flocks.

In the one-dimensional system for two flocks, the spontaneous emergence of patterns from small non-constant perturbations of the constant steady-state depends on the parameters γ and b (Potts and Lewis, 2016a). The γ parameter corresponds to *taxis* away from the interaction zone and b corresponds to the decay of the interaction zone, due to visiting areas without interactions

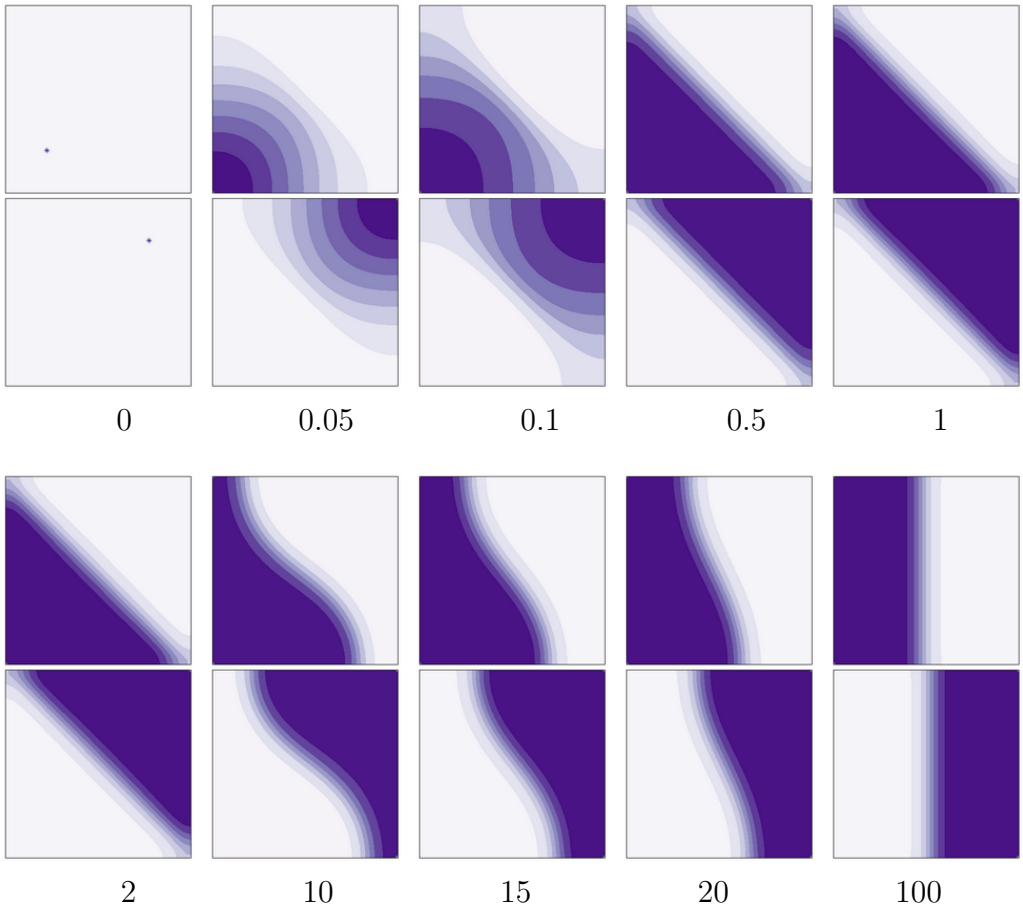

Fig. 2.1. Numerical solutions of the interaction model. Each solution is labelled with its corresponding time, t. Solutions are calculated using the numerical scheme in Appendix A.4 and it takes approximately 55 hours to reach the solution in the final panel ($t = 100$). The reasons of this particularly long computational time are investigated in §2.3.2, where it is indicated that small numerical errors may cause the system to shift between numerical steady-states. Parameter values used here are $a = 0.01$, $b = 5$, $\gamma = 10$, $m = 0$ and $\delta = 0.05$.

occurring. I focus on different values of γ and b parameters which give rise to patterns in the two-dimensional system, for multiple flocks.

2.3.1 Linear Stability Analysis

I perform LSA for the system (2.13)-(2.16) in two dimensions for two and four flocks. The system has constant steady-states $u_i^*(\mathbf{x}) = u_c$ and $k_i^*(\mathbf{x}) = k_c$. The value u_c is found by the integration condition in Equation (2.16), giving $u_c = 1$ for all i. When Equation (2.14) isn't changing over time,

$$k_c = \frac{n-1}{b+m+n-1}, \tag{2.17}$$

for all i, where n is the number of flocks in the system.

For this analysis, I assume that solutions for u_i and k_i take the form of their constant steady-states, with small spatially non-constant perturbations, $\hat{u}_i$ and $\hat{k}_i$ in the following form (which is standard, see Murray 1993)

$$u_i = u_i^* + \hat{u}_i = 1 + u_{i,0} \exp\left(\sigma t + j\boldsymbol{\kappa} \cdot \mathbf{x}\right), \tag{2.18}$$

$$k_i = k_i^* + \hat{k}_i = k_c + k_{i,0} \exp\left(\sigma t + j\boldsymbol{\kappa} \cdot \mathbf{x}\right), \tag{2.19}$$

where $j = \sqrt{-1}$ and coefficients $u_{i,0}$ and $k_{i,0}$ are arbitrarily small. The vector of wavenumbers $\boldsymbol{\kappa} = (\kappa_x, \kappa_y)$, is constant. Substituting the solutions (2.18) and (2.19) into the system (2.13)-(2.16) and ignoring non-linear terms means the system can be written in the form

$$\mathbf{M}_n \hat{\mathbf{w}} = \sigma \hat{\mathbf{w}}, \tag{2.20}$$

which is approximately valid for small times, where the non-linear terms are trivial. In Equation (2.20), $\hat{\mathbf{w}} = (\hat{u}_1, \ldots, \hat{u}_n, \hat{k}_1, \ldots, \hat{k}_n)$, $\mathbf{M}_n$ is a matrix and σ is an eigenvalue of matrix $\mathbf{M}_n$. By plotting the eigenvalue with the greatest real part against $\boldsymbol{\kappa}$, namely the dispersion relation, the existence of positive $\Re(\sigma)$ values for a non-zero range of $\boldsymbol{\kappa}$ values indicates the formation of patterns, for a given range of parameters (Murray, 1993).

To find the matrix $\mathbf{M}_n$ for the system (2.13)-(2.16), I first find a form for $\bar{k}_i$, the average of k_i over a disc of radius δ centred at $\mathbf{x}$, shown in Equation (2.8). Converting to polar coordinates this average becomes

$$\bar{k}_i(x, y, t) = \frac{1}{\pi\delta^2} \int_0^{\delta} \int_0^{2\pi} r\, k_i(x + r\cos(\theta), y + r\sin(\theta), t)\, \mathrm{d}\theta \mathrm{d}r, \tag{2.21}$$

then substituting Equation (2.19) into Equation (2.21) gives

$$\begin{aligned} \bar{k}_i =& \frac{1}{\pi\delta^2} \int_0^{\delta} \int_0^{2\pi} r k_c \, \mathrm{d}\theta \mathrm{d}r \\ &+ \frac{1}{\pi\delta^2} \int_0^{\delta} \int_0^{2\pi} r k_{i,0} \exp\left(\sigma t + j\kappa_x(x + r\cos(\theta)) + j\kappa_y(y + r\sin(\theta)\right) \mathrm{d}\theta \mathrm{d}r, \end{aligned} \tag{2.22}$$

where the first term in Equation (2.22) is equal to k_c. The integral in the second term is

$$I = \frac{\hat{k}_i}{\pi\delta^2} \left(\int_0^{\delta} \int_0^{2\pi} r \exp\left(j\kappa_x r\cos(\theta) + j\kappa_y r\sin(\theta)\right) \mathrm{d}\theta \mathrm{d}r \right), \tag{2.23}$$

$$\begin{aligned} &= \frac{\hat{k}_i}{\pi\delta^2} \int_0^{\delta} \int_0^{2\pi} r \cos\left(\kappa_x r\cos(\theta) + \kappa_y r\sin(\theta)\right) \mathrm{d}\theta \mathrm{d}r \\ &+ j\frac{\hat{k}_i}{\pi\delta^2} \int_0^{\delta} \int_0^{2\pi} r \sin\left(\kappa_x r\cos(\theta) + \kappa_y r\sin(\theta)\right) \mathrm{d}\theta \mathrm{d}r. \end{aligned} \tag{2.24}$$

The second term of Equation (2.24) is equal to zero as $\sin(\kappa_x r\cos(\theta)+\kappa_y r\sin(\theta))$ has a range $[-1,1]$ with a period of 2π and is being integrated over a full period. To evaluate the first term I use the harmonic identity $a\cos(\theta)+b\sin(\theta) = \sqrt{a^2+b^2}\cos(\theta-\phi)$ where ϕ can be set equal to zero as the integral is the same, regardless of this shift. Using $|\boldsymbol{\kappa}| = \kappa_x^2+\kappa_y^2$ the integral becomes

$$\begin{aligned} I &= \frac{\hat{k}_i}{\pi\delta^2}\int_0^{\delta}\int_0^{2\pi} r\cos\left(r|\boldsymbol{\kappa}|\cos(\theta)\right)\,\mathrm{d}\theta\mathrm{d}r, \\ &= \frac{2\pi\hat{k}_i}{\pi\delta^2}\int_0^{\delta} rJ_0\left(r|\boldsymbol{\kappa}|\right)\mathrm{d}r, \end{aligned} \tag{2.25}$$

where $J_0(x) = \frac{1}{\pi}\int_0^{\pi}\cos(x\cos(\theta))\mathrm{d}\theta$ is a Bessel function of the first kind of order 0. A Bessel Function of the first kind has the general form $J_m(x) = \frac{1}{\pi}\int_0^{\pi}\cos(x\sin(\theta)-m\theta)\mathrm{d}\theta$ for order m. Using the identity $\int uJ_0(u)\mathrm{d}u = uJ_1(u)$ and integration by substitution (where $u = r|\boldsymbol{\kappa}|$), I obtain

$$I = \frac{2J_1(\delta|\boldsymbol{\kappa}|)}{\delta|\boldsymbol{\kappa}|}\hat{k}_i, \tag{2.26}$$

which gives

$$\bar{k_i} = k_c + \frac{2J_1(\delta|\boldsymbol{\kappa}|)}{\delta|\boldsymbol{\kappa}|}\hat{k}_i. \tag{2.27}$$

Substituting (2.18) and (2.27) into Equation (2.13) gives

$$\sigma\hat{u}_i = -|\boldsymbol{\kappa}|^2\hat{u}_i - \frac{2|\boldsymbol{\kappa}|J_1(\delta|\boldsymbol{\kappa}|)}{\delta}\hat{k}_i. \tag{2.28}$$

Similarly, substituting (2.18) and (2.19) into Equation (2.14) gives

$$\sigma\hat{k}_i = \frac{m(n-1)}{a(m+b+n-1)}\hat{u}_i + \sum_{p\neq i}\frac{m+b}{a(m+b+n-1)}\hat{u_p} + \frac{-(m+b+n-1)}{a}\hat{k}_i. \tag{2.29}$$

The eigenvalues of matrix $\mathbf{M}_n$ are defined as

$$\sigma_1 = \frac{\gamma 2J_1(\delta|\boldsymbol{\kappa}|)\,[b+m(2-n)]}{\delta|\boldsymbol{\kappa}|(m+b+n-1)^2} - 1, \tag{2.30}$$

$$\sigma_2 = -\frac{\gamma 2J_1(\delta|\boldsymbol{\kappa}|)\,[b+2m(n-1)]}{\delta|\boldsymbol{\kappa}|(m+b+n-1)^2} - 1, \tag{2.31}$$

which are repeated (M_n has size $2n \times 2n$, so each eigenvalue is repeated n times). If $\max(\sigma_1, \sigma_2) > 0$ for some $\boldsymbol{\kappa}$, the steady-state solution is unstable to non-constant perturbations, suggesting patterns may form spontaneously.

In the case of two flocks ($n = 2$), the parameter values $a = 0.01$, $b = 1$, $\gamma = 10$, $m = 0$ and $\delta = 0.05$ give similar dispersion relations to Potts and Lewis (2016a) (seen by setting $\kappa_x = \kappa_y$). As the amount of flocks in the system increases (from 2 flocks to 4 flocks), the allowed range of γ and b for patterns to occur is smaller (Fig. 2.2). The range of γ and b parameters which give rise to patterns as predicted by the LSA are shown by the green areas of Fig. 2.3 (top panels).

2.3.2 An Energy Functional analysis

The energy functional method is a way of finding asymptotically-stable steady state solutions. An energy functional for the system (2.13)-(2.16) is a functional of the solution $u_i(\mathbf{x}, t)$ that gives a value, the energy, which is always decreasing through time. Before the energy functional is defined, the following assumptions are used (Potts and Lewis, 2016a). First set $\delta \to 0$, so that $\bar{k_i}(\mathbf{x}, t|\delta) = k_i(\mathbf{x}, t)$.

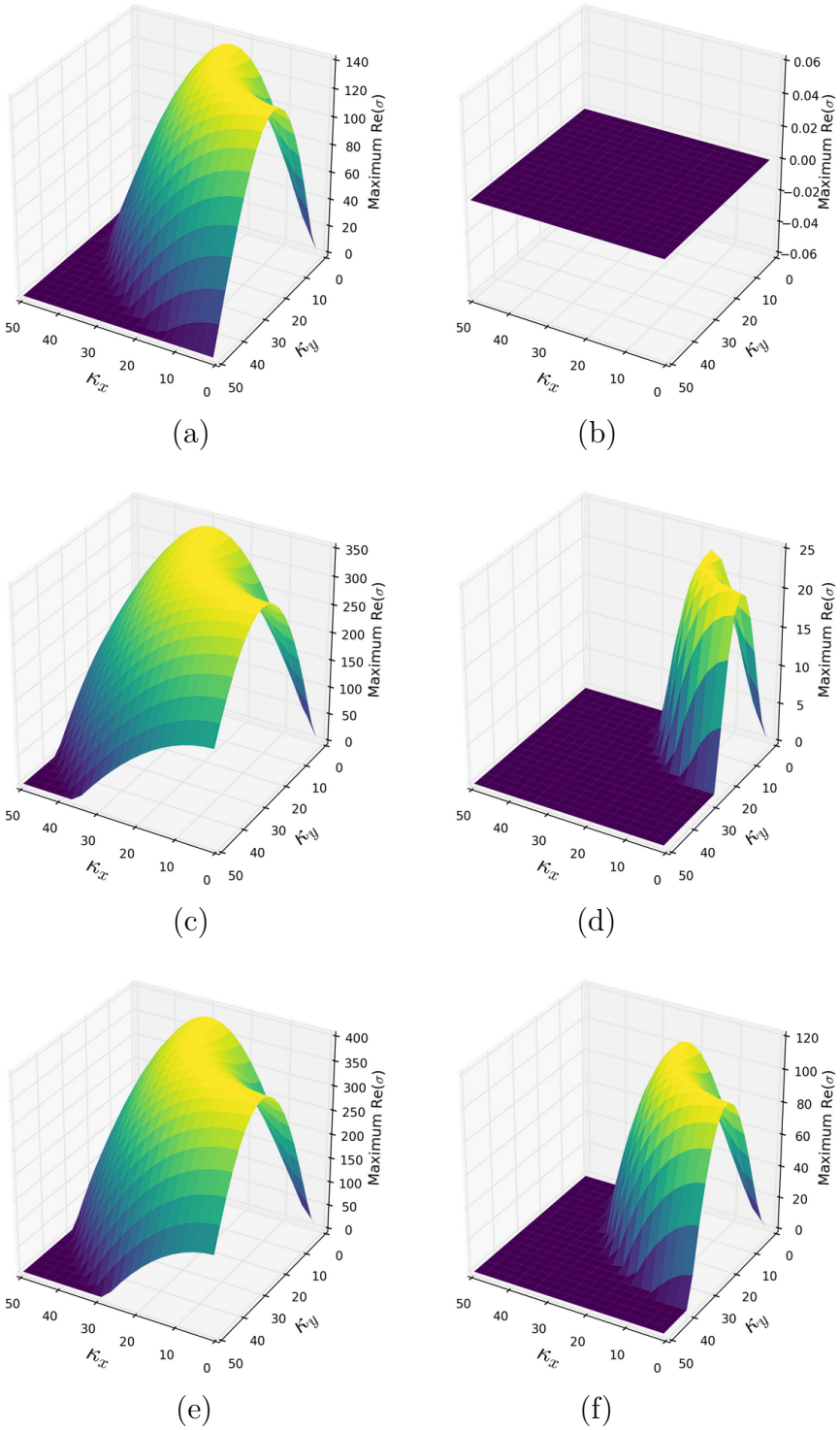

Fig. 2.2. Dispersion relations using the eigenvalues, σ_1, σ_2 (Equations 2.30 and 2.31), of the matrix M_2 (left panels) for two individuals and M_4 for 4 individuals (right panels). Panels (a) and (b) show the dispersion relation for $a = 0.01$, $b = 1$, $\gamma = 10$, $m = 0$, $\delta = 0.05$. Panels (c) and (d) increase γ to 20 and panels (e) and (f) increase b to 3.

Next, assume that Equation (2.14) reaches equilibrium quickly and set $a = 0$. Also set $m = 0$ (no decay due to finite memory). Lastly, since the integral condition (2.16) indicates a constant steady state solution $u_i^*(\mathbf{x}) = 1$, assume that $\sum_{i=1}^{n} u_i(\mathbf{x}, t) = n$, where n is the number of flocks. Using these assumptions, Equation (2.13) becomes a function of only $u_i(\mathbf{x}, t)$:

$$\frac{\partial u_i}{\partial t} = \nabla \cdot \left[\nabla u_i + \gamma u_i \nabla \left(\frac{n - u_i}{b + n - u_i} \right) \right]. \tag{2.32}$$

Equation (2.32) can then be written in the form

$$\frac{\partial u_i}{\partial t} = \nabla^2 \phi(u_i), \tag{2.33}$$

where

$$\phi(u_i) = u_i - \gamma b \ln(b + n - u_i) - \frac{\gamma b(b + n)}{b + n - u_i}. \tag{2.34}$$

I assume $b > 0$ and $u_i < b + n$, to ensure that Equation (2.34) is defined. For an energy functional, a function $\Phi(u_i)$ is defined by setting $\frac{\mathrm{d}\Phi(u_i)}{\mathrm{d}u_i} = \phi(u_i)$, so that

$$\Phi(u_i) = \frac{u_i^2}{2} + \gamma b(2b + 2n - u_i) \ln(b + n - u_i) - \gamma b(b + n - u_i). \tag{2.35}$$

Then, over the domain, $\Omega = [0, 1]^2$, the energy functional for the system (2.13)-(2.16) has the form

$$E(u_i) = \int_0^1 \int_0^1 \Phi(u_i) \, \mathrm{d}x \, \mathrm{d}y, \tag{2.36}$$

which is always decreasing since:

$$\begin{aligned}
\frac{\mathrm{d}E(u_i)}{\mathrm{d}t} &= \int_0^1 \int_0^1 \left(\frac{\mathrm{d}\Phi(u_i)}{\mathrm{d}t} \right) \, \mathrm{d}x \, \mathrm{d}y, \\
&= \int_0^1 \int_0^1 \left(\frac{\mathrm{d}\Phi(u_i)}{\mathrm{d}u_i} \frac{\mathrm{d}u_i}{\mathrm{d}t} \right) \, \mathrm{d}x \, \mathrm{d}y, \\
&= \int_0^1 \int_0^1 \left(\frac{\mathrm{d}\Phi(u_i)}{\mathrm{d}u_i} \nabla^2 \phi \right) \, \mathrm{d}x \, \mathrm{d}y. \\
&= \int_0^1 \int_0^1 \left(\phi \nabla^2 \phi \right) \mathrm{d}x \, \mathrm{d}y, \\
&= \int_0^1 \int_0^1 \left(\phi \frac{\partial^2 \phi}{\partial x^2} + \phi \frac{\partial^2 \phi}{\partial y^2} \right) \mathrm{d}x \, \mathrm{d}y, \\
&= \int_0^1 \left(\int_0^1 \phi \frac{\partial^2 \phi}{\partial x^2} \mathrm{d}x \right) \mathrm{d}y + \int_0^1 \left(\int_0^1 \phi \frac{\partial^2 \phi}{\partial y^2} \mathrm{d}y \right) \mathrm{d}x, \\
&= \int_0^1 \left(\left[\phi \frac{\partial \phi}{\partial x} \right]_0^1 - \int_0^1 \left(\frac{\partial \phi}{\partial x} \right)^2 \mathrm{d}x \right) \mathrm{d}y \\
&\quad + \int_0^1 \left(\left[\phi \frac{\partial \phi}{\partial y} \right]_0^1 - \int_0^1 \left(\frac{\partial \phi}{\partial y} \right)^2 \mathrm{d}y \right) \mathrm{d}x, \\
&= - \int_0^1 \int_0^1 \left[\left(\frac{\partial \phi}{\partial x} \right)^2 + \left(\frac{\partial \phi}{\partial y} \right)^2 \right] \mathrm{d}x \, \mathrm{d}y, \\
&< 0. \qquad (2.37)
\end{aligned}$$

The seventh line of Equation (2.37) uses integration by parts. The flux of Equation (2.33) normal to the boundary is zero, therefore, since the domain is $\Omega = [0, 1]^2$, the last line of Equation (2.37) is true. Lastly, Equation (2.37) is always negative since $\left(\frac{\partial \phi}{\partial x}\right)^2 + \left(\frac{\partial \phi}{\partial y}\right)^2$ is always positive. Therefore, the energy functional is always decreasing.

When Equation (2.33) is at steady-state, the flux $-\nabla\phi = \mathbf{c}$ is constant across the domain, by definition. The flux normal to the four boundaries is always zero, therefore at steady-state the horizontal and vertical components of $\mathbf{c}$ must both be zero, leaving $\frac{\partial \phi}{\partial x} = \frac{\partial \phi}{\partial y} = 0$. Equation (2.37) shows that the energy

is always decreasing, but when the system is at steady-state (2.37) becomes $\frac{\mathrm{d}E}{\mathrm{d}t} = 0$. Therefore, if $E(u_i)$ reaches a minimum, then this value will reached as the system reaches steady-state.

The energy functional will only reach a minimum value representing the system's steady-state if it is bounded below. Potts and Lewis (2016a) prove that in the one-dimensional system, when $m = 0$ and $\delta \to 0$, there are no non-constant classical steady-state solutions and instead search for weakly-defined solutions. The numerical solutions shown in Fig. 2.1 give evidence towards a particular biologically relevant solution where, for two flocks, the space use of each flock is concentrated on either side of the available domain. Therefore, I follow Potts and Lewis (2016a) and search for minimum energy weak solutions that correspond to the sort of home ranges that are observed numerically, whereby each flock i has most of its space use concentrated in one part of the domain, S_i, where $m(S_i) = \frac{1}{n}$ and outside of S_i space use is equal to the constant value η_i. Specifically, I search for solutions of the form

$$u_i^*(\mathbf{x}) = n - \sum_{j \neq i} \eta_j, \quad u_j^*(\mathbf{x}) = \eta_j, \qquad \text{for } \mathbf{x} \in S_i,\ j \neq i, \text{ for all } i, \tag{2.38}$$

where the sets $\{S_i\}_i$ for $1 \leq i \leq n$ partition the space $[0,1] \times [0,1]$. Substituting Equation (2.38) into Equation (2.36) gives

$$E(u_i^*) = \tfrac{1}{n}\Phi(n - \sum_{i \neq j} \eta_j) + \tfrac{1}{n} \sum_{i \neq j} \Phi(\eta_j). \tag{2.39}$$

Since $b > 0$ and $u_i < b + n$, the energy is bounded below as it is a continuous function whose domain is the compact set $[0,1]^2$.

To find values of η_j that minimise Equation (2.39), numerically for $n = 2, 4$, I search for local minima in the domain $0 < \eta_i < 1$ for all i in the parameter ranges $0 < b < 10$ and $0 < \gamma < 20$. For all values of b and γ, the minimum of Equation (2.39) is when either $\eta_i = 0$ or $\eta_i = 1$, for all i. For some values of b and γ there is a local minimum at both $\eta_i = 0$ and $\eta_i = 1$. When the energy has local minima at both $\eta_i = 0$ and $\eta_i = 1$, there are two asymptotically stable steady-state solutions, so the patterns that result as time tends to infinity are determined by the initial conditions. Home range patterns correspond to $\eta_i = 0$, since in this case each flock i is only using the space in S_i. The parameter ranges corresponding to home range patterns are shown in Fig. 2.3 (bottom panels) where the green parameter regimes show places where there is a global minimum $\eta_i = 0$ for $0 < \eta_i < 1$ for all i and the pink parameter regimes show places where there is a local minimum that is not global. The green parameter regimes correspond to the parameter regimes predicted by linear stability analysis (LSA), Fig. 2.3 (top panels).

Since the energy functional is always decreasing, if the system reaches a minimum energy solution described by Equation (2.38) with $\eta_j = 0$, for all j (corresponding the the steady-state of the system), it should not change. However, the numerical solution in Fig. 2.1 does not appear to result in a particular steady-state solution but instead slowly changes through time. I propose that due to the numerical approximation used to solve the system, it is possible that the system is becomes numerically very close to reaching a steady-state then starts moving towards another, nearby steady state solution, potentially in perpetuity. Here I explain this reasoning visually using representations of solutions to the one-dimensional system (Potts and Lewis, 2016a) and the two-dimensional system (2.13)-(2.16), for two flocks.

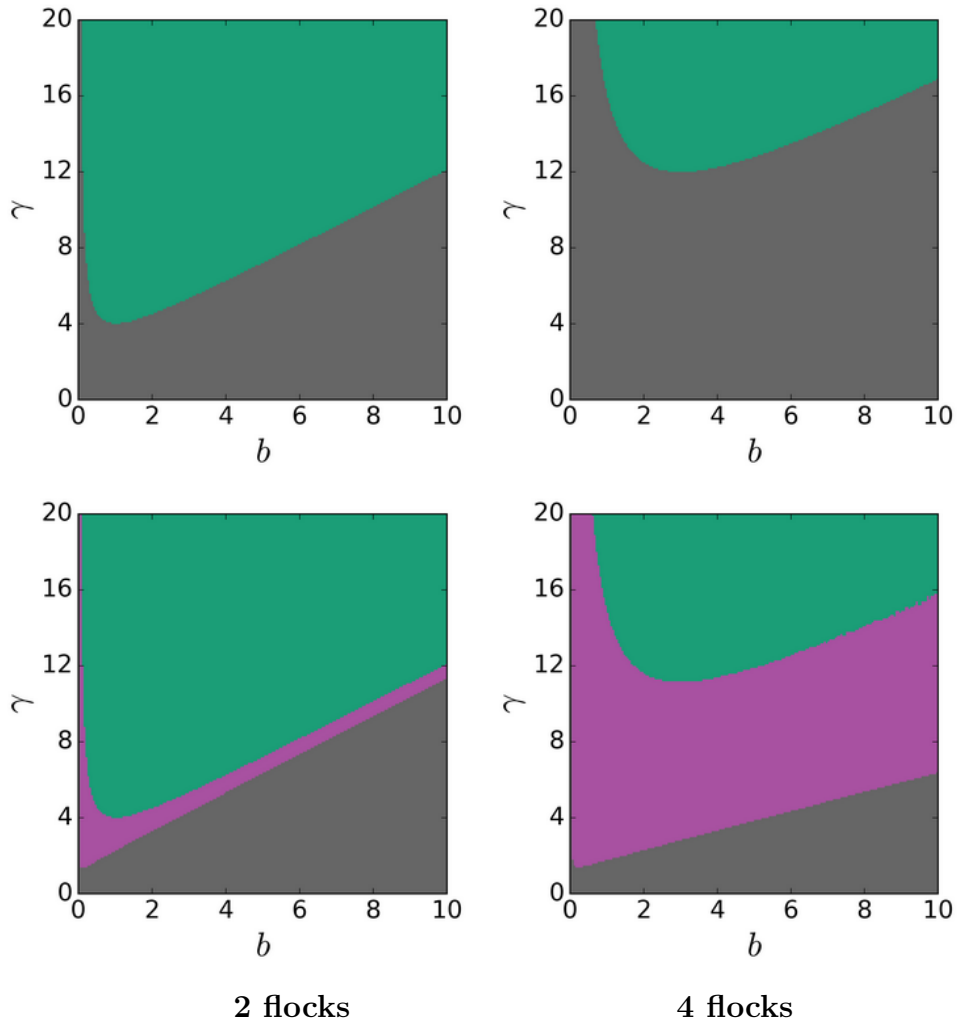

Fig. 2.3. Parameter schemes for home range pattern formation where values of b and γ shown by the green area indicate patterns. The left panels represent the interaction model with two flocks and the right panels represent the model for four flocks. The top panels are found by the linear stability analysis (LSA). The bottom panels are found by the energy functional analysis, where the green areas show values of b and γ where there was a global minimum at $\eta_i = 0$ and the pink areas show where there are local minima at $\eta = 0, 1$, where $0 \leq \eta_i \leq 1$. The pink areas correspond to steady-states which depend on the initial conditions.

The hypothetical solution shown in Fig. 2.4 shows solutions in one dimension for two flocks. Possible minimum energy solutions (Equation 3.18 in Potts and Lewis 2016a) are shown in panels (a) and (c). It is not possible to continuously move from panel (a) to (c), as to do this requires moving through non-minimum energy solutions, such in panel (b), and this requires an increase in energy.

For the two-dimensional case, possible solutions at minimum energy (defined by Equation 2.38, with $\eta_j = 0$, for all j) can be visualised in Fig. 2.5. Two solutions at minimum energy such as those in panels (a) and (b) can be arbitrarily close together. The numerical approximation of the system may find a solution very close to the steady-state then due to numerical error, it may start moving towards another solution that is very close to a different stable steady-state. Therefore, it is necessary to determine a method to find numerically the correct steady-state solution that corresponds to a given initial condition. This is the subject of §2.4.

To conclude, home range patterns form in the system (2.13)-(2.16) for the ranges of b and γ shown in Fig. 2.3. By investigating a particular type of solution, I have shown, through an analytic argument combined with numerical experiments, that the two-dimensional numerical solution of the system (2.13)-(2.16) may never settle on a steady-state. Although I have only investigated a restricted set of solutions (Equation 2.38) with the simplifying assumptions that $m = 0$ and $\delta \to 0$, the analysis agrees well with linear stability analysis of the full system (Fig. 2.3, top panels). In the next section, I detail a procedure to find numerically the steady-state of the system which corresponds to any given initial condition.

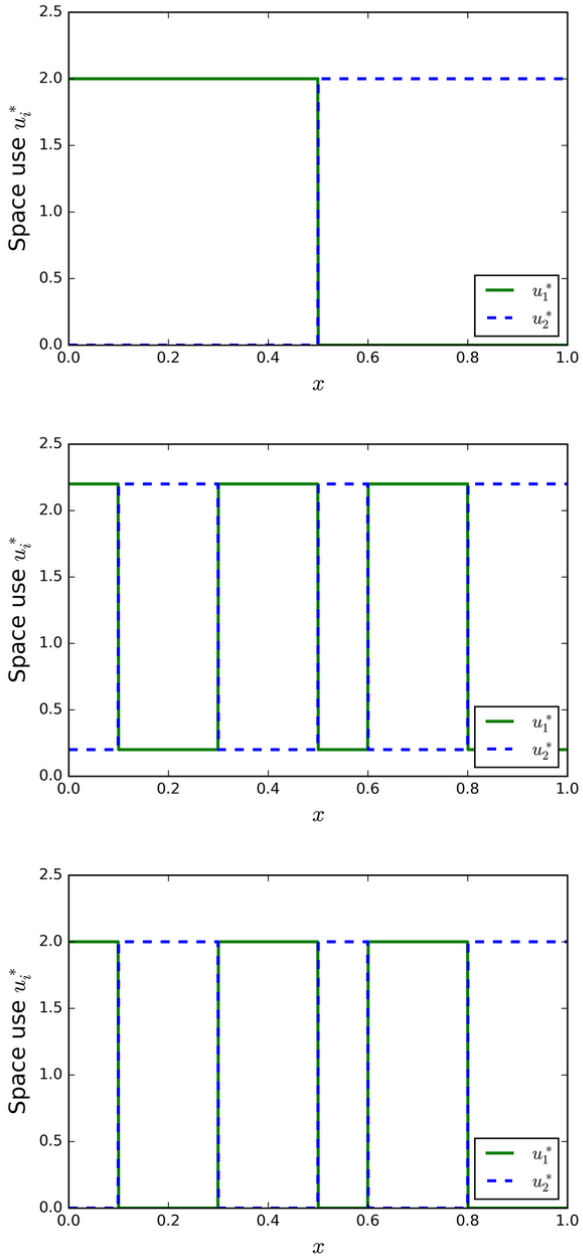

Fig. 2.4. 1D examples of solutions at minimum energy defined by a one-dimensional version of Equation (2.38) with $\eta_j = 0$, for all j. The top panel shows a solution with home ranges formed. The middle panel shows a solution which does not fit Equation (2.38) with $\eta_j = 0$, for all j, but could be moving to a solution at minimum energy. The bottom panel shows a solution at minimum energy where the home ranges are not connected. This figure shows that in one dimension it is not possible to move continuously from solution to another (e.g. from the top panel to the bottom) without minimum energy.

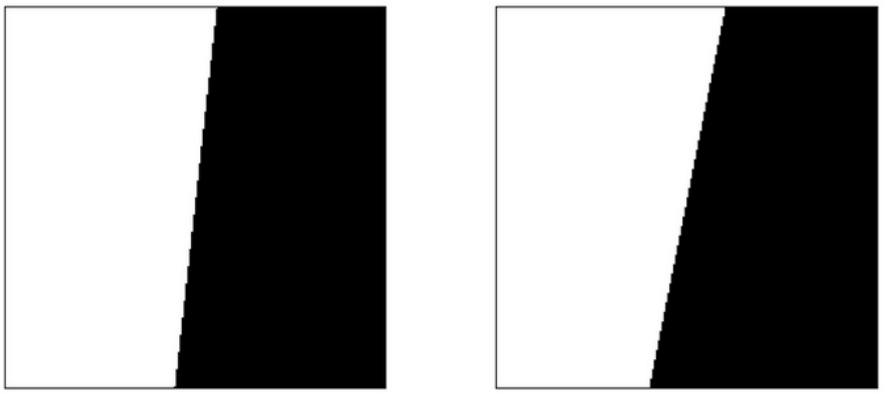

(a) (b)

Fig. 2.5. 2D examples of solutions at minimum energy defined by Equation (2.38) for two flocks, i and j, with $\eta_j = 0$. The white areas show the space use of flock i and the black areas show the space use of flock j. Panels (a) and (b) show different solutions at minimum energy. It is possible to move from solution (a) to solution (b) without moving out of a minimum energy.

2.4 Numerical methods

The numerical solution shown in Fig. 2.1 appears to move through solutions that are close to steady-state solutions predicted by the energy functional analysis (Equation 2.38 with $\eta_j = 0$, for all j). To estimate numerically the steady-state corresponding to an initial condition, I design a numerical scheme whereby the evolution of $k_i(\mathbf{x}, t)$ is halted at a point where this steady-state appears (numerically) to have been reached.

2.4.1 The evolution of $k_i(\mathbf{x}, t)$

The size of the interaction zone for each flock i is given by $\int_\Omega k_i(\mathbf{x}, t)\,\mathrm{d}\mathbf{x}$. The change in this value over time is shown in Fig. 2.6 for the system solved in Fig. 2.1. After some initial growth of the interaction zone, the numerical integral $\int_\Omega k_i(\mathbf{x}, t)\,\mathrm{d}\mathbf{x}$ appears visually to reach a saturation point. To find this

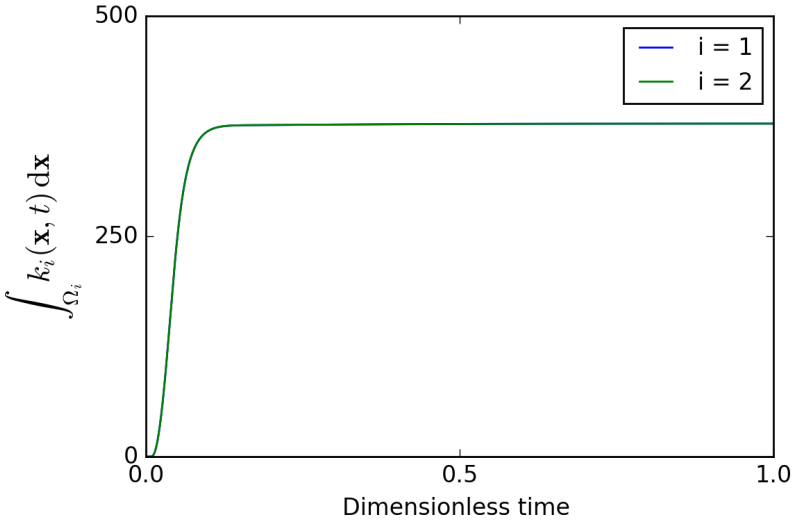

Fig. 2.6. The numerical integral of $k_i(\mathbf{x}, t)$ over the study area as the system solved in Fig. 2.1 evolves through time.

numerical saturation point, the average temporal gradient of the numerical integral $\int_\Omega k_i(\mathbf{x}, t)\,\mathrm{d}\mathbf{x}$, over 100 time steps, is given by

$$\kappa_i(t) = \int_{t' \in T_t} \left| \int_\Omega k_i(\mathbf{x}, t') - k_i(\mathbf{x}, t' + 100\tau)\mathrm{d}\mathbf{x} \right| \mathrm{d}t'. \tag{2.40}$$

where τ is equal to the numerical timestep, $\Omega = [0, 1]^2$ is the landscape and $T_t = [t, t + 100\tau]$.

The following procedure can be used to stop the evolution of k_i. At the point in time when $\kappa_i(t)$ reaches a minimum threshold value, $\kappa_{i,min}$, the evolution of the interaction zone for flock i is stopped. After this value is reached, I continue to evolve $u_i(\mathbf{x}, t)$ according to Equation (2.13), but keep $k_i(\mathbf{x}, t)$ fixed. Then I stop the numerical solution at the first point in time where $\max_{\mathbf{x}} |u_i(\mathbf{x}, t + \tau) - u_i(\mathbf{x}, t)|$ first dips below a pre-defined tolerance level for each flock i. The value of $\kappa_{i,min}$ used to stop the evolution of $k_i(\mathbf{x}, t)$ and the

tolerance level to stop the evolution of $u_i(\mathbf{x}, t)$ depends on the numerical scheme (e.g. grid spacing and time steps).

For numerical solutions in the next section, I use $\kappa_{i,min} = 0.2$. This value was found by testing a range of values and choosing the value which had the smallest difference between the stopping times for the flocks. The range of values were chosen by ensuring that the minimum value for $\kappa_{i,min}$ resulted in interaction zones that were sufficiently formed. The formation of the interaction zone was checked to be sufficient by plotting k_i and observing the size of the interaction zone. Further investigations are required to find the best quantifiable way to determine the range of $\kappa_{i,min}$ values, e.g. checking the percentage cover of the interaction zone in the domain. When fitting to data, further values of $\kappa_{i,min}$ will be explored. I stop the evolution of $u_i(\mathbf{x}, t)$ when $\max_{\mathbf{x}}|u_i(\mathbf{x}, t+\tau) - u_i(\mathbf{x}, t)| < 10^{-10}$ for a grid of 50 by 50 cells and $\tau = 10^{-5}$.

2.4.2 Numerical solutions of the interaction system

The interaction model was derived to model the home range of multiple flocks of long-tailed tits using a memory medicated avoidance mechanism. Here I show examples of numerical solutions of the interaction model for four hypothetical flocks. The interaction model is defined by Equations (2.13)-(2.16) and solved to a steady-state using the numerical schemes in Appendix A.4 and §2.4.1. Steady-state solutions correspond to utilisation distributions and these are shown in Fig. 2.7 for two different sets of initial conditions. I show solutions for different values of γ; the parameter which represents taxis away from the interaction zone. The utilisation distributions in Fig. 2.7 show that by avoiding locations where previous interactions have occurred, the interaction model can form an exclusive home range for each flock, with some small overlap.

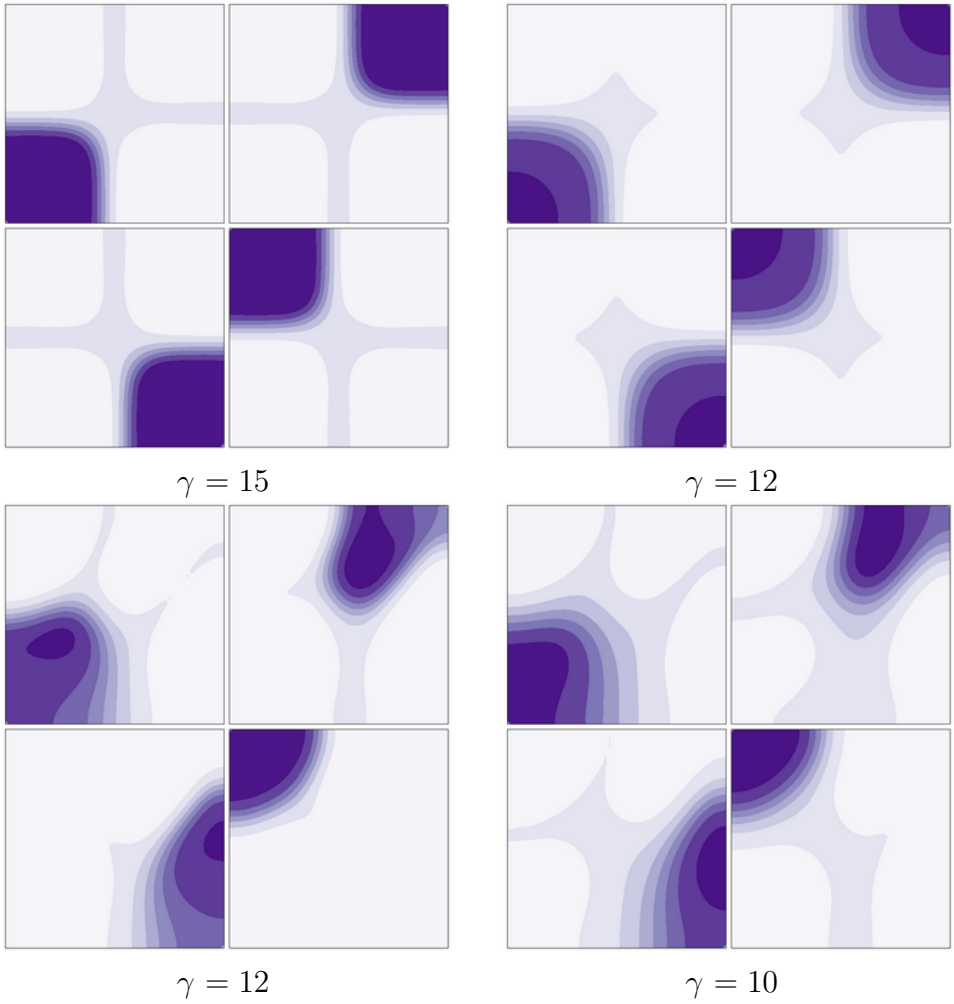

Fig. 2.7. Numerical solutions for $u_i^*(\mathbf{x})$ for the interaction system (2.13)-(2.16) for four flocks using the numerical details in Appendix A.4. Initial conditions in the top panel are Dirac delta functions which are symmetric about the vertical and horizontal lines though the middle of the domain. In the bottom panels the initial conditions are non-symmetric Dirac delta functions. The parameter values used are values are $a = 0.01$, $b = 10$, $\delta = 0.05$, $m = 0$ and $\kappa_{i,min} = 0.2$.

Parameter values which best fit the long-tailed tit study system will be found in Chapter 3, where I model space use with an extension of the interaction model.

2.5 Summary

Home range patterns of long-tailed tits in the Rivelin Valley consist of areas of exclusive space use. The purpose of this chapter was to find a mechanism to give rise to these patterns from underlying behaviours. I defined the mathematical groundwork to begin modelling the bird's home ranges using memory-mediated conspecific avoidance. I derived and analysed a two-dimensional diffusion-taxis model, the interaction model, to produce exclusive home ranges. This model uses a taxis mechanism to describe flocks of long-tailed tits avoiding locations where interactions between flocks have occurred in the past.

The extension of the interaction model into two-dimensions revealed greater numerical complications than the one-dimensional system defined by Potts and Lewis (2016a). Investigations using energy methods indicated that there is a surface of steady-state solutions and that it is possible the numerical system may shift continuously through numerical solutions close to the system's steady-states. I detailed a numerical scheme to stop the evolution of the interaction zone at a point where the change in the average value of k_i reaches a low threshold $\kappa_i(t) = \kappa_{i,min}$. The threshold represents the point in time where each flock of birds has approximately decided upon their interaction zone.

In this chapter I have explored the interaction system enough to be able to use it as an ecological model of space use for my study species. However, further

mathematical analyses are required to understand more about the behaviour of the system, without stopping the evolution of the interaction zone.

Fitting the steady-state pattern of a diffusion-taxis system, such as the interaction model to home range data is known as mechanistic home range analysis (MHRA). In previous studies, MHRA has predominantly been applied to territorial canids. This chapter shows that by extending the model of Potts and Lewis (2016a) into two spatial dimensions for multiple flocks, MHRA may be used to understand the home range formation further species, that do not have site fidelity or show territoriality. This is confirmed in the next chapter, where I show that by including a simple taxis mechanism to describe an attraction to the woodland habitat, MHRA can model home range patterns well.

Chapter 3

Mechanistic home range analyses of long-tailed tits

3.1 Introduction

Patterns of animal space use across habitats are often a combination of the home ranges of conspecifics and hetrospecifics (Bateman et al., 2015; Potts and Petrovskii, 2017). Several mechanisms have been revealed to be behind home range formation, such as the avoidance of predators (Bastille-Rousseau et al., 2015; Coleman and Hill, 2014), territorial interactions (Bateman et al., 2015; Giuggioli et al., 2011), optimising foraging (Mitchell and Powell, 2012; Moorter et al., 2009) and a site fidelity (Moorcroft and Lewis, 2006; Okubo, 1980). The ubiquity of home ranges in diverse taxa inspires the hypothesis that there are general mechanisms for the home range formation of animal species, which are yet to be uncovered (Börger et al., 2008).

Home ranges of non-breeding flocks of long-tailed tits form a complex arrangement of distinct areas and overlaps (Napper and Hatchwell 2016; Fig. 3.1). In the previous Chapter, I hypothesised that these partly-exclusive areas of space use are driven by flocks avoiding places they have previously interacted (via birdsong or sight) with other flocks, a behaviour suggested in Hatchwell et al. (2001a) and by observing the population. To describe this hypothesised behaviour, I introduced the interaction model: a model of a dynamic *cognitive map* describing the places where interactions have recently occurred, coupled with a taxis avoidance mechanism. Numerically solving the model gives rise to home range patterns (Fig. 2.7).

The interaction model provides a base model for understanding home range formation of flocks. In addition to interactions, there is a clear recognised effect of woodland habitat on the birds movement, that should be accounted for when modelling space use (Gaston 1973; Hatchwell 2016; Fig. 3.1). By including different descriptions of taxis towards the woodland habitat, I form multiple competing hypotheses that extend the interaction model (2.13)-(2.16) to form multiple different models.

As well as the effect of woodland, I also examine how the relative size of a flock (i.e. number of individuals) affects the extent to which it avoids neighbouring flocks. I hypothesise that smaller flocks will tend to have a stronger avoidance mechanism than larger flocks by assuming that smaller flocks would prefer to avoid potential conflict (Adams and Plowes, 2019; Dyble et al., 2019; Port et al., 2011). Furthermore, given that there is an apparent correlation between spatial proximity and relatedness (Hatchwell et al., 2001b; Napper and Hatchwell, 2016), I hypothesise that the relatedness of neighbouring flocks will be inversely related to the strength of the avoidance mechanism.

This study demonstrates the usefulness of mechanistic home range models for uncovering features of movement that cannot easily be detected using descriptive, statistical models. The results in this Chapter have been published in Ellison et al. (2020).

3.2 Long-tailed tits in the non-breeding season

The Rivelin Valley in Sheffield is an area composed of farmland and woodland, home to a population of long-tailed tits that has been studied for over 25 years (Hatchwell 2016, §1.3). In the non-breeding season (May-February) long-tailed tits in the Rivelin Valley live in flocks of 10-20 individuals (Gaston, 1973; Hatchwell, 2016) and their main life history goal is to forage for food. Individuals in the flock forage together and the majority of each flock usually consists of one or more fledged broods and their parents and helpers (Hatchwell, 2016). Typically, approximately 60-70% of a flock is related to at least one other member of the flock, where the coefficient of relatedness $r \geq 0.25$, meaning we consider only parents and siblings (Wright, 1922). However, birds often have relatives in other flocks as a result of dispersal after the breeding season. Flocks are not consistent between seasons and change due to mortality, dispersal and breeding events (Napper and Hatchwell, 2016). Furthermore, flock switches take place but are only common at the start of the non-breeding season (Napper and Hatchwell, 2016).

In this Chapter, I analyse data from the non-breeding seasons of 2010-13, which were first reported in (Napper and Hatchwell 2016 collected by Clare Napper), alongside data collected primarily for this study from the non-breeding season of 2018-19 (collected by Sarah Biddiscombe). The newer data contains

additional knowledge of kinship between flocks and the size of each flock. I focus on data in two different areas of the Rivelin Valley; the Fox Hagg and the Black Brook woodlands (visualised in Fig. 3.1). Data were collected in the Fox Hagg woodland of the Rivelin Valley for the 2011-12 season, in the Black Brook woodland for the 2010-11 and 2012-13 seasons and both woodlands for the 2018-19 season. Relatedness is determined by extracting DNA from blood samples collected from nestlings and adults. Field data were collected and blood samples analysed by Ben J Hatchwell, Clare Napper and Sarah Biddiscombe.

The average home range size for a single flock in this study is $0.15 \pm 0.03\text{km}^2$ (mean 95%±CI; using a 100% minimum convex polygon). Home ranges were initially calculated as minimum convex polygons to gain a rough estimate of space use for describing initial space use when modelling. As the flocks forage, they usually stay in each tree for less than a minute before moving on (B. J. Hatchwell, pers. obs.). Consequently, tracking data of the birds consists of GPS locations, recorded at time intervals of one minute. Locations were recorded on a Garmin Geko 201 GPS with a standard error of 10m. Observations were made by locating a flock in the study site by recognising their calls and then identifying ringed individuals.

An observation period began when a flock was first encountered and the first location was recorded. The observation period ended when sight of the flock was lost. One location was recorded every minute to give a trajectory for each observation period. There were 19 ± 2 (mean ±95% CI) locations per observation period. Data from six of eight flocks that were followed in the non-breeding season of 2011-12 in the Fox Hagg woodland are included in this study. I removed two flocks from the analysis of the 2011-12 season as these

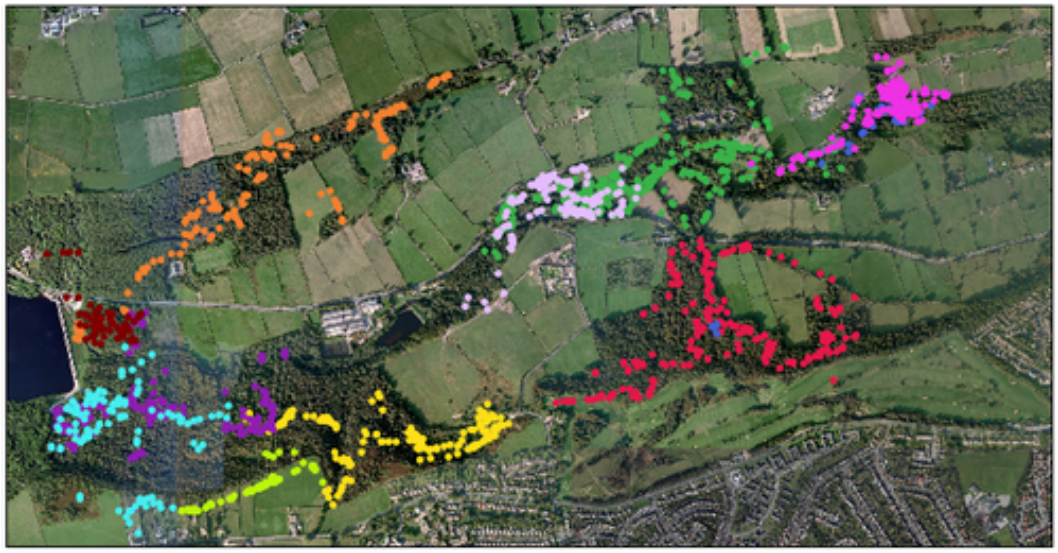

Fig. 3.1. Recorded locations for 11 flocks of long-tailed tits in the 2018-19 non breeding season, each color represents a different flock. The overlapping home ranges are generally split into the two separate woodlands of Fox Hagg (left) and Black Brook (right) in all recorded data sets.

contained only 4 and 7 locations, collected over one observation period, so this was not enough data to estimate home ranges. Data sets for the six remaining flocks consisted of 155, 341, 140, 110, 152 and 83 locations, recorded over a range of 5-21 observation periods between May 2011 and February 2012. In addition to the 2011-12 data, the results are validated using data from the 2010-11, 2012-13 and 2018-19 data sets. For the validation sets I followed a similar procedure to remove from the analysis any flocks that had data collected over only one observation period. In each case, there were at most 18 locations per flock in the removed datasets. Each flock used has >40 recorded locations taken over >1 observation periods. The 11 flocks used in the non-breeding season of 2018-19 are shown in Fig. 3.1, for both the Fox Hagg and Black Brook woodlands.

3.2.1 Testing for effects of kinship and the size of the flock

In the 2018-19 data, the individual birds which each flock was comprised of were observed and recorded. Using this information the size of the flocks can be estimated, additionally the identity of close kin (parents, offspring and siblings) is known for 108 of the 192 birds. Table 3.1 shows the size of each flock and the number of kin-connections between them, for five flocks.

Table 3.1. The number of kin-connections between flocks (A-E) and the size of flocks for the second data set in 2018-19 shown in the bottom panels of Fig. 3.6. There is a kin connection if two birds are related by either being siblings, parents or offspring. The size of the flocks is the number of birds in a flock, if a bird has been seen in different flocks it is given a value of 0.5 in both (no birds here were seen in more than two of the flocks).

Kin-connections	A	B	C	D	E
A	-	11	7	0	1
B	11	-	6	0	1
C	7	6	-	2	4
D	0	0	2	-	1
E	1	1	4	1	-
Size of Flock	29.5	39.5	12	9.5	8.5

Prior to modelling the space use of the flocks using mechanistic home range analysis (MHRA), I perform some preliminary analyses. I show that questions of space use dependent on kinship and flock size for the data in this study are unable to be answered using a commonly-used method to estimate home ranges (Worton, 1989), known as kernel density estimation (KDE). Estimating home ranges using KDE assumes that space use is normally distributed around each

known location of a flock. Home ranges are then estimated by taking the sum of the normal distributions, so the resulting space use description does not have any behavioural origins. I focus on the second data set from the season 2018-19, with kinship and flock size shown in Table 3.1. The Python 3.4 function `gaussian_kde` from the `scipy.stats.kde` library is used to calculate the KDEs and this implements automatic bandwidth determination using Scott's Rule (Scott, 1992). The Bhattacharyya coefficient (Bhattacharyya, 1946) is used to represent the overlap of two flocks' home ranges and is calculated as follows:

$$BC_{ij} = \int_{\Omega} \sqrt{U_i(\mathbf{x})U_j(\mathbf{x})}\mathrm{d}\mathbf{x}, \tag{3.1}$$

where $U_i(\mathbf{x})$ and $U_j(\mathbf{x})$ are utilisation distributions for flocks i and flock j estimated using KDE and Ω is the available domain. The relationship between two home ranges is further represented by calculating the distance between the centroids of the two ranges d_{ij}. Kinship is tested using both the number of connections between flock i and flock j and also by correcting for the size of the flock. The corrected kin relatedness is calculated as $\kappa_c = \frac{2\kappa_{ij}}{s_i+s_j}$, where s_i is the number of birds in flock i. Fig. 3.2 and Table 3.2 show the results.

The results show that there is no evidence of any correlation between the overlap of the KDE home ranges of two flocks (nor the distance, d_{ij}, between the home ranges) and the relative size of the flocks (using two different measures of size, κ_{ij} or κ^c_{ij}). Since all the R^2 values were less than 0.06 and all p-values are greater than 0.5, there is insufficient evidence to suggest that either kin relatedness or relative flock size explain much of the variation in home range overlap. Instead I test these effects using MHRA, detailed in the next section.

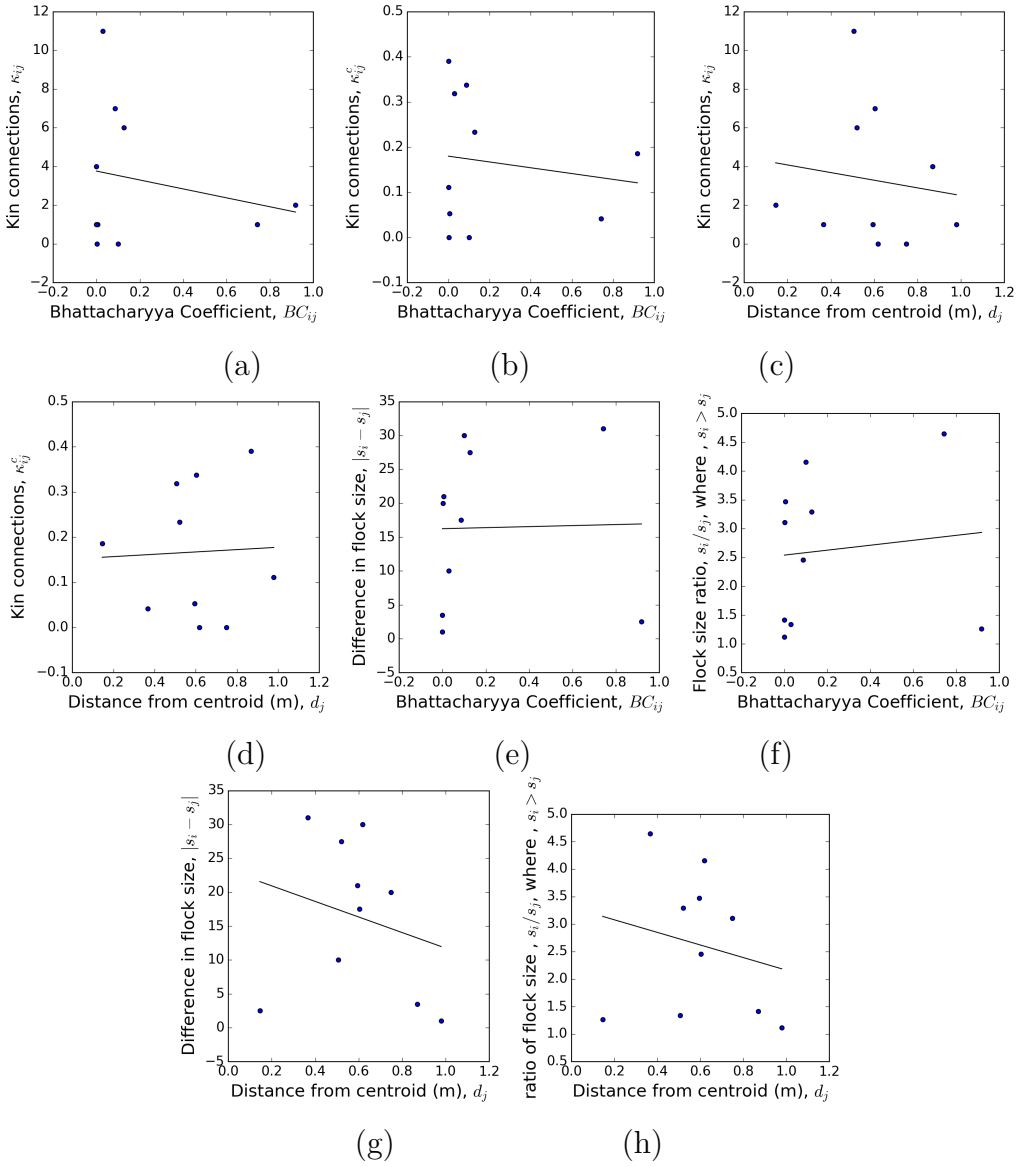

Fig. 3.2. Scatter plots to show the correlation between KDE home ranges of each flock and the kin relatedness and size difference of each flock. Regression lines are plotted and the corresponding correlation coefficients are shown in Table 3.2.

Table 3.2. Relationships between the overlap of home ranges of each flock compared with the kin relatedness and relative size difference in turn where R^2 is Pearson's Correlation Coefficient. The overlaps are measured in two ways after estimating the home ranges using KDEs (1) by Bhattacharyya's coefficient BC_{ij} and (2) using the distance between central point of the home range d_{ij}. The two measures of overlap are compared separately with the amount of kin connections κ_{ij} and also those corrected for the size of the flock κ^c_{ij}. The relative size difference of each flock was also measured by $|s_i - s_j|$ and s_i/s_j, where s_i is the number of birds in flock i.

	Measure 1	Measure 2	R^2	p-value
(a)	BC_{ij}	κ_{ij}	0.045	0.56
(b)	BC_{ij}	κ^c_{ij}	0.022	0.68
(c)	d_{ij}	κ_{ij}	0.017	0.72
(d)	d_{ij}	κ^c_{ij}	0.0018	0.91
(e)	BC_{ij}	$\lvert s_i - s_j \rvert$	0.0005	0.95
(f)	BC_{ij}	s_i/s_j, $s_i > s_j$	0.013	0.76
(g)	d_{ij}	$\lvert s_i - s_j \rvert$	0.057	0.51
(h)	d_{ij}	s_i/s_j, $s_i > s_j$	0.045	0.56

3.3 The interaction model with habitat

Woodland structure is complex in the Rivelin Valley, encompassing dozens of species of trees and shrubs of varying sizes. I simplify the landscape by viewing woodland as a binary variable: either present or absent. A more detailed picture of the woodland environment is explored in Chapter 4 where movement in response to different types of tree is investigated. In this section, I detail different models to describe this more simple attraction to woodland by defining different vector fields.

3.3.1 An attraction towards woodland areas

To define the woodland, the landscape is discretised into a grid and any cell with more than half tree coverage is defined to be in a woodland area. Each woodland area is defined visually using a procedure detailed in Appendix

B.1. Attraction to woodland areas is introduced into the interaction model by defining a vector field $\mathbf{v}_M(\mathbf{x})$, where different models describing different behaviours are indicated by M. Each of the vector fields can be visualised in Fig. 3.3 for the Fox Hagg and Black Brook woodlands. Corresponding descriptions of the vector fields are defined here

$M = 0$, no attraction to woodland,

$M = 1$, taxis acts solely on the woodland edges, to draw flocks in (Fig. 3.3b),

$M = 2$, taxis acts both on the edges and within the woodland to draw flocks towards the centre of a woodland area (Fig. 3.3c),

$M = 3$, taxis acts on the woodland edges and all space outside of the woodland areas to draw the flocks towards the woodland (Fig. 3.3d),

$M = 4$, inside the woodland the flocks are drawn towards the centre of the woodland area and outside they are drawn in (Fig. 3.3e),

$M = 5$, no taxis mechanism away from the interaction zone and $\mathbf{v}_M(\mathbf{x})$ corresponds to the best fitting model from Models 0-4.

Attraction to the central parts of woodland areas is defined using a function of the distance to the edge of the woodland are, where locations at a greater distance are more attractive. The mathematical form for the vector fields corresponding to each of these models on the discrete landscape is defined in Appendix B.1. Each $\mathbf{v}_M(\mathbf{x}|\omega_M)$ depends upon a parameter ω_M, which controls how much the birds are attracted to woodland. The model that includes both

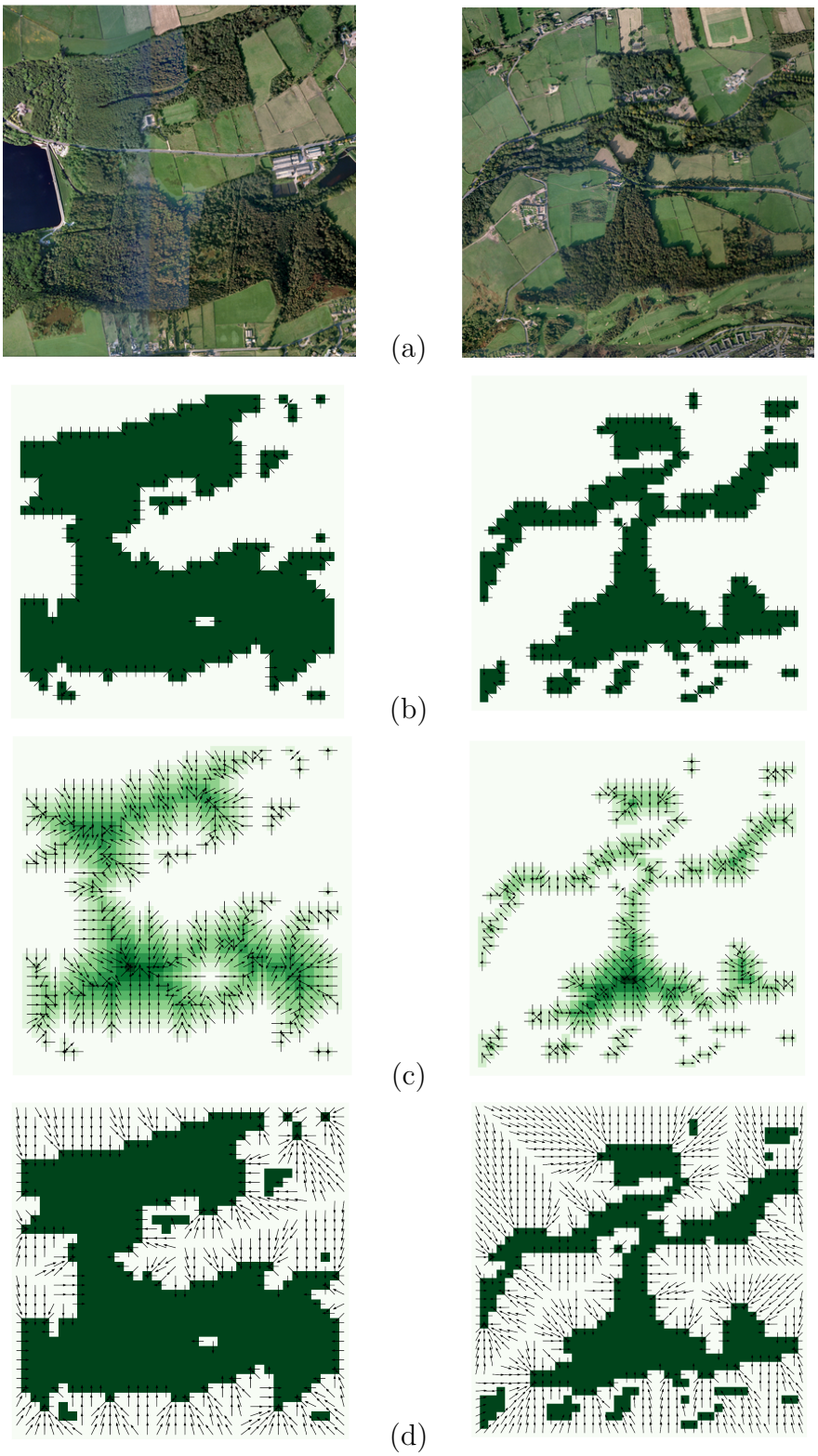

Fig. 3.3

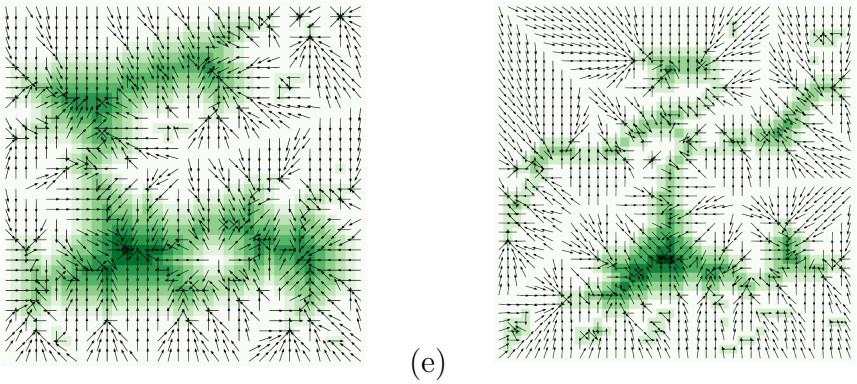

(e)

Fig. 3.3. Panel (a) shows the real landscape taken from satellite images for the Fox Hagg (left) and Black Brook (right) woodlands, which are the study sites for the data sets 2011-12 and 2012-13 respectively. Panels (b)-(e) show the vector fields $\mathbf{v}_M$ for the Models 1-4 respectively, corresponding to the woodland images (a) on their respective row. Each of these models represents an attraction into a woodland area, following the vector fields.

inter-flock interactions and response to woodland has the following form

$$\frac{\partial u_i}{\partial t} = \nabla^2 u_i + \nabla \cdot \left[\gamma u_i \nabla \bar{k}_i - \zeta u_i \mathbf{v}_M\right], \tag{3.2}$$

$$a\frac{\partial k_i}{\partial t} = u_i \Sigma_{i \neq j} u_j (1 - k_i) - b k_i u_i, \tag{3.3}$$

$$\left|\mathbf{n} \cdot \left[\nabla u_i + \gamma u_i \nabla \bar{k}_i - \zeta u_i \mathbf{v}_M\right]\right|_{\partial\Omega} = 0, \tag{3.4}$$

$$\int_\Omega u_i \, \mathrm{d}\mathbf{x} = 1, \tag{3.5}$$

where ζ controls the strength of taxis along the vector field $\mathbf{v}_M$. The system (3.2)-(3.5) is solved using the same finite difference methods as Chapter 2 (Appendix B.2). Note that I have simplified the cognitive map of interactions for each flock by setting $m = 0$ (Equation 2.14) so that there is no decay of the interaction zone over time. Therefore the interaction zone decays only due to each flock visiting locations and no interactions occurring.

The system is solved numerically and the numerical scheme (Appendix B.2) defines space and time discretely. The initial conditions used to solve System (3.2)-(3.5) numerically define uniform space use over estimated home ranges using minimum convex polygons (MCPs) with the overlaps removed. The discrete form of the initial conditions for the 2011-12 data set is shown in Fig. 3.4(a) with the data show in Fig. 3.4(d).

For the interaction model to reach a *steady-state*, it is necessary to stop the evolution of the *interaction zone* at a particular threshold value of the average value of $k_i(\mathbf{x}, t)$ for all $\mathbf{x}$, calculated as $\kappa_i(t)$, shown in Equation (2.40). Using the described initial conditions with parameters $a = 0.01$, $b = 10$, $\delta = 0.05$, $\gamma = 10$, $\omega_M = 1$ and $\zeta = 10$, I tested a range of threshold values for $\kappa_i(t)$. The testing process was as follows: for each candidate threshold value the difference between time t for $\kappa_i(t)$ of the first flock to reach the threshold value and t for the last flock to reach the threshold value was calculated. I chose the threshold value which gave the smallest difference in t, so the evolution of the interaction zone is stopped at the first point in time when $\kappa_i(t) \leq 0.2$ for all i.

3.3.2 Fitting models to data

Models are fitted by maximising the likelihood function

$$L(b, \gamma, \delta, \zeta, \omega_M | X) = \prod_{i=1}^{N} \prod_{n=1}^{N_i} u_i^*(\mathbf{x}_{i,n}), \tag{3.6}$$

where $\mathbf{x}_{i,n}$ is the nth location of flock i, $X = \{\mathbf{x}_{i,n}\}_{i,n}$ is the set of all locations, u_i^* is the numerical steady-state solution of u_i, N is the number of flocks and N_i is the number of locations in the data set for flock i. I use model selection to find the best-fit model of $M = 0, \ldots, 5$. The Nelder-Mead maximisation

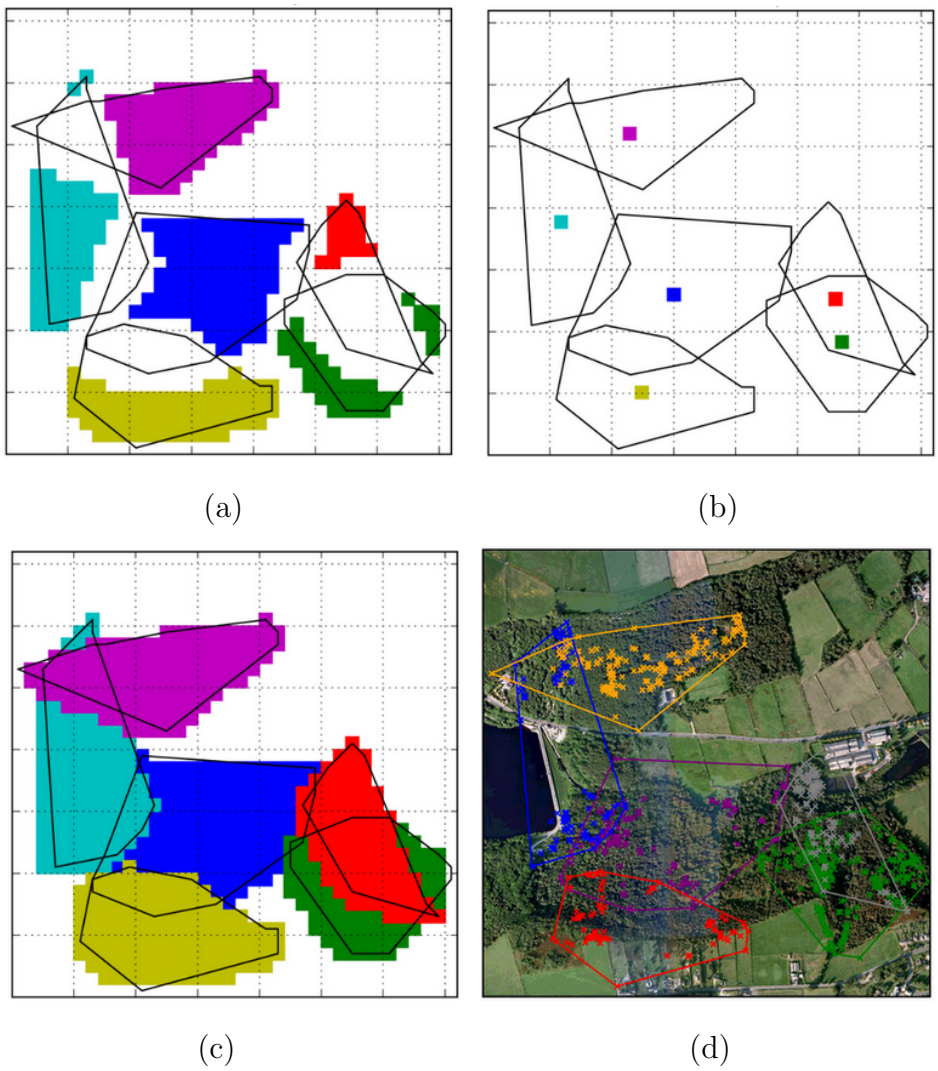

Fig. 3.4. Panels (a)-(c) show three different types of initial conditions with the minimum convex polygons plotted over. Panel (d) shows the data for the 2011-12 data set with minimum convex polygons plotted over.

algorithm (Nelder and Mead, 1965) is used to maximise Equation (3.6) and the best model is selected based on bayesian information criterion (BIC) scores (Schwarz, 1978), a commonly used measure of model fit that penalises models with greater parameters. The BIC is calculated as

$$\mathrm{BIC} = k \ln \left(\sum_{i=1}^{N} N_i \right) - 2 \ln (L) , \tag{3.7}$$

where k is the number of parameters, L is the likelihood and N_i is the number of locations for flock i. Two models, M_1 and M_2, can be compared using the Bayes Factor

$$\mathrm{BF}(M_1, M_2) = \exp \left(-\frac{1}{2} \left| \mathrm{BIC}_{M_1} - \mathrm{BIC}_{M_2} \right| \right) , \tag{3.8}$$

where a Bayes factor of more than 10 gives strong evidence for the better fitting model over the other (Kass and Raftery, 1995).

Measurements of flock locations are taken at one minute intervals, However, the likelihood function in Equation (3.6) requires that data are independent relocations. In general, it is not possible to determine independence with absolute certainty, as no matter how large the time interval, the relocation of a flock will depend their locomotive capabilities and the environment. However, it is possible to perform a statistical test of locational independence by calculating the serial correlation in location (Benhamou et al., 2014) as

$$r_{\mathbf{z}} = 1 - \frac{E(D_s^2)}{2E(D_c^2)}, \tag{3.9}$$

where $E(D_s^2)$ is the mean distance squared between successive relocations in time interval τ and $E(D_c^2)$ is the mean distance between the locations and their centroid. Obtaining a $r_{\mathbf{z}}$ value close to 1 indicates that the distances between locations are very small compared to the home range size. A value of $r_{\mathbf{z}} < 0.5$ indicates that, on average, the distance between relocations is greater than the distance to the home range centre, suggesting that relocations show locational independence. I calculate $r_{\mathbf{z}}$ for four different data sets, each corresponding to a different time interval between relocations, τ. The four data sets are S_1, S_{10}, S_{30} and S_{day} corresponding to data sampled every 1 minute, 10 minutes, 30 minutes and one data point sampled each day.

It is necessary to check that the choice of initial conditions does not affect the results. In addition to the initial conditions shown in Fig. 3.4(a), I repeat the model selection for the 2011-12 dataset using two other initial conditions for the Models 1-4, first with the initial space use for each flock concentrated at the centre of their corresponding MCPs, (Fig. 3.4b) and another where the initial space use for each flock was uniformly distributed over their MCP (Fig. 3.4c).

3.4 Further drivers of space use patterns

3.4.1 The effect of the landscape on kinesis

Both the woodland and the interaction zone may have an effect on kinesis (i.e. the diffusion coefficient in Equation 1.1) as well as the taxis mechanism. To test this I use the following model

$$\frac{\partial u_i}{\partial t} = \nabla^2 \left[\Phi_i u_i\right] + \nabla \cdot \left[\gamma u_i \nabla \bar{k}_i - \zeta u_i \mathbf{v}_M\right], \tag{3.10}$$

where $\Phi_i(\mathbf{x}, t)$ is a function of space, and depends upon the presence of woodland and/or the interaction zone. The vector field $\mathbf{v}_M(\mathbf{x})$ is the function from the best-fit model out of Models 0-5. I use the following three functional forms for Φ_i

$$\Phi_i^{(1)}(\mathbf{x}) = \exp(\mu w(\mathbf{x})), \tag{3.11}$$

$$\Phi_i^{(2)}(\mathbf{x}, t) = \exp(\psi \bar{k}_i(\mathbf{x}, t)), \tag{3.12}$$

$$\Phi_i^{(3)}(\mathbf{x}, t) = \exp(\mu w(\mathbf{x}) + \psi \bar{k}_i(\mathbf{x}, t)), \tag{3.13}$$

where $w(\mathbf{x})$ is the density value of the woodland. The value of $w(\mathbf{x})$ depends on whether the best-fit taxis model includes taxis towards the centre of woodland. Without this central attraction, when extending Model 1 or 3 to incorporate (3.11)-(3.13), $w(x) = 1$ for x in woodland and $w(x) = 0$ for x outside woodland. When the extending a model including attraction towards the centre of woodland (Model 2 or 4), $w(x) = S(\mathbf{x})^{\omega_M}$ for x in woodland, where $S(x)$ is the distance from x to the woodland edge, and $w(x) = 0$ outside woodland. Here, Equation (3.11) models a situation where the presence of woodland alone has an effect on kinesis. In Equation (3.12), only the interaction zone has an effect on kinesis. Equation (3.13) incorporates both effects. I investigate this effect on kinesis both with and without the taxis term in Equation (3.10). For simplicity in reporting results, when the functions (3.11)-(3.13) are included in the best-fit taxis model, I denote these extended models as Models 6-8 respectively. Alternatively, when the functions (3.11)-(3.13) are included in

Equation (3.10) with the second term equal to zero, the models are denoted as Models 9-11 respectively.

3.4.2 The effect of kinship and flock size

The extended interaction model (3.2)-(3.5) assumes that each flock of birds is equally worth avoiding, where in reality this avoidance may depend on the relationship of two flocks. I use the best-fit model from Models 0-11 as a null model to answer further biological questions by varying the amount of avoidance depending on the relationship between two flocks. This model is used to test effects on movement of (a) relative flock size and (b) inter-flock relatedness. The null model is modified by assuming that the interaction zone of each flock develops at a different rate for interactions with each of the other flocks, dependent on either its kin-connections or relative size. Including these dependencies, Equation (3.3) is changed to

$$a\frac{\partial k_i}{\partial t} = u_i \Sigma_{i \neq j} \alpha_{ij} u_j (1 - k_i) - b k_i u_i, \tag{3.14}$$

where the various α_{ij} take different values depending on the kin-connections between two flocks or their relative flock size (in §3.3.1-3.4.1, $\alpha_{ij} = 1$ for all flocks i and j). A larger α_{ij} means that flock i is less likely to visit places that it has previously interacted with flock j than if it were to have a smaller α_{ij}. I set α_{ij} to be a function of either the relative size of flock j compared to flock i and/or the number of kin-connections between i and j, denoted κ_{ij}. For this,

there are three functional forms

$$\alpha_{ij}^{(1)} = 1 + \sigma_1 \frac{s_j}{s_i}, \tag{3.15}$$

$$\alpha_{ij}^{(2)} = \frac{\sigma_2}{\kappa_{ij}^{\sigma_3}}, \tag{3.16}$$

$$\alpha_{ij}^{(3)} = \alpha_{ij}^{(1)} \alpha_{ij}^{(2)}, \tag{3.17}$$

where s_i (resp. s_j) is the size of flock i (resp. j).

Equation (3.15) tests the hypothesis that a flock is less likely to consider a location safe if they have observed it being used by a larger flock, than if the same location were observed being used by a smaller flock. A higher value for $\alpha_{ij}^{(1)}$ is obtained when $s_j > s_i$ than when $s_j < s_i$, meaning the probability that a location will be considered to be in the interaction zone of flock i will be higher if flock j is larger. Equation (3.16) means a flock would be less likely to consider a location part of its interaction zone if it had observed a highly related flock there than if it had observed a less related flock in the same location. The function $\alpha_{ij}^{(2)}$ is smaller if there are more kin connections between flock i and j. Equation (3.17) combines the two hypotheses. The parameters σ_1, σ_2 and σ_3 are fit using the functions (3.15)-(3.17). BIC (Equation 3.7), is used both to select between the three models and examine whether they are an improvement on the null model ($\alpha_{ij} = 1$ for all i, j).

3.5 Results of the mechanistic home range analysis

3.5.1 An attraction to the woodland

Analyses of the 2011-12 season indicate that two aspects of movement- a flock's response to the habitat and conspecifics- combine to give the key ingredients in the formation of long-tailed tit home ranges. A combination of both the interaction mechanism and an attraction towards central woodland models the home ranges best (shown in Fig. 3.5a), and the particular best-fit model is Model 4 (Fig. 3.5b). This contrasts with the relatively poor fit of the base models that included inter-flock interactions only (Model 0; Fig. 3.5c) and with attraction to woodland only (Model 5; Fig. 3.5d), which can be considered as null models for the purpose of illustrating the value of Model 4 in capturing the home range patterns.

Similar findings hold across the four other non-breeding seasons and different parts of the study site (Fig. 3.6), where best-fit models reveal that flocks are always being drawn to the centre of the woodland. For three of the other data sets (2010-11, 2018-19$_1$, 2018-19$_2$), the best fitting model is confirmed to be Model 4, and for one (2012-13) it is Model 2 (Table 3.3). These models are the only two which describe movement towards the centre of woodland (Fig. 3.3). The data sets and their corresponding utilisation distributions are shown in Fig. 3.6 and in Appendix B.4.

Some variation in the parameters is notable in Table 3.3, in particular the parameter controlling the decrease of the interaction zone due to safe visits b (1.14-13.3), where the outlier is the 2010-11 season ($b = 1.14$). This is likely

to do with the smaller number of flocks analysed in this season compared to others. The first term in Equation (2.14) is a sum that increases with the number of flocks. Therefore one might expect the parameter b to increase with the number of flocks, providing a part explanation for this inconsistency. There is a smaller amount of variation between seasons for γ (7.7-10) which controls the taxis away from the interaction zone, ζ (12.9-25.9) which controls the taxis towards central woodland and δ (0.047-0.096) which is the flocks' *perceptual range*. The mean value of δ, when converted into metres is approximately 80m, so the models suggest that the birds are, on average, considering an area with a radius of 80m around their present location when making movement decisions. By considering the mean squared displacement of the data (Appendix B.3) I find that on average the birds take around 10 days to form their interaction zone.

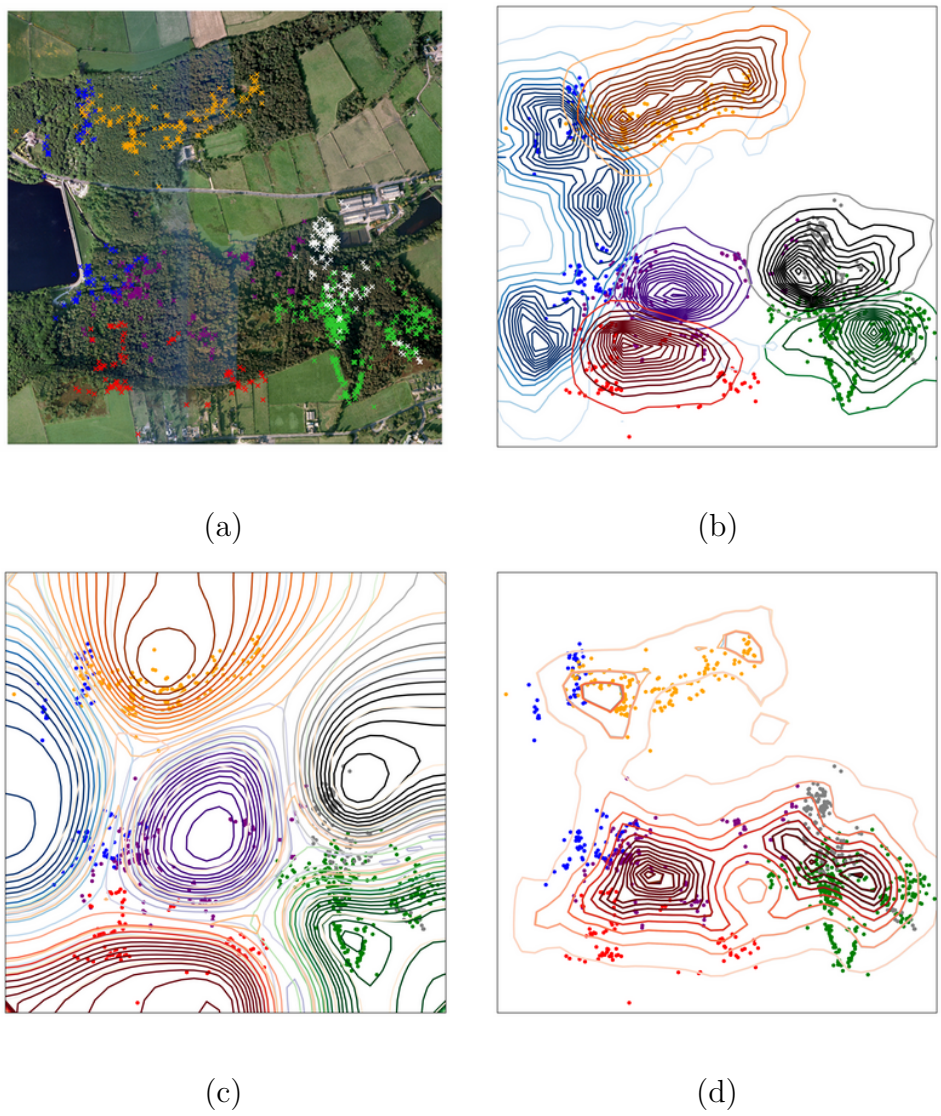

Fig. 3.5. Utilisation distributions informed by fitting the steady-state of Equations (3.2)-(3.5) to data from the non-breeding season of 2011-12. Flock locations are shown on top of a photograph of the landscape in panel (a) where each color represents a different flock. Panels (b)-(d) show the steady-state solution of Equations (3.2)-(3.5) together with observed locations (dots), here darker contour lines mean a higher probability density. Panel (b) shows the corresponding utilisation distribution for the best-fit model (Model 4). Panel (c) shows the the utilisation distribution for Model 0, where there is no attraction to woodland. Panel (d) shows the utilisation distribution for Model 5, where there is no directed movement away from other flocks. Here the contour lines coincide since there are no interactions. Both movement in response to the environment and in response to other flocks are necessary to create home range patterns which capture the data well.

Table 3.3. Best fitting models, their parameter values and their bayesian information criterion (BIC) scores for all of the data sets. The BIC values from each data set can be compared with the other models which were tested by using the last column in the table. The subscripts on the 2018-19 data sets refer to the two data sets collected that season. The parameter a is not reported as its value does not affect the steady-state distribution $u_i^*(\mathbf{x})$. The ΔBIC is calculated from next best fitting model for each data set.

Data set	Best-fit Model	Number of flocks	b	γ	δ	ζ	ω_M	BIC	ΔBIC
2010-11	4	4	1.14	8.0	0.054	12.9	2.1	3411	227
2011-12	4	6	13.3	9.6	0.072	18.1	0.51	11089	29
2012-13	2	4	2.9	10.0	0.074	19.9	0.74	6399	258
2018-19$_1$	4	6	9.2	9.7	0.096	23.5	0.64	10905	151
2018-19$_2$	4	5	11.7	7.7	0.047	25.9	1.1	14297	283

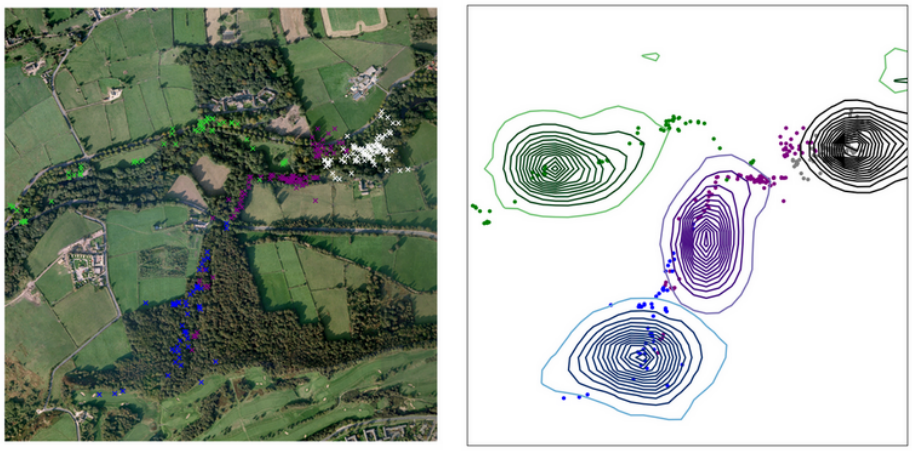

2010-11

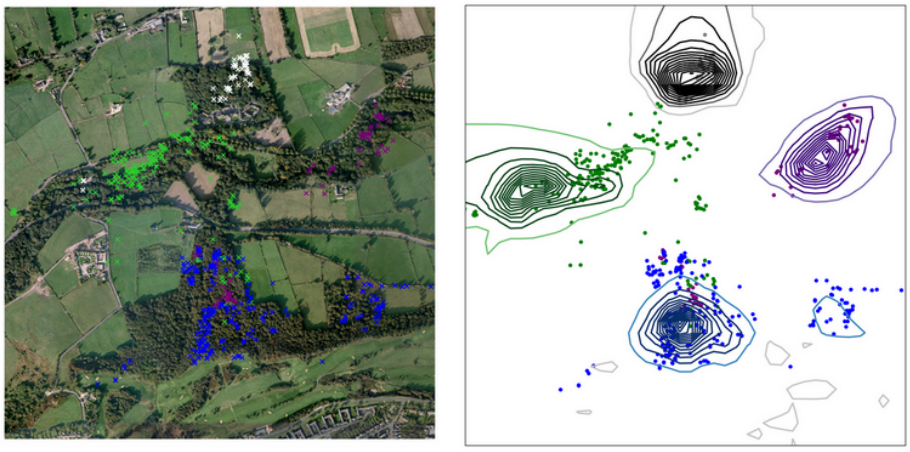

2012-13

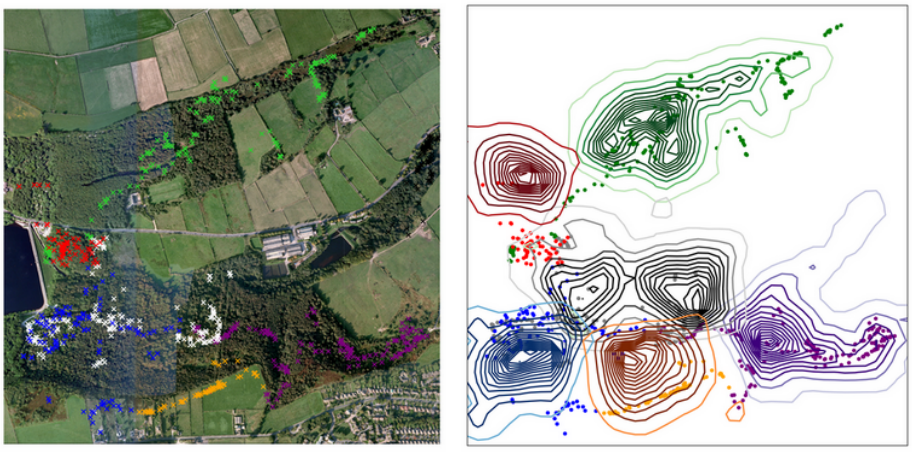

2018-19$_1$

Fig. 3.6

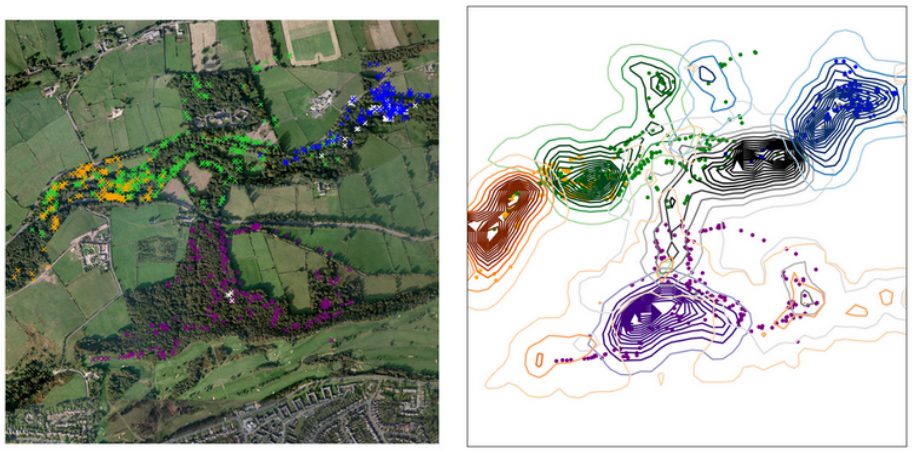

2018-19$_2$

Fig. 3.6. Results for the best-fit model for the seasons 2010-11, 2012-13 and 2018-19 with the corresponding utilisation distributions for the best fitting models shown. Model 4 is the best fitting model from all data sets apart from 2012-13 which gives Model 2. Models 2 and 4 are the only models that direct movement into woodland and away from the woodland edges.

3.5.2 Effect of the Initial Conditions

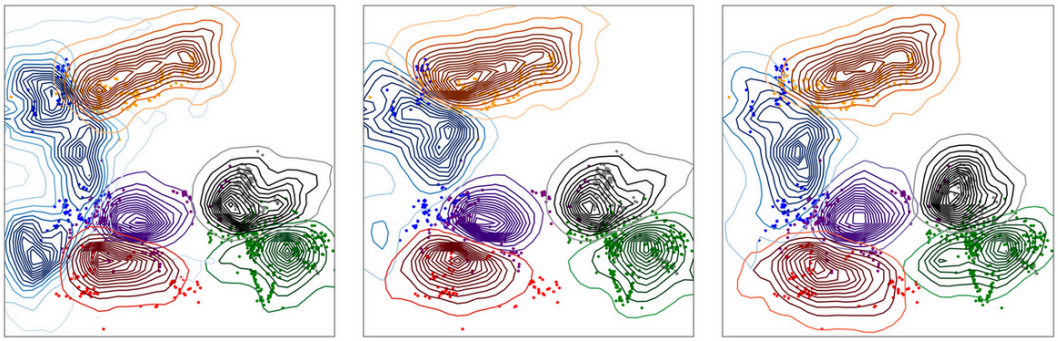

(a) (b) (c)

Fig. 3.7. The utilisation distributions for Model 4 for initial conditions (a)-(c) (Fig. 3.4) are shown below. Panel (a) shows the initial conditions used in all other sections. Panel (b) shows the solution where space use is initially concentrated at the centre of the MCP for each flock. Lastly, Panel (c) shows the solution where initial space for each flock use uniformly covering the whole of the corresponding MCP.

All initial conditions tested (Fig. 3.4) for the 2011-12 data (Models 1-4) indicate Model 4 to be the best-fit model, shown in Table 3.4 and visualised in Fig. 3.7. This indicates that the results of model selection appear to be robust to reasonable choice of initial condition.

Table 3.4. The results for fitting Models 1-4 for the data set collected in 2011-12 using initial conditions (a)-(c) visualised in Fig. 3.4. Model 4 is the best fitting model in all cases.

	BIC		
Model	(a)	(b)	(c)
1	11859	11833	12135
2	11118	11473	11047
3	11790	11836	11843
4	**11089**	**11436**	**10978**

3.5.3 The independence of data

The value of $r_{\mathbf{z}}$ (Equation 3.9) for seasons 2011-18 and data sets S_1, S_{10}, S_{30} and S_{day} is shown in Table 3.5. The results indicate that data used in the study (S_1) and those sampled every 10 minutes (S_{10}) are highly locationally correlated. The locational correlation for sub-sampling data every 30 minutes (S_{30}) varies across years and sub-sampling each day (S_{day}) shows little locational correlation, which indicates independence.

Table 3.5. The results of calculating $r_{\mathbf{z}}$ using Equation (3.9) to indicate locational independence in the full data and sub-samples. Values close to 1 indicate that the distances between locations are very small relative to the home range size and values close to 0 indicate locational independence. The results show that only locations sampled each day indicate a consistent lack of independence over seasons.

	S_1		S_{10}		S_{30}		S_{day}	
Year	locations	$r_{\mathbf{z}}$	locations	$r_{\mathbf{z}}$	locations	$r_{\mathbf{z}}$	locations	$r_{\mathbf{z}}$
2010-11	219	0.96	45	0.76	29	0.55	27	-0.21
2011-12	666	0.96	127	0.77	66	0.83	59	0.04
2012-13	381	0.97	69	0.86	38	0.09	34	0.35
$2018\text{-}19_1$	486	0.99	99	0.81	47	0.48	32	0.06
$2018\text{-}19_2$	750	0.98	130	0.61	62	0.16	44	-0.22

Given the evidence of a lack of locational independence in the full data set, I test whether the key results of the study are robust to the data sub-sampled each day. To test this I fit the S_{day} data for each of the 2010-13 seasons to Models 1-4 to understand how this sub-sampling affects the model selection. Table 3.6 shows that the model selection procedure returns the same best-fit models for the 2010-11 and 2012-13 seasons, regardless of sub-sampling regime. Furthermore, the models are visually relatively similar (Fig. 3.8b-c) to those using the full data set (Fig. 3.8a), but the latter gives a slightly tighter fit. The refined data set for 2011-12 indicates that Model 2 is the best fit and the full data set indicates Model 4. However, both models describe an attraction towards the centre of the woodland, so are biologically similar, and the difference in BIC (ΔBIC=10.9) is not dramatic. Therefore it is reasonable to use the complete data sets when fitting models to ensure I utilise the full known space use of the birds, despite violating the independence assumption.

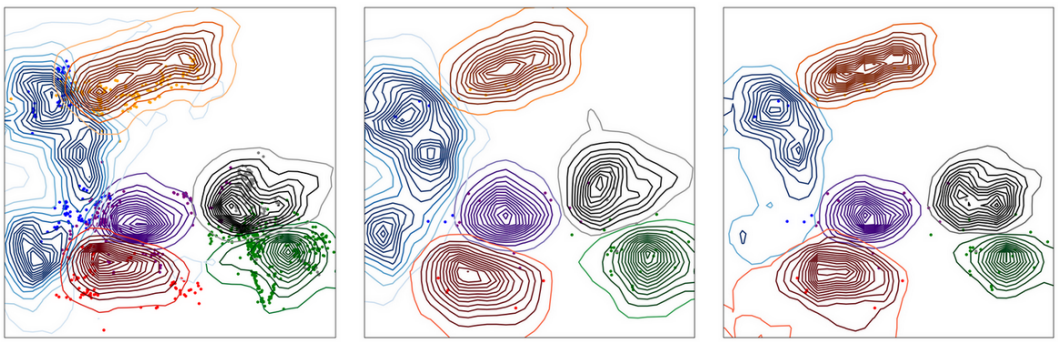

(a) (b) (c)

Fig. 3.8. Utilisation distributions for the full data set and data sampled each day for the season 2011-12. Panel (a) shows the results of using the full data set with best fitting Model 4 with all locations. Panel (b) shows the results of fitting Model 4 to the daily sub-sampled data and Panel (c) shows the best fitting Model 2 for the sampled data with the sub-sampled locations. Model 2 and Model 4 both contain the mechanisms describing a preference to forage in the centre of woodland.

Table 3.6. Results for model selection for the seasons 2010-11, 2011-12 and 2012-13 for the full data set and the data set with one location sampled per day. The model selection procedure indicates Models 2 and 4 (preference towards the centre of woodland) regardless of sampling regime.

	BIC					
	2010-11		2011-12		2012-13	
Model	All data	One per day	All data	One per day	All data	One per day
1	3666	332.5	11859	704.2	6746	455.3
2	3643	338.4	11118	**667.6**	**6399**	**442.1**
3	3638	343.6	11790	709.5	7079	464.2
4	**3411**	**317.5**	**11089**	678.5	6657	**442.1**

3.5.4 The effect on kinesis

When considering the effect of a landscape-varying kinesis mechanism on the space use of the flocks, there is no improvement in the model fit. Including the effect of landscape on kinesis into the best-fit models (Models 6-8 in Table 3.7;

Table 3.7. Results for including landscape-varying kinesis in the best fitting model of Models 0-5, for data collected in the three seasons between 2010-13. Models 6-8 include the functions (3.11)-(3.13) in the Main Text, respectively, with taxis. Models 9-11 use the same functions, respectively, but without taxis. The table reports BIC results for the three data sets and The ΔBIC column gives the difference with the best fitting taxis model for that data set. This shows that including kinesis does not improve the previous best fit models and without taxis they are a poor fit.

	Model	BIC	ΔBIC	Model	BIC	ΔBIC
2010	6	3415	4	9	4030	619
	7	3415	4	10	4238	827
	8	3416	5	11	3925	514
2011	6	11096	7	9	13428	2338
	7	11095	6	10	13765	2675
	8	11103	14	11	13309	2220
2012	6	6397	2	9	7550	1151
	7	6400	1	10	7616	1217
	8	6400	1	11	6706	307

Fig. 3.9) from the study gives larger BIC values than the models without such a kinesis effect. Furthermore, when fitting models where landscape only affects kinesis (Models 9-11 in Table 3.7; Fig. 3.9) and not taxis, the fit is very poor compared with models with landscape-driven taxis. These results show that including kinesis in the best fit taxis models do not improve them and without taxis, modelling behaviours as effecting only kinesis is a poor fit for each data set.

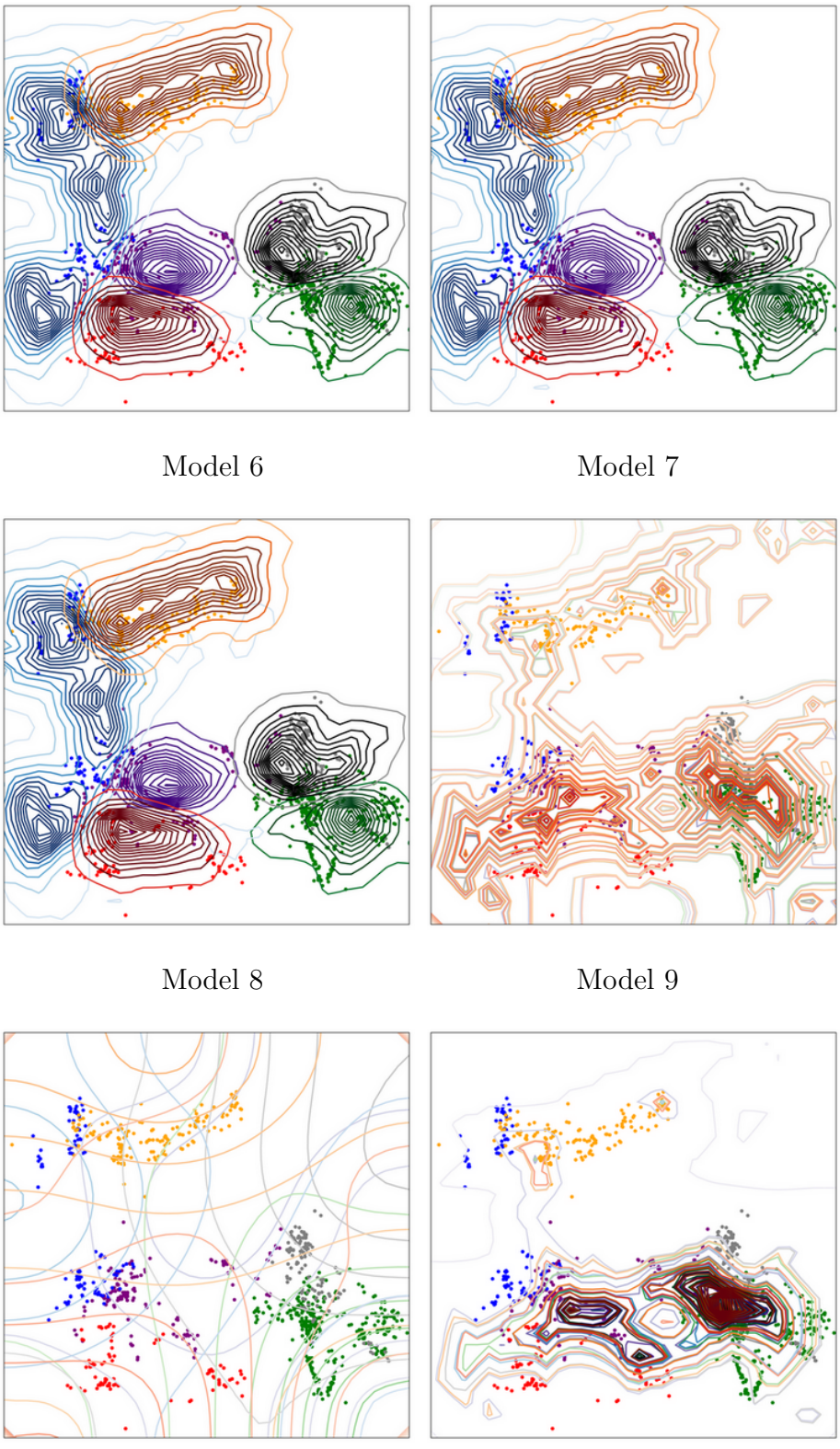

Model 6 Model 7

Model 8 Model 9

Model 10 Model 11

Fig. 3.9. Utilisation distributions for landscape-varying kinesis in the best fitting model of Models 0-5 (Models 6-8) and as a standalone model (Models 9-11) for data collected in 2011-12.

3.5.5 The effect of kinship and flocksize

Finally, the model selection procedure was extended for the 2018-19 data to test for an effect of flock size and relatedness between flocks on home range utilisation. Here, I assume no effect on kinesis. In the absence of this additional mechanism, Model 4 was the best fitting model (Table 3.3; Fig. 3.10a), and Model 2 was the next best fit, both indicating avoidance of other flocks and movement towards the centre of woodland. Model 4 is extended to incorporate flock size and relatedness. Although visually there is not a dramatic improvement in the fit between predicted and observed ranges (Fig. 3.10b-d), the extended model results in a reasonable improvement in BIC values (ΔBIC 48-67). More specifically, the results show that smaller flocks avoided larger flocks and larger flocks were less likely to avoid smaller flocks, while avoidance decreased as inter-flock relatedness increased (Table 3.8). These effects of kinship and flock size on avoidance behaviour were not found when analysed using KDE overlap (§3.2.1).

Table 3.8. The extended version of Model 4, where parameters ω_1-ω_3 (Equations 3.15-3.17) are fit in addition to the previous parameters, with the second 2018-19 data set, their parameter values and their BIC scores corresponding to Fig. 3.10. The BIC values can be compared with the previous Model 4 (BIC=14297) using the last column in the table, ΔBIC.

Model	b	γ	δ	ζ	ω_M	σ_1	σ_2	σ_3	BIC	ΔBIC
α_{ij}^1	14.4	7.8	0.050	25.8	1.9	0.068	-	-	14233	64
α_{ij}^2	11.8	7.8	0.048	25.9	1.2	-	0.088	1	14248	48
α_{ij}^3	11.6	8.9	0.047	25.9	1.2	0.087	0.99	0.058	14230	67

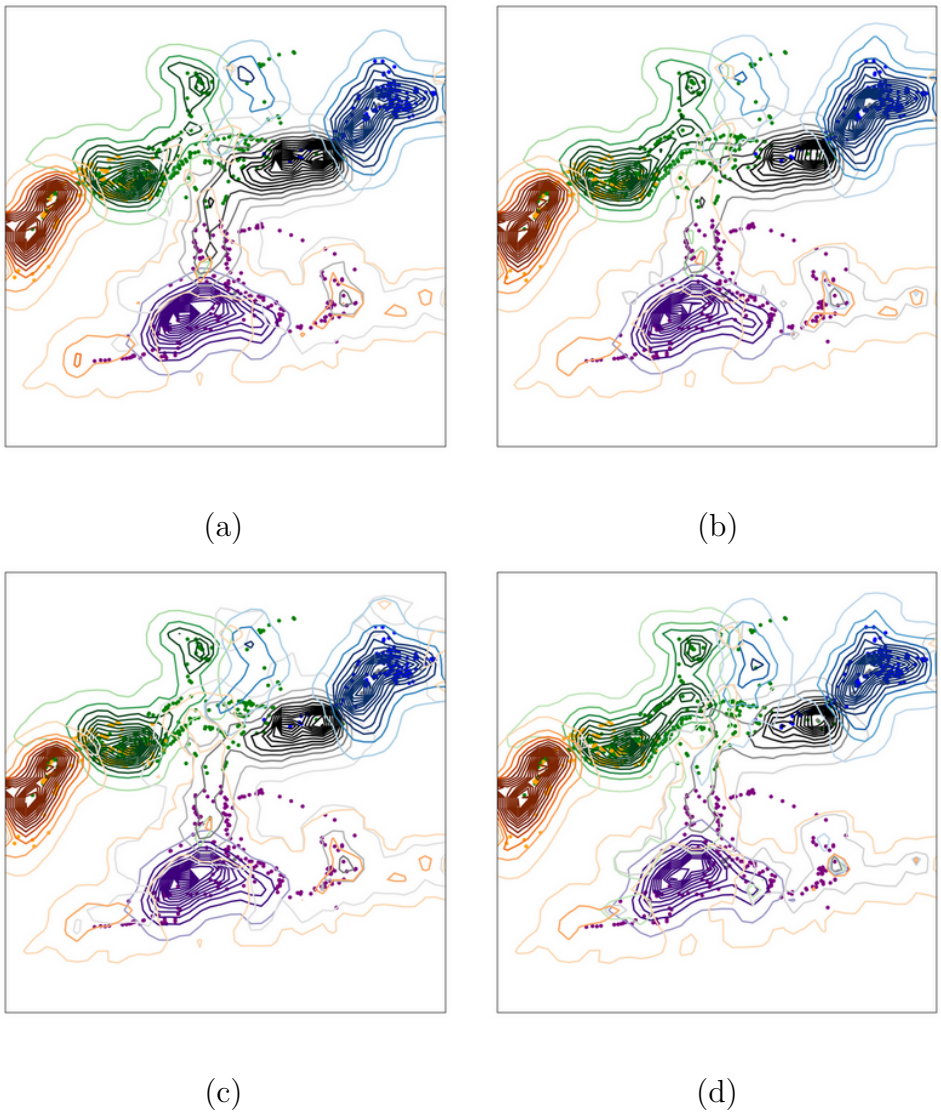

Fig. 3.10. Panel (a) shows the best fitting model (Model 4) for the second 2018-19 data set (Fig. 3.6d). Panels (b)-(d) show Model 4 with α_{ij} defined in (3.15)-(3.17) respectively. Although there is little change visually from the previous best fitting model where $\alpha_{ij} = 1$ (Panel (a)) there is a reasonable improvement in the BIC values (Table 3.8).

3.6 Summary

The home range patterns produced by foraging flocks of long-tailed tits are formed from a combination of conspecific avoidance and attraction towards the centre of woodland. Furthermore, flocks are less likely to avoid locations where they have interacted with other flocks and smaller flocks are more likely to avoid larger flocks.

Woodland is described simply as present or absent and will be explored further in the next Chapter. By modelling the attraction towards the woodland either uniformly or weighted towards the centre, the latter was discovered to be a much better fit for all data sets, indicating that flocks prefer foraging away from the edges of woodland areas. The effects of inter-flock interactions and the woodland affect the taxis aspect of movement but not kinesis.

Both kinship and flock size have a noticeable effect on conspecific avoidance. More closely-related flocks are less likely to avoid each other and this confirms the findings of (Hatchwell et al., 2001a), who showed there was more spatial overlap between more closely related flocks. I discuss the implications of these findings further in Chapter 5.

In conclusion, in addition to the new behavioural findings of this study I have shown that MHRA using partial differential equations is a suitable method to model the home ranges of flocks of long-tailed tits, where previously it has only been applied to model the home ranges of territorial animals or those with a central place attraction.

Chapter 4

The woodland habitat selection of nest building long-tailed tits

4.1 Introduction

Unravelling an animal's fine-scale selection of habitat is an important part of identifying areas for focussing conservation management (Klar et al., 2008; Morris, 2003). Fine-scale habitat-selection has been studied in a range of wild animals, from dolphins (*Tursiops truncatus*, Allen et al. 2001) to ungulates (van Beest et al. 2012) to feral cats (*Felis catus*, McGregor et al. 2014). The selection of locations by animals in heterogeneous landscapes can be analysed by comparing recorded locations of an animal with the available habitat (Manly et al., 2002). However, the question of how individual-level movement decisions are influenced by habitat requires the analysis of habitat-selection and movement mechanisms simultaneously (Avgar et al., 2016).

Chapter 3 showed that one of the main mechanisms driving the home ranges of non-breeding flocks of long-tailed tits is an attraction towards the centre of woodland. In this Chapter, the same population of long-tailed tits is revisited in the nest building season of 2019, to determine how the fine-scale distribution of different trees affects movement decisions. The Rivelin Valley, Sheffield, contains a complex structure of woodland where many species of trees are thought to be used by long-tailed tits throughout the year. Evidence of long-tailed tits foraging selectively comes from Gaston (1973), who suggested that a population of long-tailed tits in Oxford, in the pre-nesting season, prefer sycamore, when compared with oak and ash. I investigate which species of trees 18 pairs of long-tailed tits in the Rivelin Valley selected over a 50-day observation period. The space use of the birds in the Rivelin Valley has been studied since 1994, yet the study in this Chapter is the first to map the distribution of woodland habitat and question how different trees are influencing the foraging decisions of long-tailed tits.

Field workers studying long-tailed tits in the Rivelin Valley devote the majority of their time to finding nests each season. The species of nesting trees are recorded each year (Hatchwell, 2016), but the birds' favoured tree species for foraging in is not known. Understanding the selection of foraging trees can have a practical impact on field work by allowing data collection to be targeted on preferred foraging and nesting trees, therefore saving time. Furthermore, it is important to understand the birds distribution, variation in survival and productivity (i.e. fitness) in different habitats. In the nest building season, birds are easier to locate and observe due to their site fidelity and their small home range (relative to the non-breeding season). Additionally, whilst nest

building, the birds' main energy expenditure is foraging, rather than caring for offspring.

To unravel the effects of the woodland structure on movement, I determine which species of trees the birds tend to select as they move. The size of trees in this Chapter is represented by how much they cover at canopy and low level, providing a way to describe the birds' selection for the magnitude of each type of tree and indicate which types are preferred. It is important to understand how the birds are selecting their preferred tree species, therefore different models describing different ways of selecting a set of trees are tested. For example, given a set of tree species, would a foraging pair prefer a location with a larger magnitude of tree cover or more diversity?

The field observations used to collect data for this study were designed to estimate and record when the birds' decisions to move are made, rather than at arbitrary points in time. Using the results of the field work, decisions are analysed by developing a model using an integrated step-selection analysis (iSSA) framework (1.5; Avgar et al. 2016). I determine (a) which trees are preferred, (b) how the birds are selecting for the set of preferred trees and (c) space use estimations by calculating *utilisation distribution*s from the models.

4.2 Long-tailed tits in the nesting season

4.2.1 Data collection

Field studies were conducted on 18 breeding pairs of nest building long-tailed tits (*Aegithalos caudatus*) in the early breeding season of 2019 by Tobit Dehnen. Pairs build intricate nests, that may take over a month to construct (Lack and

Lack, 1958) and in this period, both birds in the pair typically forage and move around in close proximity. Since both birds in the pair forage together whilst nest building, I model each pair as one individual entity. Data were collected over 50 days in the Rivelin Valley, Sheffield, UK (§1.3) in an area covering approximately 1.2km^2 (Fig. 4.1). Similar to the flocks in Chapter 3, pairs of birds were followed on foot and identified using coloured rings on their legs. Whilst recording locations, the observer followed the birds at a distance of at least 5m to reduce observer bias. When birds could not be closely followed (e.g. when they crossed a river) but were still in sight, locations were later corrected. Pairs were usually located at the nest site. Once located, each pair was followed until sight was lost.

Successive animal locations are often recorded through time at constant intervals (Kays et al., 2015), however this is unlikely to correspond to the times when the animal decided to move. To capture the pairs' movement decisions, locations were recorded when the observer noted that the pair had moved a significant distance. *Significant movement*s were defined to be when a pair moved to a location estimated to be more than 10m away from the previously recorded location. By recording these significant movements, an estimated time for when the birds decide to move was obtained.

Although the birds within the study site have a very large landscape available to them, they use a relatively small home range within their available landscape in which habitat data was collected. One reason for this method is that the birds spend the breeding season within these home ranges, meaning that it is reasonable to assume that their habitat knowledge is omniscient throughout the range. This means that when modelling decisions to move, the birds aren't just deciding within a *perceptual range* of their current location, but making

decisions based on the whole home range. Furthermore, recording the cover of trees throughout the entire study site is extremely time consuming and unnecessary if the birds occupy only a small portion of it.

Home ranges were estimated using the recorded locations for each pair as a 95% minimum convex polygon (Burt 1943, MCP) and environmental data were subsequently collected inside the home ranges. This simple method of describing space use was used to efficiently obtain habitat information to define availability and was not considered a definitive model of the pair's home range. I use the term *tree type* to denote different grouped tree and shrub species that were recorded in the study. Each tree type, s, used in this Chapter belongs to a set of twenty-two types of tree thought to be used by long-tailed tits when nest building. The set is denoted as S_{22} and listed in Appendix C.4.1.

A method of describing the cover of different tree types within the Rivelin Valley was designed by Tobit Dehnen and Ben Hatchwell. Each MCP was split into a grid of 25m by 25m squares and data were collected at the intersections of the squares, these intersections are denoted as *habitat locations*. At each habitat location, data were collected at two different foraging heights: the shrub layer (1-7m) and canopy layer (>7m). The data collection is described below and is further illustrated with a diagram in Appendix C.2.

For the shrub layer, each habitat location had a 10m by 10m square defined around it and this was split into quarters. For each quarter the most dominant tree type (or no tree type) was estimated for each 10% of the quarter. The most dominant tree type inside a square was decided by choosing the tree type covering the largest area of the square, by comparing all types of tree in the square.

For the canopy layer, a transparent acrylic square with side length 25cm was split into 25 equal small squares and held above the observer's head at each habitat location, at a constant height. Subsequently, the tree type (or no tree type) that covered the greatest proportion of each of the 25 small squares was recorded. An approximate percentage estimate, $T_s(\mathbf{x})$, of the cover of each tree type, s, in the area of each habitat location is calculated by averaging the shrub and canopy percentages equally. The distribution of types of tree is reported in Table C.1, showing that the majority of tree types are accessible to at least 10 pairs.

I assume that the percentage of each tree type for any location in the landscape can be represented by the nearest habitat location. Any location > 25m away from any habitat location is not included in the analysis. The habitat locations for an example pair of birds are shown in Fig. 4.2. Recorded locations for the birds are assigned to the nearest recorded habitat location, represented as a Voronoi Diagram[1] (Fig. 4.2, Aurenhammer 1991). Additionally, the type of tree that each nest resides in was recorded and is reported in Fig. C.2, the most preferred nesting plant is bramble.

Recorded locations are shown on a satellite image of the study site in Fig. 4.1. Each linear displacement between two successive recorded locations is denoted as a *step*. A sequence of steps recorded in succession without stopping is denoted as a *path*. In total, 1124 steps were recorded with a median of 4 steps per path. The mean *step length* (distance between recorded locations) for all pairs was 19 ± 0.7m (95% CI), the mean *step time* (time taken between recorded points) was 66 ± 5 (95% CI) seconds and the mean *step speed* (step

[1]For a set of two-dimensional points in space, $\mathbf{x}_n$, Voronoi diagrams partition space into regions of convex polygons each containing only one $\mathbf{x}_n$, where any point inside the polygon is closest to the corresponding $\mathbf{x}_n$ rather than any other $\mathbf{x}_n$ in the set

length divided by step time) was 1.5 ± 0.2m/s (95% CI). For two steps in succession, a *turning angle* can be calculated, this is the angle the pair turns through from one step to the next. I denote the turning angles, step times, step lengths and step speeds collectively as *movement attribute*s.

From the 1124 steps, 1073 steps were recorded with habitat data attached. Analyses in this Chapter are performed using all 1073 steps from the population of birds to uncover population level behaviours. Some of the recorded steps end at the same habitat location as the nest, removing steps ending at the nest leaves 811 steps. I additionally perform some analyses of tree selection on the reduced data set of 811 steps. The analysis on the reduced data set is to ensure that a location is chosen due to the woodland structure, rather than visiting the nest. The data sets may be reduced further to remove observer bias from the first encounter of the birds by removing the first step from each path. Repeating the analyses with data reduced for observer bias does not change the overall results of the study and is reported in Appendix C.4.3.

4.2.2 Hypotheses of habitat selection

To understand fine scale habitat-selection within home ranges, I develop hypotheses and subsequently write models to test them. Hypotheses are tested by describing each one using mathematical formulae within mathematical models and fitting each model to the data described earlier in §4.2.1. Each hypothesis can be categorised into two general behaviours for the nest building pairs: (A) a preference for places close to the nest site and (B) movement towards preferred types of trees, dependent on how much area the trees cover.

Fig. 4.1. Recorded GPS locations for 18 pairs of long-tailed tits, plotted over the study site in the Rivelin Valley, Sheffield, UK. Each colour shows the locations for a different pair of birds and their nest sites are shown with a star icon. The locations for the pair of birds visualised in orange on the left side of the landscape are shown with corresponding habitat locations in Fig. 4.2.

I include a preference for places close to the nest site as it separates the selection of woodland habitat from the fidelity to the nest. I test two hypotheses that describe the following: pairs are more likely to select a location if

A1) it is close to the nest site. Since pairs are building nests, I hypothesise that the pair prefer to choose a place close to the nest.

A2) When the pair are are far away from the nest site, the pair have a greater preference for locations in the direction of the nest site. This behaviour assumes that the attraction for places close to the nest site depends on how far away the pair is.

To examine how long-tailed tits use their woodland habitat selectively whilst nest building, I investigate hypotheses describing behaviour (B). I first examine whether there is a set of preferred tree types within the 22 recorded types of

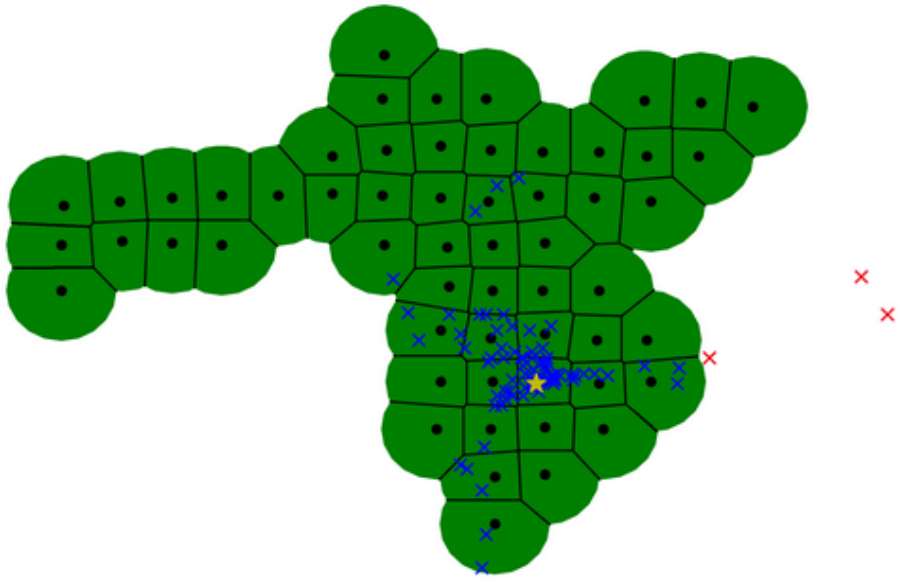

Fig. 4.2. Locations for an example pair of birds, shown as blue crosses, plotted over habitat locations, shown as black dots. Each recorded location for a pair is attached to the nearest habitat location, forming a landscape structured as a Voronoi Diagram. Each location resides inside a closed area and is assumed to have the same attributes as the habitat location which resides inside the area. The edges of the landscape are shaped such that any location more than 25m from a habitat location is discarded from the analysis (shown in red) and only locations in the green parts of the diagram are included in the analysis (shown in blue). Each habitat location shows where the percentage of 22 types of trees was estimated at a spacing of approximately 25m apart vertically and horizontally. The pair in this figure is represented on a satellite image of the landscape with orange locations in Fig. 4.1.

tree and if there are specific ways that the tree types are being selected. To model behaviour (B), the hypotheses are tested on a set of tree types, S. The set S is either equal to S_{22} (the set of all tree types) or a subset of S_{22}. The hypotheses are as follows: pairs are selecting locations

B1) with a different preference for each tree type in S,

B2) based on the presence or absence of any of the tree types in S,

B3) based on the diversity of tree types in S,

B4) based on the percentage cover of the tree types in S.

Hypothesis (B1) aims to understand the selection for each tree type separately, which will in turn indicate a set of preferred types of tree. I detail the process of finding this set in §4.4.3, after introducing the modelling methods. Furthermore, I describe each of the hypotheses (A1)-(B4) using mathematical formulae in §4.4.

4.3 Statistical methods

To quantify the birds' selection for each of the twenty-two types of trees, recorded steps are compared to control steps that could have been taken. To understand this habitat-selection, I use iSSA, a general framework for the inference of movement and habitat-selection across continuous space in discrete time (Avgar et al., 2016). I introduced iSSA in §1.5, where I noted that the movement model is denoted as a step-selection function (SSF, Equation 1.6) and may include two functions: a *movement kernel*, defining movement independent of habitat and the *habitat-selection function*, defining habitat selection, independent of movement. In this section, a movement kernel and a habitat-selection function are defined for the nest building long-tailed tits to form a step-selection model.

The formulation of iSSA requires locations to be recorded at regular intervals, so the time between successive locations is constant (Avgar et al., 2016; Thurfjell et al., 2014). Recording movements at regular intervals in time has the advantage of the movement kernel being dependent on only spatial measures (e.g. the step lengths and turning angles). However, it is unlikely that animals make their decisions to move at equally spaced points in time. Furthermore,

the time scale of step-selection analyses have shown to influence space use estimates (Schlägel et al., 2016). In this Chapter, the birds' locations were recorded when significant movements were made (see §4.2.1), resulting in steps recorded over varying intervals of time. To analyse these steps I use a recently developed extension of iSSA that allows varying step times (Munden et al., 2020).

To form the step-selection model I first define the movement kernel, $\phi(\mathbf{x}_j, \tau_j|\mathbf{x}_{j-1}, \mathbf{x}_{j-2})$. The movement kernel describes movements of any pair in the population from location $\mathbf{x}_{j-1}$ to $\mathbf{x}_j$. Following Munden et al. (2020), the kernel is formed of three probability density functions that are fit to the turning angles α_j, the step lengths l_j and the step times τ_j. Measurements can be visualised in Fig. 4.3, for the path of a hypothetical individual. The movement kernel has the form

$$\phi(\mathbf{x}_j, \tau_j|\mathbf{x}_{j-1}, \mathbf{x}_{j-2}) = g_1(\alpha_j)g_2(\tau_j)g_3(l_j|\tau_j), \tag{4.1}$$

where it is convenient to fit the distribution g_3 to the empirical step speeds (step length divided by step time). The probability distributions $g_1 - g_3$ will be defined by finding the best fit distributions from those in Appendix C.1.

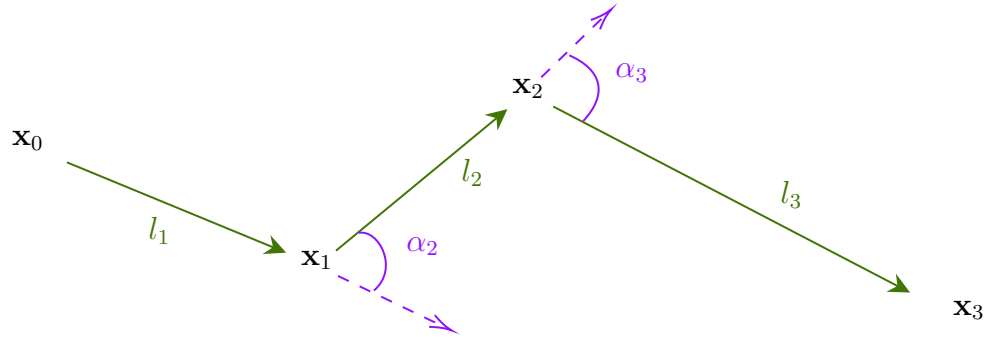

Fig. 4.3. A hypothetical path of steps, showing the step lengths, l_j (in green) and the turning angles, α_j (in purple). Shown is the trajectory through locations $\mathbf{x}_0$, $\mathbf{x}_1$, $\mathbf{x}_2$ and $\mathbf{x}_3$ (shown in black).

The habitat-selection function, $\Psi_i(\mathbf{B} \cdot \mathbf{Z}_i)$, has the general form shown in Equation (1.5). The covariates $\mathbf{Z}_i = \mathbf{Z}_i(\mathbf{x}_j, \mathbf{x}_{j-1}, \mathbf{x}_{\text{nest},i})$ describe behaviours which may depend on the start of the step, the end of the step and the nest location $\mathbf{x}_{\text{nest},i}$ of pair i. The mathematical forms of the covariates which describe the hypotheses in §4.2.2 are defined precisely in §4.4. The associated parameters $\mathbf{B} = (\beta_1, \ldots, \beta_n)$ are inferred in the fit of the model.

The probability density of a pair of long-tailed tits moving from location $\mathbf{x}_{j-1}$ to location $\mathbf{x}_j$ over time interval τ_j is modelled as

$$f_i(\tau_j, \mathbf{x}_j | \mathbf{x}_{j-1}, \mathbf{x}_{j-2}, \mathbf{x}_{\text{nest},i}) = K^{-1} \phi(\tau_j, \mathbf{x}_j | \mathbf{x}_{j-1}, \mathbf{x}_{j-2}) \Psi_i(\mathbf{B} \cdot \mathbf{Z}_i), \tag{4.2}$$

where $K = \int_{\Omega_i} \int_T \phi(\mathbf{x}'_j, \tau'_j | \mathbf{x}_{j-1}, \mathbf{x}_{j-2}) \Psi_i(\mathbf{B} \cdot \mathbf{Z}'_i) \mathrm{d}\tau'_j \mathrm{d}\mathbf{x}'_j$ is a normalisation constant, ensuring f_i is a probability density function and $\mathbf{Z}'_i = \mathbf{Z}_i(\mathbf{x}'_j, \mathbf{x}_{j-1}, \mathbf{x}_{\text{nest},i})$. The landscape available to pair i is Ω_i and T is the set of all possible step times that the pair could move from $\mathbf{x}_{j-1}$ to $\mathbf{x}'_j$.

4.3.1 Representing Availability

In this study, each pair of long-tailed tits has a different home range that was initially estimated using a minimum convex polygon (MCP) in which habitat data was collected. The collection of habitat data in this way means pairs have different available habitats. The spatial domain, Ω_i, represents availability as it defines the entire landscape of possible locations.

Fitting Equation (4.2) to data requires calculating the integral K for each trial set of parameter values. This can be computationally expensive, so instead it is typical in step-selection studies to use a Monte-Carlo approximation (Reiher, 1964) in place of the integral. This turns out to have the added advantage of being equivalent to conditional logistic regression (CLR): a quick and well-used technique in ecological research. This approximation works by sampling control steps from the set of all possible steps that start at $\mathbf{x}_j$ and end at Ω_i. As is standard for resource- and step-selection analysis, each step in the data is called a *used step* and the control steps are termed as *available step*s. I match each used step to 100 available steps. The set of available steps can be thought of as steps the birds could have taken instead of the used step. Fig. 4.4 illustrates available steps and used steps for a hypothetical pair.

Available steps are sampled from an availability kernel (Avgar et al., 2016), which has the following form

$$\tilde{\phi}(\alpha_j, \tau_j, l_j) = \tilde{g_1}(\alpha_j)\tilde{g_2}(\tau_j)\tilde{g_3}(l_j|\tau_j), \tag{4.3}$$

where $\tilde{g}_k$ has the same functional form as g_k (Equation 4.1), for each k, but may not have the same parameter values.

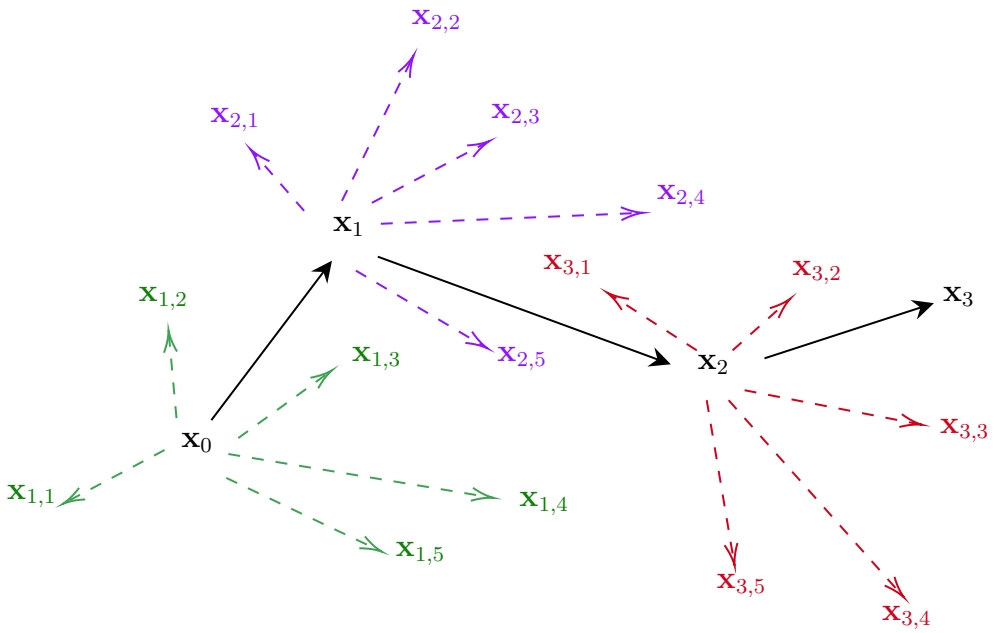

Fig. 4.4. An example path for a hypothetical pair of long-tailed tits with availability modelled as five alternative available steps for each used step. The diagram shows used steps (black lines) moving from locations $\mathbf{x}_0$, $\mathbf{x}_1$, $\mathbf{x}_2$ and $\mathbf{x}_3$ with available steps shown by the dashed lines. For example, the green available steps are steps that could have been taken instead of the used step from $\mathbf{x}_0$ to $\mathbf{x}_1$, the purple from $\mathbf{x}_1$ to $\mathbf{x}_2$ and the red from $\mathbf{x}_2$ to $\mathbf{x}_3$.

The probability distribution $\tilde{g}_1(\alpha_j)$ is derived by fitting uniform and Von Mises distributions to the turning angles and choosing the best fitting distribution. Distributions $\tilde{g}_2(\tau_j)$ and $\tilde{g}_3(l_j|\tau_j)$ are formed by fitting step times and step speeds respectively to the exponential, half-normal, log-normal and gamma distributions and choosing the best fitting distributions (Avgar et al., 2016).

The parameters for each distribution are inferred by maximising the likelihood functions

$$L_1(p_1, \ldots, p_P|\mathrm{D}) = \prod_{j \in \mathrm{D}} \tilde{g_1}(\alpha_j), \tag{4.4}$$

$$L_2(p_1, \ldots, p_P|\mathrm{D}) = \prod_{j \in \mathrm{D}} \tilde{g_2}(\tau_j), \tag{4.5}$$

$$L_3(p_1, \ldots, p_P|\mathrm{D}) = \prod_{j \in \mathrm{D}} \tilde{g_3}(l_j|\tau_j), \tag{4.6}$$

for $\tilde{g_1}$, $\tilde{g_2}$ and $\tilde{g_3}$ respectively, where $p_1, \ldots, p_P$ are the P parameters in each of the probability density functions (Appendix C.1) and j corresponds to a step in the set of all steps for all pairs, D. Equations (4.4)-(4.6) are maximised using a Nelder-Mead algorithm (Nelder and Mead, 1965) and the `minimize` function in Python 3.4. The best fitting distributions are chosen by comparing bayesian information criterion (BIC) values. The form of each distribution used is reported in Appendix C.1.

Available steps are sampled from the availability kernel (4.3) in a three step process: first sampling a turning angle from $\tilde{g_1}(\alpha_j)$, then sampling a step time using $\tilde{g_2}(\tau_j)$ and last sampling a step length from $\tilde{g_3}(l_j|\tau_j)$. Combining the turning angle, step time and step speed distributions with the start of the used step, $\mathbf{x}_{j-1}$ gives an available end location $\mathbf{x}_{j,a}$ using the formula

$$\mathbf{x}_{j,a} = \mathbf{x}_{j-1} + l_a \begin{pmatrix} \cos(\alpha_a) \\ \sin(\alpha_a) \end{pmatrix} \tag{4.7}$$

where l_a is the step length of the sampled step and α_a is the turning angle of the sampled step.

4.3.2 Fitting the step-selection function

To fit Equation (4.2) to the data described in §4.2.1 I use the iSSA methods of Avgar et al. (2016) which I describe briefly here. I begin by constructing a weighting function

$$W_i(\tau_j, \mathbf{x}_j, \mathbf{x}_{j-1}, \mathbf{x}_{j-2}, \mathbf{x}_{\text{nest},i}) = \exp\left(\mathbf{B} \cdot \mathbf{Z}_i + C\right). \tag{4.8}$$

Here, $\mathbf{B}$ and $\mathbf{Z}_i$ are as defined in Equation (4.2), and C is a function that corrects for the fit of the availability kernel (4.3) with the form

$$C(\tau_j, \mathbf{x}_j, \mathbf{x}_{j-1}, \mathbf{x}_{j-2}) = C_1(\tau_j, \mathbf{x}_j, \mathbf{x}_{j-1}, \mathbf{x}_{j-2}) + \cdots + C_N(\tau_j, \mathbf{x}_j, \mathbf{x}_{j-1}, \mathbf{x}_{j-2}). \tag{4.9}$$

Equation (4.9) corrects for any discrepancy between each function $\tilde{g}_n$ in the availability kernel (Equation 4.3, that is parametrised using Equations 4.4-4.6) and the corresponding g_n in the habitat-independent movement kernel (Equation 4.1), which I am aiming to estimate. I give an example of how to use the correction function in Appendix C.3. The conditional logistic regression procedure maximises the following likelihood function

$$L_2(\mathbf{B}, \mathbf{K}|\mathrm{D}) = \prod_{i=1}^{18} \prod_{j \in \mathrm{D}_i} \frac{W_i(\tau_j, \mathbf{x}_j, \mathbf{x}_{j-1}, \mathbf{x}_{j-2}, \mathbf{x}_{\text{nest},i})}{\sum_{a \in D_{i,j,a}} W_i(\tau_{j,a}, \mathbf{x}_{j,a}, \mathbf{x}_{j-1}, \mathbf{x}_{j-2}, \mathbf{x}_{\text{nest},i})}, \tag{4.10}$$

where D is the set of recorded locations for the population, D_i is the set of recorded locations for pair i, $\mathrm{D}_{i,j,a}$ is the set of available steps for pair i, for used step j. The end location and the step time of each available step are $\mathbf{x}_{j,a}$ and $\tau_{j,a}$, respectively (see Fig. 4.4). Equation (4.10) is maximised using CLR with the `clogit` function in the R 3.6.1 package `survival`. Finally, to parametrise

Equation (4.2), I just need to set the movement kernel as $\phi = \tilde{\phi}\exp(C)$ and the habitat-selection function as $\Psi_i = \exp(\mathbf{B} \cdot \mathbf{Z}_i)$.

4.4 Mathematical models for different movement behaviours

The step-selection function (SSF) model shown by Equation (4.2) depends on a vector of covariates $\mathbf{Z}_i(\mathbf{x}_j, \mathbf{x}_{j-1}, \mathbf{x}_{\text{nest},i})$, where each covariate describes a different behaviour for pair i. The behavioural hypotheses that will define these covariate functions were defined in §4.2.2 and different models are defined by different combinations of the covariates. Here I detail mathematical formulae to describe each of the hypotheses and define different forms of $\mathbf{Z}_i$.

4.4.1 Fidelity to the nest

I define mathematical forms to describe hypotheses (A1) and (A2), both describing an attraction to the nest location. Each hypothesis has a candidate function associated with it

$$Z_{A1}(\mathbf{x}_{\text{nest},i}, \mathbf{x}_j) = |\mathbf{x}_{\text{nest},i} - \mathbf{x}_j|, \tag{4.11}$$

$$Z_{A2}(\mathbf{x}_{\text{nest},i}, \mathbf{x}_j, \mathbf{x}_{j-1}) = |\mathbf{x}_{\text{nest},i} - \mathbf{x}_{j-1}|\cos(\theta_i). \tag{4.12}$$

Where $\theta_i(\mathbf{x}_{j-1}, \mathbf{x}_j, \mathbf{x}_{\text{nest},i})$ is the angle pair i would need to turn through to relocate from $\mathbf{x}_j$ to $\mathbf{x}_{\text{nest},i}$, after the step from $\mathbf{x}_{j-1}$ to $\mathbf{x}_j$. The function Z_{A2} describes hypothesis (A2) in the following way: Z_{A2} becomes larger in magnitude, proportional to the distance $|\mathbf{x}_{\text{nest},i} - \mathbf{x}_{j-1}|$, and is at its largest when $\cos(\theta_i) = 1$ (the location $\mathbf{x}_j$ is on the line from $\mathbf{x}_{j-1}$ to $\mathbf{x}_{\text{nest},i}$). When

$|\theta| < \frac{\pi}{2}$, the function Z_{A2} is positive (increasing f_i) and when $|\theta| > \frac{\pi}{2}$, Z_{A2} is negative (decreasing f_i). This means that when a pair of birds is choosing a location, the further away the pair currently is from the nest, the greater preference they have for locations in the direction of the nest. To summarise, hypothesis (A1) describes the behaviour that a pair prefers locations closer to the nest whereas (A2) tests whether the preference is dependent on how far away the pair currently is and the angle to turn through to get back to the nest.

To choose the best covariate to represent movement in response to the nest, $\mathbf{Z}_i$ in Equation (4.8) is set equal to covariates (4.11) and (4.12) in turn and Equation (4.10) is maximised. In each case, I test whether the increase in likelihood is sufficient to reject the null hypothesis that $\mathbf{B} = 0$. Then, I find the best model out of Equation (4.11) and (4.12) using their BIC.

The null model and the models containing covariates (4.11) and (4.12) are denoted as Models 0, 1 and 2 respectively and are summarised in Table 4.1. The best fitting nest covariate is denoted $Z_A^*(\mathbf{x}_j, \mathbf{x}_{j-1}, \mathbf{x}_{\text{nest},i})$.

4.4.2 Woodland habitat-selection

Hypotheses (B1)-(B4) in §4.2.2 correspond, respectively, to the following covariate functions

$$Z_{B1}^s(\mathbf{x}_j) = T_s(\mathbf{x}_j), \quad \text{where } s \in S \tag{4.13}$$

$$Z_{B2}(\mathbf{x}_j) = P_S(\mathbf{x}_j), \tag{4.14}$$

$$Z_{B3}(\mathbf{x}_j) = \mathrm{V}_S(\mathbf{x}_j), \tag{4.15}$$

$$Z_{B4}(\mathbf{x}_j) = \sum_{s \in S} T_s(\mathbf{x}_j). \tag{4.16}$$

The function $T_s(\mathbf{x})$ is equal to the estimated percentage of tree type s at location $\mathbf{x}_j$. Equation (4.13) describes hypothesis (B1) by fitting a separate covariate for each tree type in $s \in S$. The presence of any of the tree types in S is described by $P_S(\mathbf{x})$, which is equal to 1 if any tree type from set S is present at location $\mathbf{x}_j$ or 0 otherwise. The diversity of tree types, $V_S(\mathbf{x})$, is equal to the number of tree types in set S estimated to be present at location $\mathbf{x}_j$.

4.4.3 Inferring the preferred types of trees

Since covariates $Z_{B1} - Z_{B4}$ depend on a set of tree types S, I determine a set of preferred tree types $S = S_r$ to be used in models. The types included in S_r are found by fitting a covariate representing each of the 22 tree types in S_{22}. The parameters $\mathbf{B}$ are inferred by setting $\mathbf{Z}_i$ in Equation (4.8) to be a vector including nest covariate Z_A^* and another 22 covariates equal to $Z_{B1}^s(\mathbf{x}_j)$ (Equation 4.13), one for each tree type $s \in S_{22}$. For each inferred parameter β_s, $\exp(\beta_s)$ is the increase in the odds of a step occurring due to one percentage point increase in the abundance of the tree type s, keeping all other covariates constant. For example, $\exp(\beta_s) = 1.1$ indicates that the odds of a step occurring due to the percentage cover of tree type s increases by approximately 10% for each percentage point of s present. Positive parameters in $\mathbf{B}$ indicate selection for a covariate. I evaluate the p-values of all positive inferred parameters as this indicates the significance of the covariate.

The parameters representing the selection of covariates are estimated for the full data set of 1073 steps and again for the reduced data set of 811 steps (see §4.2). The reduced set of 811 steps are steps that do not end at the same habitat location as the nest. Analysing this reduced set separately, allows for

the interpretation of selection on foraging movements, rather than visiting the nest.

Long-tailed tits are insectivorous so their movement may depend upon bud burst as their prey species tend hatch to coincide with these bursts (Gaston, 1973), therefore the preference of a tree type may change over time. I explore whether there is a difference in the estimated parameter values for particular tree types over time. The data is split in half, with each half corresponding to 25 consecutive days. Inferring parameters in separate halves of the data means that if the magnitude of the parameter is significantly different in each half, the selection of that tree type could be dependent on time.

4.4.4 Model selection

After defining the preferred subset of tree types, S_r, I perform model selection to test hypotheses (B1)-(B4). Each of the models are fitted by maximising Equation (4.10) using different combinations of covariates (4.13)-(4.16) in the weighting function (4.8). All models are fitted with the previously chosen covariate Z_A^* (either Equation 4.11 or 4.12) using the full 50 days of data.

Model 3 includes covariates $Z_{B1}^s(\mathbf{x}_j)$ (Equation 4.13) for $s \in S_r$ to test hypothesis (B1). Models 4-6 test hypotheses (B2)-(B4) by fitting covariates $Z_{B2}(\mathbf{x}_j)$ to $Z_{B4}(\mathbf{x}_j)$ (Equations 4.14-4.16), respectively. Model 7 fits the covariates $Z_{B2}(\mathbf{x}_j)$ and $Z_{B3}(\mathbf{x}_j)$ together, to test combined effects of the presence and diversity of tree types in S_r. Model 8 fits covariates $Z_{B2}(\mathbf{x}_j)$ and $Z_{B4}(\mathbf{x}_j)$ together, to test the effects of the presence and the percentage of the tree types combined. The covariates included in all models are summarised in Table 4.1. The parameters

in each model, **B**, are estimated using CLR with the likelihood function shown in Equation (4.10).

Table 4.1. The covariates that are included in each model summarized. Models 1 and 2 are initially fit and compared with Model 0 to find the best nest covariate, Z_A^*. Models 3-8 are fit and compared to find the best fitting model.

Model, M	Covariates	Hypotheses	Equations
0	C	The null model	
1	C, Z_{A1}	(A1)	(4.11)
2	C, Z_{A2}	(A2)	(4.12)
3	C, Z_A^*, Z_{B1}	(B1)	(4.13)
4	C, Z_A^*, Z_{B2}	(B2)	(4.14)
5	C, Z_A^*, Z_{B3}	(B3)	(4.15)
6	C, Z_A^*, Z_{B4}	(B4)	(4.16)
7	C, Z_A^*, Z_{B2}, Z_{B3}	(B2) & (B3)	(4.14),(4.15)
8	C, Z_A^*, Z_{B2}, Z_{B4}	(B2) & (B4)	(4.14),(4.16)

4.5 Results of the step-selection analysis

4.5.1 Defining movement

The distributions of the movement attributes (turning angles, step times etc) with the fitted probability distributions super-imposed (Appendix C.1) are shown in Fig. 4.5. The turning angles are fitted to a uniform distribution (BIC= 3047) and the Von Mises distribution (BIC=3011, Equation C.5). Although the Von Mises distribution is a better fit (ΔBIC=36), the simpler uniform distribution of turning angles to reduce the parameters in the model.

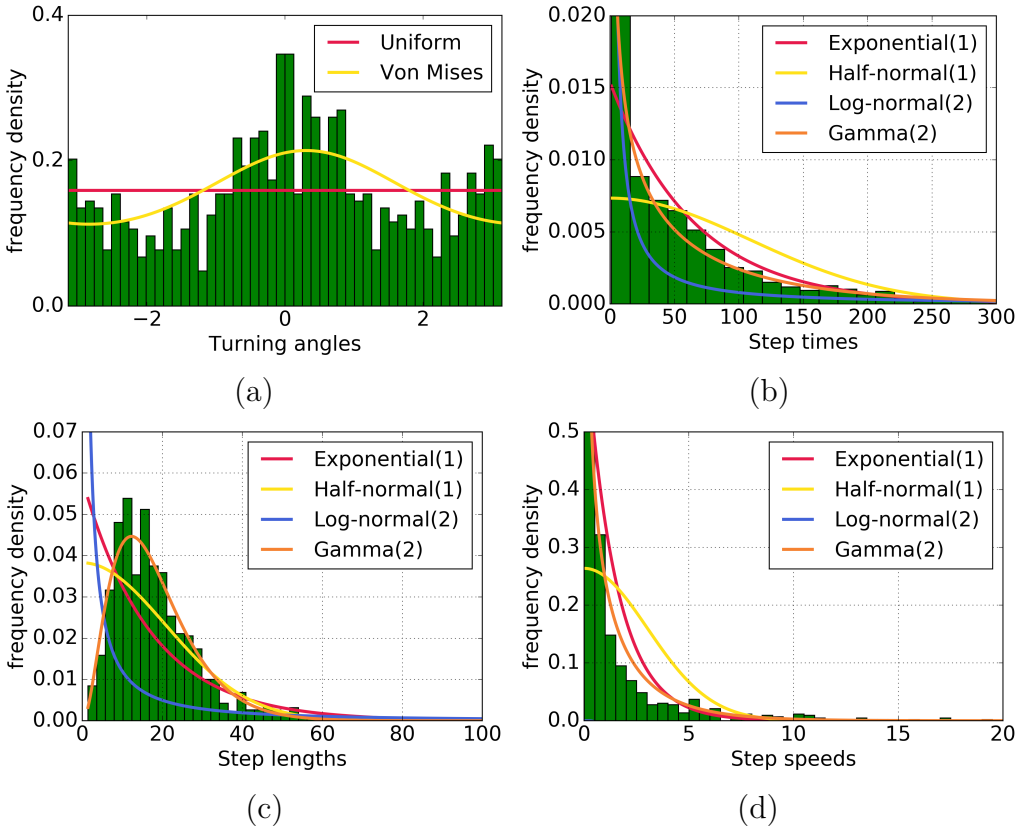

Fig. 4.5. Histograms of the movement attributes for the population of birds with best fit probability distributions (Appendix C.1) super-imposed. The empirical distributions for the turning angles (a), step times (b), step lengths (c) and step speeds (d) are shown. The best fitting exponential, half-normal, log-normal and gamma distributions are super-imposed on the step times, lengths and speeds. The legend labels show the number of parameters in each model. BIC values for each fit are shown in Table 4.2.

Table 4.2. Results from fitting the various candidate models (C.1-C.4) to the availability kernel. The best fitting distributions for each of the movement attributes are shown in bold

PDF	parameters	BIC (time)	BIC (length)	BIC (speed)
Exponential	1	9466	10442	8772
Half-normal	1	9893	10283	9548
Log-normal	2	9403	10130	**8370**
Gamma	2	**9355**	**10127**	8584

The best fit model is determined by the BIC values in Table 4.2. The step times best-fit a Gamma distribution and the step speeds best-fit a Log-Normal distribution, giving the following form for the availability kernel

$$\tilde{\phi}(\mathbf{x}_j, \tau_j | \mathbf{x}_{j-1}) \propto \frac{\tau_j^k}{|\mathbf{x}_j - \mathbf{x}_{j-1}|} \exp\left(-\frac{\tau_j}{\theta} - \frac{(\ln(|\mathbf{x}_j - \mathbf{x}_{j-1}|/\tau_j) - \mu)^2}{2\sigma^2}\right), \quad (4.17)$$

with the best fit parameters $\theta = 109$s and $k = 0.563$, $\mu = 0.6$, $\sigma = 1.44$ are dimensionless parameters. As the weighting function is in log-linear form, it is also useful to write

$$\tilde{\phi}(\mathbf{x}_j, \tau_j | \mathbf{x}_{j-1}) \propto \exp\left(-\frac{\tau_j}{\theta} + (k-1)\ln(\tau_j) + \left(\frac{\mu}{\sigma^2} - 1\right)\ln\left(\frac{|\mathbf{x}_j - \mathbf{x}_{j-1}|}{\tau_j}\right) - \frac{1}{2\sigma^2}\ln\left(\frac{|\mathbf{x}_j - \mathbf{x}_{j-1}|}{\tau_j}\right)^2\right). \quad (4.18)$$

The weighting function $W_{i,M}$ (Equation 4.8), which depends on the Model, M (Table 4.1) has the form

$$W_{i,M}(\mathbf{x}_j, \mathbf{x}_{j-1}, \tau_j) = \exp\left(C + \mathbf{B} \cdot \mathbf{Z}_{i,M}\right), \quad (4.19)$$

with the correction function corresponding to Equation (4.18) being

$$C = \kappa_1 \tau_j + \kappa_2 \ln\left(\tau_j\right) + \kappa_3 \ln\left(\frac{|\mathbf{x}_j - \mathbf{x}_{j-1}|}{\tau_j}\right) + \kappa_4 \ln\left(\frac{|\mathbf{x}_j - \mathbf{x}_{j-1}|}{\tau_j}\right)^2. \quad (4.20)$$

4.5.2 An attraction to the nest

The next part of the analysis is to find a covariate to describe an attraction to the nest using methods described in §4.4.1. The model fit results of fitting both nest covariates in turn are shown in Table 4.3.

Table 4.3. The best fit covariate function to represent the birds' movement in response to the nest. In all cases, Model 1 fits best by having the lowest BIC value.

Model, M	Covariates	BIC
0	C	9781
1	C, Z_{A1}	**9547**
2	C, Z_{A2}	9787

The BIC values show that Model 1 is a much better fit than Model 2 and Model 0 is a similar fit to Model 2. The fit of Model 1 suggests that the birds are more likely to choose locations close to the nest. Therefore there is evidence towards hypothesis (A1). The poor fit of Model 2 suggests that being further from the nest does not mean the birds are more likely to turn towards the nest, giving little evidence for hypothesis (A2). Therefore, $Z_{A*}(\mathbf{x}_j) = Z_{A1}(\mathbf{x}_j)$ (shown in Equation 4.11) is used to represent attraction towards the nest site in further analyses.

4.5.3 The preferred types of trees

I introduce woodland habitat into the analysis by first defining a preferred subset of tree types, S_r, using methods described in §4.4.3. The results of fitting the covariates Z_{A1} and Z^s_{B1} for $s \in S_{22}$ are shown in Table 4.4. Before any inference on the parameter values, I investigate only the types which have

$p \lesssim 0.1$, to ensure there is sufficient data to analyse the result (explained further in §4.4.3). This leaves eight types of trees (shown in bold text) and the tree type with the highest parameter value is chestnut where $\exp(\beta_s) = 1.131$.

However, further inspection of the data (Table C.1, Appendix C.4) reveals more conclusions. Firstly, locations containing chestnut and larch were only visited by one pair of birds and their home range resides in a small plantation of woodland, not used by other pairs in the study. To visualise the plantation area, the locations for the pair selecting chestnut and larch are shown in black in Fig. 4.1. Larch is not present in the home ranges of any other pairs making it hard to analyse on a population level as it could mean that either this pair has individual specific tastes or larch wasn't available to other pairs.

There are two locations containing chestnut in the entire study site. The first is in sparse woodland and close to the nest of the pair using the location. The other location contains a chestnut tree that is 40m from the closest nest and alone in an open field. The second location containing chestnut is not visited by any pair, which may be because it requires flying outside of the woodland. Analysing only the seventeen pairs in the natural woodland indicates that the preferred tree type is brambles, which is also the chosen nest species for 11 of the 18 nests.

To understand more about the selection of trees whilst the birds are foraging, the fit of Z_{A1} and Z^s_{B1} is repeated with the set of 811 steps that do not end at the same habitat location as the corresponding nest site (4.2). The results for significant tree types are shown in Table 4.5. This analysis reveals different conclusions for the selection of the tree types, particularly chestnut and brambles. Firstly, chestnut is not included in the analysis, as all steps to chestnut were to

Table 4.4. The results of fitting separate covariate functions for each of the 22 types of trees. The parameter values $\exp(\beta_s)$ and their 95% confidence intervals are shown. Chestnut is found to be the most preferred tree type with $\exp(\beta_s) \approx 1.13$. The fit of a different covariate for each of the recorded 22 tree types is prior to fitting Models 3-8. The fit indicates a subset of tree types, S_r, used to fit further models using the threshold p-value< 0.1 (shown in bold font).

	$C + Z_{A1} + Z_{B1}$			
Covariate for	$\exp(\beta_s)$	$\text{CI}_{95,L}$	$\text{CI}_{95,H}$	p-value
Sycamore	1.008	1.004	1.013	0.00025
Oak	1.009	1.005	1.014	3×10^{-5}
Holly	0.999	0.990	1.009	0.89290
Hawthorn	1.003	0.990	1.017	0.66210
Birch	1.005	0.998	1.012	0.14735
Brambles	1.038	1.023	1.053	4.5×10^{-7}
Alder	1.021	1.007	1.034	0.00217
Ash	0.999	0.987	1.010	0.83263
Lime	1.007	0.993	1.021	0.34301
Beech	1.004	0.996	1.012	0.33832
Willow	1.008	0.997	1.018	0.15242
Hazel	1.015	0.997	1.034	0.09519
Elder	1.018	0.996	1.040	0.10716
Cherry	1.002	0.988	1.017	0.74250
Chestnut	1.131	1.030	1.241	0.00951
Cypress	1.054	0.983	1.131	0.13979
Elm	1.015	0.997	1.033	0.10539
Gorse	0.998	0.971	1.025	0.86591
Larch	1.013	1.006	1.021	0.00036
Rowan	1.012	1.003	1.022	0.01021
Norway Spruce	0.998	0.984	1.013	0.80716
Sikta Spruce	0.974	0.898	1.056	0.51984

Table 4.5. The results of fitting separate covariate functions for each of the 22 types of trees with all steps to the nest location removed. Results are reported for any tree type with p-values less than 0.1 and the tree types are listed in the order of preference indicated by the parameter values with the 95% confidence intervals are shown.

	$C + Z_{A1} + Z_{B1}$			
Covariate for	$\exp(\beta_s)$	$\text{CI}_{95,L}$	$\text{CI}_{95,H}$	p-value
Gorse	1.057	1.020	1.096	0.002
Elder	1.030	1.007	1.054	0.01
Alder	1.026	1.012	1.040	0.0002
Larch	1.019	1.011	1.027	3.6×10^{-6}
Birch	1.010	1.003	1.018	0.007656
Oak	1.010	1.006	1.015	1.9×10^{-5}
Sycamore	1.007	1.002	1.012	4.6×10^{-3}
Brambles	0.941	0.912	0.972	0.0002

the same habitat location as the pair's nest. Therefore the selection of chestnut is likely to be due to the tree type's proximity to the nest, rather than being preferred for foraging. Movement in response to bramble, has now changed to show that whilst foraging the birds are actually selecting locations without bramble. This result again suggests that the apparent selection of bramble in the previous analysis is due to many birds nesting in the plant. Additionally for this reduced data set, the p-values of rowan and hazel are high (> 0.1), indicating that there is not enough evidence to infer the section of these tree types. In conclusion, by analysing all steps that do not end at the nest, I find the birds are selecting for gorse predominately, followed by elder, alder, larch, birch, oak and sycamore in approximately that order.

I performed two alternative model fit procedures using the covariate $Z^s_{B1}(\mathbf{x}_j)$. One analysis uses the data collected over the first 25 days and the other analysis uses data from the second 25 days. The results are shown in Table C.2 in Appendix C.4.2. Oak, alder and elder have significant values in both halves of

the data set. The preference for oak and elder increases by a small amount in the second half of the data set and the preference for alder stays the same.

To conclude, I have found evidence that whilst foraging in the nest building season, the birds are selecting for gorse, elder, alder, larch, birch, oak and sycamore, approximately in that order.

4.5.4 Inferring ways of selecting preferred trees

In this section, I infer how a set of preferred tree types, S_r are selected by a pair of the birds using methods described in §4.4.4. The models are fit to the full data set of 1073 steps as I eventually aim to find a space use model to represent the birds' true movement in the nest building season. Three candidate subsets were trialled to find the best fitting S_r by fitting Models 3-8. I trialled: (a) the preferred tree types indicated by all steps (Table 4.4), (b) the preferred tree types indicated by foraging steps (Table 4.5) and (c) the types of trees in both (a) and (b). All subsets indicated the same best fitting model and the subset described by (c) gave the lowest BIC value of all with a difference of ΔBIC=5 with method (a) and ΔBIC=30 with method (b). Using the subset (c), the set S_{22} is reduced to the subset

$$S_r = \{\text{chestnut, brambles, gorse, elder, alder, larch, birch, hazel, rowan, oak, sycamore}\}, \tag{4.21}$$

Note that while I have shown that birds are not selecting for brambles when foraging, including brambles in a model using all steps fits best. This may be due to many of the nest sites being very close to or inside brambles, as 11 of 18 pairs are nesting in brambles. I further test whether including the actual

Table 4.6. The results for fitting Models 3-8 compared with the null Model 0 and the model with no habitat selection, Model 1. Models were fit using the preferred tree types shown in Equation (4.21). The ΔBIC column shows the difference between the current BIC value and the lowest BIC value. Including both the covariates Z_{B2} and Z_{B4} in the model gives the lowest BIC value, but not by a large difference. There is evidence that Models 4, 7 and 8 all fit the data similarly well.

Model , M	Covariates	Parameters	BIC	ΔBIC
0	C	4	9781	293
1	C, Z_{A1}	5	9547	58
3	C, Z_{A1}, Z_{B1}	16	9550	62
4	C, Z_{A1}, Z_{B2}	6	9492	4
5	C, Z_{A1}, Z_{B3}	6	9512	24
6	C, Z_{A1}, Z_{B4}	6	9507	19
7	C, Z_{A1} , Z_{B2}, Z_{B3}	7	9494	6
8	C^G, Z_{A1}, Z_{B2}, Z_{B4}	7	9488	0

nest tree type into the models with subset (a) gives a better fit than subset (c). I found the fit was not better that the subset (c) with ΔBIC=14.

Models 3-8 were fit by maximising Equation (4.10) and the results are shown in Table 4.6. The best fitting model is Model 8, but there is little difference (see ΔBIC in Table 4.6) between the BIC values for Models 4, 7 and 8. The covariates describing diversity and the spatial cover of trees in the set S_r do not fit as well alone (Models 5 and 6 respectively). However, including a covariate for the presence of any of tree type in the set improves the fit (Models 7 and 8 respectively). I conclude that the birds appear to be moving in response to the set of tree types S_r and there is evidence that the birds choose places because of both the presence of preferred tree types and the spatial cover of tree types in the set S_r (Model 8). By comparing the BIC values of Model 1 and Models 3-8 in Table 4.6, there is evidence towards the birds choosing locations based on the presence of tree types (B2), the diversity of tree types (B3) and the total

cover of trees in S_r (B4). However, there is less evidence towards the birds having a different preference for each percentage cover of tree type in S_r (B1).

Analyses reported in Tables 4.4, 4.5 and 4.6 are repeated with the first step of each path removed to reduce observer bias and the conclusions are shown to be the same in Appendix C.4.3.

4.5.5 The best-fit model

The best fitting model is Model 8, with a set of 11 tree types in the set S_r (Equation 4.21). Model 8 combines the nest covariate $Z_{A1}(\mathbf{x_j}) = |\mathbf{x}_{\text{nest},i} - \mathbf{x}_j|$ with the presence of preferred trees $Z_{B2}(\mathbf{x_j}) = P_S(\mathbf{x})$ and the percentage sum of preferred tree types $Z_{B4}(\mathbf{x_j}) = \sum_{s\in S} T_s(\mathbf{x})$, where $S = S_r$. This model describes the birds preferring locations that are close to the nest, have one or more of the tree types in S_r present, where these have a large magnitude of cover. This suggests that the birds choose locations where the total cover of preferred trees is substantial. The SSF has the form

$$f_i(\mathbf{x}_j, \tau_j|\mathbf{x}_{j-1}) = \frac{\phi(\mathbf{x}_j, \tau_j|\mathbf{x}_{j-1})\Psi_i(\mathbf{B}, \mathbf{Z}_i(\mathbf{x}_j))}{\int_{T_j}\int_\Omega \phi(\mathbf{x}'_j, \tau'_j|\mathbf{x}_{j-1})\Psi_i(\mathbf{B}, \mathbf{Z}_i(\mathbf{x}'_j))\mathrm{d}\mathbf{x}'_j\mathrm{d}\tau'_j}, \tag{4.22}$$

where

$$\begin{aligned}\phi(\mathbf{x}_j, \tau_j|\mathbf{x}_{j-1}) = \exp\Bigg(&\left(\kappa_1 - \frac{1}{\theta}\right)\tau_j + (\kappa_2 + k - 1)\ln\left(\tau_j\right) \\ &+ \left(\kappa_3 + \frac{\mu}{\sigma^2} - 1\right)\ln\left(\frac{|\mathbf{x}_j - \mathbf{x}_{j-1}|}{\tau_j}\right) \\ &+ \left(\kappa_4 - \frac{1}{2\sigma^2}\right)\ln\left(\frac{|\mathbf{x}_j - \mathbf{x}_{j-1}|}{\tau_j}\right)^2\Bigg),\end{aligned} \tag{4.23}$$

$$\Psi_i(\mathbf{B}, \mathbf{Z}(\mathbf{x}_j)) = \exp\left(\beta_1|\mathbf{x}_{\text{nest},i} - \mathbf{x}_j| + \beta_2 P_S(\mathbf{x}_j) + \beta_3\sum_{s\in S} T_s(\mathbf{x_j})\right), \tag{4.24}$$

with dimensionless parameters $\kappa_2 = 0.57$, $\kappa_3 = 0.66$, $\kappa_4 = 0.086$, $\beta_1 = -0.026$, $\beta_2 = 0.47$, $\beta_3 = 0.0053$ and $\kappa_1 = -0.0011\text{s}^{-1}$.

4.6 Calculating space use

One way of calculating a utilisation distribution for a pair of long-tailed tits is to simulate Equation (4.22). However this would be computationally expensive, particularly with sampling non-constant step times as well as step headings and step lengths. Instead I use results from Moorcroft and Barnett (2008) and Potts and Schlägel (2020) to parametrise a diffusion-taxis equation using the parametrised best-fit SSF. The resulting diffusion-taxis equation is solved to calculate the steady-state and therefore obtain a utilisation distribution for each pair.

I show the derivation of a diffusion-taxis equation from an individual-based model (IBM) in Appendix A.1. In this derivation a redistribution kernel is used to define the probability of moving from location $\mathbf{x}$ to another location $\mathbf{x}'$. The redistribution kernel builds a diffusion-taxis equation and the diffusion and taxis coefficients (Equations A.6 and A.7 respectively) are dependent on the form of the redistribution kernel. Potts and Schlägel (2020) derived the diffusion and taxis coefficients for a diffusion-taxis equation where the redistribution kernel is equal to a SSF. I use their result to parametrize a diffusion-taxis equation using the SSF in Equation (4.22). The variables $(\mathbf{x}_{j-1},\mathbf{x}_j,\tau_j)$ from §4.1-4.5 are redefined to be $(\mathbf{x}', \mathbf{x}, \tau)$, for notational purposes.

A general SSF for a pair i, for non-constant step times, has the form

$$f_i(\mathbf{x}|\mathbf{x}',\tau) = \frac{\phi(\mathbf{x},\tau|\mathbf{x}')\Psi_i(\mathbf{x})}{\int_{\Omega_i}\int_T \phi(\mathbf{x}'',\tau'|\mathbf{x}')\Psi_i(\mathbf{x}'')\mathrm{d}\mathbf{x}''\mathrm{d}\tau'}, \tag{4.25}$$

where Ω_i is the landscape that is available to pair i and T is the set of all possible step times that the pair could move from $\mathbf{x}'$ to $\mathbf{x}''$. The habitat-selection function is kept general, so that the appropriate function for each of the Models 3-8, can be inserted into the diffusion-taxis equation and has the form

$$\Psi_{i,M}(\mathbf{x}) = \exp\left(\mathbf{B}\cdot\mathbf{Z}_{i,M}(\mathbf{x})\right). \tag{4.26}$$

The derivations in Moorcroft and Barnett (2008) and Potts and Schlägel (2020) require a movement kernel that does not vary with time. Here the movement kernel is integrated over all possible step times from $\mathbf{x}$ to $\mathbf{x}'$ to give

$$\phi_{\delta t}(|\mathbf{x}-\mathbf{x}'|) = \int_0^\infty \phi(|\mathbf{x}-\mathbf{x}'|,\tau)\,\mathrm{d}\tau, \tag{4.27}$$

where δt is the now a constant step time for moving from $\mathbf{x}'$ to $\mathbf{x}$. The redefined SSF has the form

$$f_{\delta t,i,M}(\mathbf{x}|\mathbf{x}') = \frac{\phi_{\delta t}(|\mathbf{x}-\mathbf{x}'|)\Psi_{i,M}(\mathbf{x})}{\int_{\Omega_i}\phi_{\delta t}(|\mathbf{x}''-\mathbf{x}'|)\Psi_{i,M}(\mathbf{x}'')\mathrm{d}\mathbf{x}''}. \tag{4.28}$$

Following the derivation in Appendix A.1 with $p(\mathbf{x}|\mathbf{x}') = f_{\delta t,i,M}(\mathbf{x}|\mathbf{x}')$ (Equation A.1), I arrive at the diffusion-taxis equation (A.5). The functions $\mathbf{A}(\mathbf{x},t)$ and $D(\mathbf{x},t)$ (Equations A.6 and A.7 respectively) are derived in Potts and Schlägel (2020) and lead to the diffusion-taxis equation

$$\frac{\partial u_{i,M}}{\partial t} = D_{\delta t}\nabla^2 u_{i,M} - 2D_{\delta t}\nabla \cdot \left[u_{i,M}\nabla\left(\mathbf{B}\cdot\mathbf{Z}_{i,M}(\mathbf{x})\right)\right], \tag{4.29}$$

where $u_{i,M}(\mathbf{x},t)$ is a utilisation distribution for pair i for model M and $D_{\delta t}$ is a constant found by integrating the movement kernel over space and taking the limit as $\delta t \to 0$. Lastly, Potts and Schlägel (2020) show that there is a steady-state solution of Equation (4.29), found by inspection when

$$u^*_{i,M}(\mathbf{x}) = K^{-1}\exp\left(2\mathbf{B}\cdot\mathbf{Z}_{i,M}(\mathbf{x})\right), \tag{4.30}$$

where K is a normalising constant. Equation (4.30) gives an explicit utilisation distribution for each pair of birds. The utilisation distribution depends only on $\mathbf{B}$ and $\mathbf{Z}_{i,M}$ and these were parametrised in §4.5. Fig. 4.6 shows the utilisation distributions for Model 8 and Model 3 and all other Models are shown in Appendix C.5.

4.7 Summary

In this Chapter, I apply integrated step-selection analysis (iSSA) to a population of nest building passerines. Data were collected in the nesting season and this bias is accounted for by including a preference for locations close to the nest site whilst investigating movement in response to the woodland structure.

I test two hypotheses regarding the nest location: (A1) a preference for locations closer to the nest (Equation 4.11) and (A2) a preference for turning back to the nest when far away from the nest (Equation 4.12). The model describing

the former is a much better fit, therefore, further models include a covariate describing a preference for locations close to the nest.

Analyses of habitat selection in response to the percentage estimate of 22 types of trees initially aims to understand the birds preference for each type of tree separately. Birds show significant preference for eight tree types (chestnut, brambles, alder, hazel, larch, rowan, oak, sycamore). However, some of this preference is biased by movement towards the nest site. Once I control for this, by removing any steps that ended at the nest site, I find that gorse is the most selected tree type followed by elder, alder larch, birch, oak and sycamore in that order.

As well as investigating the preference for a particular tree type, I also examined three different hypotheses regarding how the structure of woodland affects movement decisions. In particular, I examined which of the following explains best the birds' movements: (a) the percentage cover of each tree type separately, (b) the presence or absence of "preferred trees", (c) the tree diversity, measured as the number of preferred tree types present, (d) the percentage cover consisting of any of the preferred trees. The resulting model selection procedure indicated that both the presence and total percentage of preferred tree cover explain movement decisions best (Table 4.6). However, the ΔBIC values were not large, suggesting the model selection procedure was unable to separate these competing hypotheses with high confidence.

Lastly, the utilisation distributions for each of the models are calculated for nine pairs of long-tailed tits. The plots for the best fitting model (Model 8) and the worst fitting model (Model 3) are shown in Fig. 4.6 (Models 4-7 are shown in Appendix C.5).

In conclusion, there is evidence that whilst nest building the birds are selecting predominantly gorse and to a lesser extent elder and alder with little selection of oak and sycamore. Previous to the study in this Chapter it was thought that in this season the birds were selecting for mostly oak (B.J. Hatchwell, pers. obs.) and sycamore (Gaston, 1973). Yet, further field work is required to understand the differences in foraging selection whilst provisioning nests and whilst flocking in the non-breeding season. I discuss the implications of this Chapter, alongside previous research in Chapter 5.

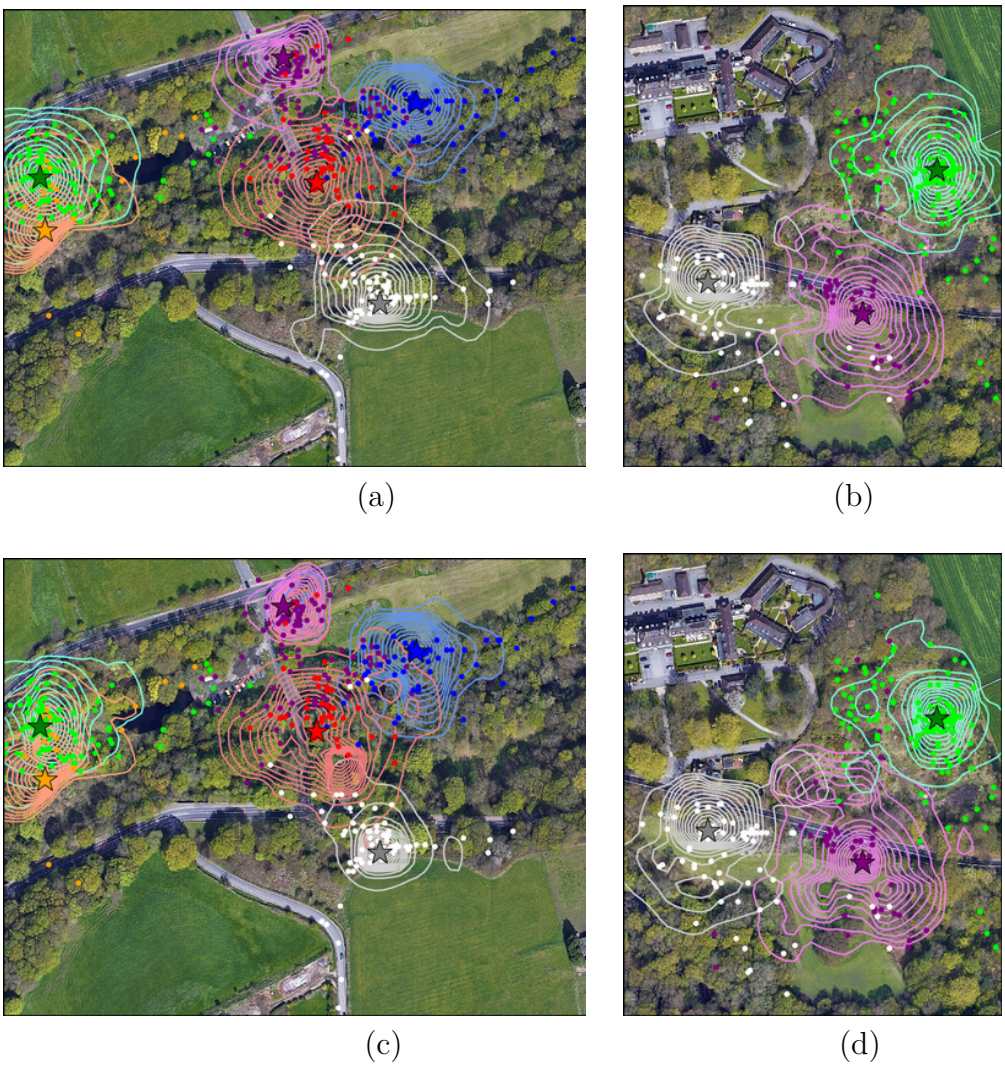

Fig. 4.6. Utilisation distributions (Equation 4.30) for nine pairs of long-tailed tits calculated from fitted SSF functions. The top panels show the utilization distributions as contour plots as described by the best-fit model, Model 8. Corresponding locations for each pair are shown as dots in a similar colour to the contour lines and nest locations are shown using a star icon. The bottom panels show the utilization distributions for the same pairs using a lesser fitting model, Model 3. Model selection was conducted by comparing BIC values.

Chapter 5

Discussion and conclusions

5.1 Introduction

Mathematical modelling provides tools to evaluate the elaborate interplay between the movement decisions and space use of wild animals, in response to their available landscape and other individuals. I have explored the movement drivers of the space use patterns of long-tailed tits, whilst they live both in flocks and as nest building pairs. Here, I discuss the implications of these findings and further directions.

Home ranges are often produced using descriptive methods in ecological studies (Carter et al., 2013; Coleman and Fraser, 1989; Ferguson et al., 1999; Napper and Hatchwell, 2016), yet stationary home ranges are the outcome of dynamic movement processes (Börger et al., 2008; Moorcroft et al., 1999). This thesis focusses on understanding the behaviours that drive the patterns, rather than analysing just the eventual space use description. The conclusions on long-tailed tit movement behaviour gathered here not only advance our knowledge of

this species, but demonstrate the versatility of mathematical modelling in understanding biological processes, when extensive experimentation is not available.

5.2 A home range model to describe interaction driven space use

Observations of long-tailed tits from a previous study (Hatchwell et al., 2001a) suggest that there could be a discrete avoidance mechanism between flocks that causes their home ranges to consist of exclusive areas of space use and overlaps (Fig. 3.1). In Chapter 2, I extended and analysed a mechanistic space use model (Potts and Lewis, 2016a) to describe flocks avoiding places they had interacted with other flocks in the past.

Analysing each flock's movements with the simultaneous movements of other flocks by parametrising an individual-based model (IBM, Giuggioli et al. 2011; Railsback and Grimm 2011), may be a natural first step in understanding interaction-driven movements for a species where numerous animals are able to be tracked simultaneously (Kernohana et al., 2001; Macdonald et al., 1979). Long-tailed tits are too small to be GPS tagged, instead the birds are followed and data is collected by direct observations (Napper and Hatchwell, 2016). Researchers observing the long-tailed tits cannot record the movements of flocks simultaneously without a large number of field assistants. To overcome a similar problem, Potts et al. (2014a) parametrised an IBM using the movements of flocks of birds which were not simultaneously tracked, however these birds were conspicuous and the model assumed that each flock could always detect the movements of other flocks. The home ranges of flocks of long-tailed tits

are too large, relative to their approximated perceptive radius to assume that they can always detect the movement of other flocks. Therefore, parametrising an IBM for the movements of each flock in response to other flocks would mean simulating the model and fitting to the overall space use. This would be extremely computationally expensive, such that this approach would not be practically viable.

A partial differential equation (PDE) model of space use can be obtained by scaling an IBM and forming a diffusion-taxis equation. This method has the advantage of being able to obtain a deterministic pattern of space use from underlying stochastic movement rules. The corresponding space use pattern can then be fit to location data. This process of forming a diffusion-taxis model and fitting to location data is named mechanistic home range analysis (MHRA, Moorcroft and Lewis 2006). Instead, the movement of flocks in response to other flocks can be modelled in the underlying movement processes of the diffusion-taxis equation. I extended the one-dimensional memory driven PDE model introduced by Potts and Lewis (2016a) into two dimensions, redefining the territorial conflicts as conspecific interactions and defining it as the interaction model.

After forming the interaction model, I discovered that in two dimensions there are numerical complexities not observed in the one-dimensional system. In particular there may be a surface of stable *steady-state* solutions that can lead to the numerical approximation of the model not finding a steady-state. By visually analysing the numerical solution through time, it is revealed that the numerical solution moves close to a steady-state then shifts towards another, without settling on one. To overcome this problem, the dynamic cognitive map of each flock was stopped from evolving when the space use solution

reached a point in time which is estimated to correspond to the steady-state of the given initial condition. Specifically, this is when a threshold value for the average value of the cognitive map is reached. I later showed that this method provides a suitable home range model for the birds, however the shortcoming is that the method relies on the threshold value. This value was estimated by searching through a range of values and comparing them with the utilisation distributions visually. Keeping this value constant and varying the parameter γ (controlling taxis away from the interaction zone), produces variations in the spatial overlaps of the utilisation distribution of each flock (Fig. 2.7). The threshold value is kept constant in the later fitting procedures, but more detailed investigations are required to determine the best way of choosing this threshold value. Furthermore, numerical investigations into different approximation methods of the differential equations are required to understand the most efficient and accurate way to estimate the steady-state of the interaction model. For example, using the method of lines (Schiesser, 1991) or trialling an alternative approximation of the taxis term as in Gerisch and Chaplain (2006) may lead to a system which describes the stable steady-states more accurately than the approximation of the diffusion-taxis system using finite-differences. Moreover, additional investigation is required to understand if these techniques are necessary when extending other diffusion-taxis models to more than one dimension. One particular example is the scent marking model of Potts and Lewis (2016b), where a diffusion-taxis equation models space use in response to a dynamic map of scent marks, similar to the cognitive map of interactions. For the scent marking model, numerical stable steady-states of the one-dimensional system are found, however the two-dimensional system is not investigated.

It is common in spatial studies to infer conspecific behaviour using the overlaps of home ranges that are estimated with statistical methods, such as a kernel density estimation (KDE) or a MCP (Fieberg and Kochanny, 2005). Such studies have indicated that there are effects of kinship (Oli et al., 2002), body size and population density (Pearce et al., 2013) on the overlaps for various study species. In particular, Hatchwell et al. (2001a) used a convex peeling technique to infer the effects of kin on this population of long-tailed tits. Whilst these descriptive studies reveal a relationship between conspecifics and space use, space use is an outcome of movement. Therefore, modelling the underlying movement process, as the interaction model does, is necessary to reveal explicit behavioural drivers of animals. Nonetheless, these studies have merit in indicating the necessity for investigations using mechanistic modelling or more detailed experimentation.

The interaction model is able to capture the patterns of exclusive areas and overlaps, from underlying behavioural mechanisms observed in this population of long-tailed tits. The steady-state solutions shown in Fig. 2.7 show such home range patterns and how they vary with different values of the parameter γ (taxis away from the interaction zone). These solutions indicate the suitability of the interaction model for forming non-territorial home ranges, prior to fitting to data. In the interaction model, flocks move in response to the average value of their cognitive map of interactions, over a disc. For simplicity, perception is assumed to be a binary quantity: perceived within the δ-disc and not perceived outside this disc. However, it would also be possible to consider other non-local formalisms, such as exponential decay (Avgar et al., 2015).

Overall, the methods detailed in Chapter 2 not only introduce a two-dimensional version of an existing PDE system to model non-territorial space use without

an attractive potential, but also demonstrate the possible complexities of numerically solving such PDEs in two dimensions. Furthermore, the methods present a detailed example of moving from a two-individual one-dimensional system, often seen in the literature (Fagan et al., 2020; Potts and Lewis, 2016b), to a multi-individual, two-dimensional system, required to fit to data.

5.3 The home range drivers of flocks of long-tailed tits

The interaction model provides a suitable base model to describe taxis driven by the memory of conspecific interactions. Chapter 3 is dedicated to extending the model to include interactions with the environment. Previous studies (Gaston, 1973; Hatchwell, 2016) indicate that long-tailed tits prefer to forage in woodland and visually this idea agrees with the recorded locations (e.g. Fig. 3.1). In Chapter 3, I discovered that the interaction model fits the data well when coupled with an attraction to the centre of woodland and avoidance behaviour in response to relatedness and flock size.

I extended the interaction model to include different ways of modelling taxis towards the woodland, by modelling the woodland as simply being present or absent. The best-fit mechanistic home range analysis (MHRA) models all describe taxis towards the centre of woodland and this result was consistent through seasons. The discovery that flocks prefer foraging in the centre of woodland was not considered in previous studies (Hatchwell et al., 2001a; Napper and Hatchwell, 2016) and this conclusion means future data collection can be initially focused in central areas to save time. Possible hypotheses result from this central foraging behaviour. First, it may be related to avoiding

predation, as studies on several taxa indicate that foraging in the centre of woodland habitats provides greater protection from predators (Angkaew et al., 2019; Hansen et al., 2019; Valentine et al., 2019). However some studies reported the reverse, that there is lower predation risk in edge habitats when compared with the centre (Newmark and Stanley, 2011; Šálek et al., 2010). A second hypothesis for the birds foraging in the centre of woodland is a potential difference in food availability or quality (Rosli et al., 2018; Terraube et al., 2016). These hypotheses call for further investigation, but quantifying the predation rate in the non-breeding season and sampling food availability for insectivores feeding at canopy level requires extensive data collection. Hence, the mechanistic modelling techniques used in this study demonstrate their worth in uncovering such behaviours otherwise only discovered by considerable amounts of field work.

Attraction to the centre of woodland coupled with memory mediated conspecific avoidance mechanism models the data well (Fig. 3.5). The avoidance behaviour appears to act as a proxy for territoriality, causing distinct home ranges to form without requiring directly-observable aggressive behaviour. Yet, the question of why flocks avoid each other remains unanswered. I offer three hypotheses regarding the avoidance behaviour, with the first being that flocks are avoiding antagonistic social interactions (Sharp et al., 2005) so that there is no need to defend territories. Simulations of intrusive birds entering long-tailed tit flocks using playback experiments prompt small amounts of aggression that may deter interactions (Napper and Hatchwell, 2016). The best-fit MHRA model indicates that small flocks are more likely to avoid large flocks, which would make sense if the birds intend to avoid aggression. Avoidance dependent on group size appears to be unusual among social vertebrates, perhaps since

the exclusive space use of these non-territorial birds is rare. Yet this behaviour is seen in territorial gray wolves (*Canis lupus*, Brandell et al. 2020) and models of battles between social insect colonies, where the outcome of conflicts over space may be determined by relative colony size (Adams and Plowes, 2019; Adler et al., 2018).

Secondly, it is possible that living in large flocks is an effective anti-predator strategy and that the flocks separate to optimise some energetic maximum (Pulliam and Caraco, 1984). Flocking to limit individual risk of predation is commonly observed in ornithological studies. For example in chaffinches (*Fringilla coelebs*, Lindström 1989) and mixed flocks (Gaddis 1980), sometimes the size of flocks (Cresswell 1994; Siegfried and Underhill 1975; Vine 1973) or particular flocking structures affect predation risk (Carere et al. 2009; Procaccini et al. 2011).

A final explanation for the conspecific avoidance between flocks is a potential social benefit in strengthening relationships within flocks for the later breeding season. Long-tailed tits are cooperative breeders and their helping behaviour is kin-selected (Hatchwell et al., 2014; Leedale et al., 2018; Russell and Hatchwell, 2001). Helping decisions in the breeding season are influenced by association during the non-breeding season (Napper and Hatchwell, 2016), where vocal cues are learnt for recognition (Sharp et al., 2005). Therefore maintaining contact with kin whilst flocking during the non-breeding season, and avoiding diluting those relationships by recurrent interactions with non-kin in other flocks, may lead to greater breeding success. Extending the best-fit MHRA model to include avoidance dependent on kin shows that flocks are less likely to avoid other flocks that they are related to and supports the idea that separate flocks are socially beneficial. A positive relationship between home range overlap

and kinship has been previously observed in the study population (Hatchwell et al., 2001a) as well as in several other taxa, including mammals (Sera and Gaines, 1994; Støen et al., 2005; Walker et al., 2008), lizards (While et al., 2009) and fish (Griffiths and Armstrong, 2002). Thus, the mechanistic description of avoidance dependent on kin may also drive the space use of many animal species.

The memory capacity of small passerines is hard to quantify or test biologically, as little is known about the cognitive abilities of small birds in general, regardless of species (Emery, 2006). However the models in the MHRA suggest that flocks remember visual or vocal interactions and choose to avoid those places in the future. Even a visual analysis of the location data suggests the birds must have a capacity for memory to enable the boundaries of the home ranges. Without memory, birds would only respond to present interactions and this would not explain the segregated patterns. Therefore, including memory as an indirect inferred behaviour is often necessary and has an abundance of previous applications (Avgar et al., 2015; Fagan et al., 2013; Merkle et al., 2014, 2017).

The mechanistic models used in this section could theoretically be further analysed using posterior predictive checks, e.g. simulating replicated data using the fitted model and comparing it to the real data. Here this could be done by sampling locations from the utilisation distribution with some variation on the parameters, known as bootstrapping. One of the reasons this hasn't been done here is that the computational time required to perform such analyses is infeasible, likely taking years to obtain 95% confidence interval, despite being coded in C++. Instead, plotting the utilization distributions over the location data, (e.g. Figure 3.5b) gives evidence towards the home range models being a good fit.

One advantage of diffusion-taxis models for studying home range patterns is that they allow users to reveal the behavioural decisions that can give rise to the recorded space use patterns, using independent recorded locations. These mechanistic methods are in contrast with statistical models that only give descriptors of the home range, such as the methods of MCPs and KDEs. An alternative way to estimate home ranges with mechanistic origins is to correct for the bias due to autocorrelation in KDE, namely autocorrelated kernel density estimation (AKDE, Fleming et al. 2015). Inferring behaviour based on the overlap of home ranges predicted by AKDE (Winner et al., 2018) uses movement in an attempt to improve on the statistical estimates of KDE, but the method does not incorporate explicit behavioural processes into the underlying movement model. Therefore, AKDEs are unable to make inferences about specific behavioural drivers of space use. That said, AKDE's advantage over MHRA is that it allows for autocorrelation in movement. A combination of AKDE and MHRA may emerge as the way forward, allowing for both behavioural mechanisms and autocorrelation in an efficient way, but this is highly non-trivial and has yet to be forthcoming.

Some aspects of movement can be included into home range analysis using Brownian bridge methods by assuming that movement between locations is Brownian motion (Horne et al., 2007). Furthermore, the biased Brownian bridge (Benhamou, 2011) incorporates taxis movement into the Brownian motion. The diffusion-taxis models developed in Chapters 2 and 3 are based on a diffusion-taxis equation which results in a utilisation distribution for biased Brownian motion. Therefore, combining the two methods by including behaviourally-informed interpolations of space use between successive recorded locations fixes may be a natural next step.

In previous MHRA studies, models describe an attraction towards a central place or territoriality (Bateman et al., 2015; Moorcroft and Lewis, 2006; Moorcroft et al., 1999), behaviours which are not observed by long-tailed tits outside the breeding season. The application of MHRA in this thesis not only advances avian ecology by uncovering the effects of conspecific avoidance and foraging in the centre of woodland areas, but also shows how the best fit MHRA model can be used to expose more subtle behaviours, such as the effects of kinship and flock size. This study demonstrates not only the flexibility of MHRA but that it can be used to uncover behaviours in animal species that traditional statistical methods can not.

5.4 The woodland habitat drivers of pairs of long-tailed tits

Succeeding the study in the non-breeding season, I explored how pairs of nest building long-tailed tits use their woodland habitat selectively, depending on the available tree types in their home range. For the study in the non-breeding season, the birds' directed-movement within woodland was modelled as either undirected or towards the centre of the woodland area. Thus the complex distribution of tree species in the Rivelin Valley was not accounted for. In Chapter 4, I showed that long-tailed tits use their habitat selectively, preferring to forage in particular types of trees rather than others by analysing movements using integrated step-selection analysis (iSSA, Avgar et al. 2016). Subsequently, a mechanistic space use model was defined that included a mechanism to describe an attraction to the nest site. Similar to the study in the non-breeding season, these analyses used methods to infer behaviours based on reasonably

coarse location data, in comparison to animals fit with tracking devices. Here I discuss the results and implications of the study.

In this study, the movements of long-tailed tits in the nesting season were analysed as the pairs are easier to follow at this time of year due to their fidelity to the nest. I first asked if there were particular types of trees that the birds prefer to forage in. I found that the birds are predominantly selecting the tree type gorse followed by elder, alder, larch, birch, oak and sycamore. A previous study by Gaston (1973) suggested that nest building long-tailed tits in a study site 120 miles from the Rivelin Valley prefer to forage in sycamore when compared with oak and ash. However, these conclusions were based on measurements of time spent in the tree species and did not account for availability related to the birds current location or the magnitude of the tree cover. I additionally found that whilst foraging, pairs are not selecting locations with brambles, known to be the preferred nesting species of many pairs. An avoidance of brambles could be due to removal of all the movements towards the nest. Or further reasons, such as a lack of foraging benefit or the reluctance to enter other birds' nest areas due to attracting predators, as found in field sparrows (*Spizella pusilla*, Burhans 2000).

In the nesting season, long-tailed tits are cooperative breeders and the birds are much more likely to help pairs they are related to (Russell and Hatchwell, 2001). I found that one pair (shown in black in Fig. 4.1) appeared to select mostly chestnut and larch, which were not available to the rest of the pairs. However the selection of the location containing chestnut was unable to be untangled from visits to the nest. This finding leads to more questions aimed at understanding whether or not this pair is using chestnut. If so, whether the preference for both chestnut and larch is due to individual differences or the

lack of the tree types in other areas. Another question to ask is why this pair chose to build their nest in a location with quite different trees to the other pairs in the study site. One possible explanation is that this was the only safe chestnut tree to use (being small and inside woodland). This leads to another hypothesis, that these birds are unrelated to the other pairs and therefore more likely to nest in the small woodland alone (Hatchwell et al., 2001b; Russell and Hatchwell, 2001; Sharp et al., 2008). Further analysis of long-term data to test whether pairs without relatives breed in more isolated sites than those with nearby relatives would be worthwhile.

Different ways that the birds select for the population's set of preferred trees were explored, where preferred trees were identified for the population using all recorded movements. Four ways selecting tree types based on the percentage cover of the trees at a location were trialled. The ways of selecting the tree types are described as follows: a location is selected based on (a) the percentage of each tree type, each with a different selection parameter, (b) the presence of any tree type, (c) the diversity of tree types and (d) the sum of the percentage cover of all tree types. Comparing the model fit of different combinations of the four mathematical formulae reveals that the birds are predominantly selecting locations due to the presence of any preferred tree and magnitude of cover of the set of preferred trees, with some evidence for movement decisions biased towards locations with more diversity. There is less evidence for a mechanism where the birds are choosing locations based on different preference rates for each tree type, specifically where a different parameter is fit for the selection of each type of tree. The analyses of these data lead to the conclusion that the birds do have preferred tree types, but choose locations based on how much cover those trees have in total rather than the particular type of tree. A preference for a

greater amount of canopy cover and alternative measure of tree size, such as trunk diameter is seen in other insectivore studies (VanderWerf, 1993; Virkkala and Liehu, 1990; Zwicker and Walters, 1999) sometimes alongside a preference for higher density of leaves (Holmes and Robinson, 1981; VanderWerf, 1993).

Mapping out the complex and dense tree species that define the woodland areas in the Rivelin Valley would provide an ideal estimate of habitat availability. However, this would require a comprehensive study, taking a considerable amount of field work over years, as in Fuller and Henderson (1992) and Skroblin and Legge (2012). Instead the birds' habitat-selection was investigated within the descriptively estimated home ranges of each pair a method which is feasible with the availability of field workers and similarly seen in a study on various insectivorous birds (Hodgson et al. 2006).

The advantage of tracking the birds on foot, compared with studies on tagged animals, allows the observer to estimate when the pair's decisions to move were made. Where many previous step-selection analysis (SSA) studies use data taken over constant time intervals (e.g. every 1 minute, Thurfjell et al. 2014), the recorded locations of the long-tailed tits instead correspond with the estimated time of the decision to move. Since the data are recorded over non-constant time intervals, the movement kernel includes a distribution of the time difference in observations as well as spatial measures. I use a recent method by Munden et al. (2020) to include the time difference between locations. However, Munden et al. (2020) estimate decisions to change direction from movement data acquired using accelero-magnetometers (Potts et al., 2018), in contrast to the estimation of decisions from direct observations in Chapter 4.

A space use model was developed by parametrising a SSF that included a preference for places close to the nest so that it captured the pairs' usual movements. It may be that this preference is dependent on time away from the nest. However, it was not known how long each pair had been away from the nest in many of the observations. To approximate home ranges, I use a diffusion-taxis equation to model the utilisation distribution of each flock, moving as described by a movement kernel that is parametrised by the best-fit SSF (Potts and Schlägel, 2020). The diffusion-taxis equation can be analytically solved to produce an explicit space use model. This recently-introduced method provides an accessible way to obtain a utilisation distribution from iSSA. Since the analyses infer parameters at the population level, the model has a predictive use in further seasons, once nests are located and the habitat is mapped. Deriving a diffusion-taxis equation to describe space use resulting from movement defined by the iSSA removes the requirement to perform multiple simulations to estimate space use (Avgar et al., 2016), which are particularly computationally costly when simulating non-constant time steps as well as step lengths.

Long-tailed tits are predominantly insectivorous and the availability of insects depends on the species of tree and the time of year (Moorman et al., 2007; Tellería et al., 1997). A previous study by Gaston (1973) found that the selection of sycamore, oak and ash varied over a 3-4 month period and appears to depend on when the trees come into leaf, similar to that seen in other bird species (Hodgson et al., 2006; Tellería et al., 1997) and mammals (Chamberlain and Leopold, 2000; Dahl, 2005; Rosalino et al., 2005). The data in Chapter 4 were collected over 50 days and by splitting the data in half to give two sets of 25 days I performed the SSA again to investigate differences. I found that

the selection parameter for elder had almost doubled and since elder comes into bud (attracting pre of long-tailed tits) much earlier than the time of data collection, this increase in selection could be due to nest building materials. However some p-values were too high to be analysed (oak was included but not sycamore or ash). Therefore, further observation is required to understand how the habitat selection differs temporally throughout the year.

The study has led to new conclusions on the woodland habitat selection of long-tailed tits, resulting in a predictive model of space use and new behavioural knowledge which can be applied to reduce time spent in field work studies. Where many other studies infer habitat-selection without accounting for movement (McGarigal et al., 2016), the iSSA methods here accommodate movement steps over varying time intervals. I provided a definitive example of flexible modelling methods that may be used to understand more about a species, where the fine scale habitat is mapped and movement decisions can be estimated.

5.5 The next steps for long-tailed tit ecology

Many of the conclusions obtained from methods in this thesis are yet to be explored by further observations and experiments. A preference for foraging in the centre of woodland may be difficult to observe directly, but could be further analysed by interpreting habitat-selection movement paths such as with a SSA. Investigations to understand potential edge effects on the predation rate of adults and juveniles would be very worthwhile, but it is complicated to understand these edge effects on possible predation rate outside of the nesting season due to immigration and natural deaths. However, a study is

currently being conducted by Ben Hatchwell on the effects of habitat type on nest predation rate.

Measuring directly the tendency of flocks to avoid one another would require analysis of synchronous observations of many flocks, which is a difficult task for field work. Simulated interactions using the playback of calls from birds in neighbouring flocks offers an experimental alternative to direct observation of interactions (Napper and Hatchwell, 2016), but these are difficult to conduct and suffer from a number of flaws. Instead, MHRA provides a way of making such inferences with much less data.

The conclusions generated for the long-tailed tits are at the population level and individual differences are not specifically analysed. There are various reasons for this. First, in the MHRA of Chapter 3 I inferred the values of six parameters when fitting models. If I instead estimated different parameters for each flock, these parameters would have increased by a multiple of the number of flocks. For context, fitting a model with six parameters takes on average 13±4 hours (mean ±95% CI), however this depends on the the machine used (the machine used here is described in Appendix A.4). Secondly, flocks do not reform year on year so understanding population level drivers is more useful for understanding the space use of flocks in future years.

The computational time for fitting the step-selection models of Chapter 4 for the nest building pairs is much quicker compared with MHRA and individual level inference is much more viable (e.g. Osipova et al. 2019; Prokopenko et al. 2017). The reason I fit models to the steps of the population, rather than individual pairs, is because of the amount of available data and the predictive capability of models. In general, individual differences in movement behaviour

are notable and common throughout animal species (Nilsson et al., 2014) and it may be worthwhile understanding the extent of individual differences within long-tailed tits to estimate the variability of population-level results.

A considerable amount is already known about the social behaviour of the Rivelin Valley long-tailed tits in the breeding season due to extensive genetic studies, behavioural and life history observations and experiments. Related pairs are generally more likely to nest close to each other (Hatchwell et al., 2001b; Leedale et al., 2018; Russell and Hatchwell, 2001; Sharp et al., 2008) and a study on the relatedness of the pairs in Chapter 4 could uncover more. However, further studies are currently being conducted by Ben Hatchwell to investigate the relationship between the spatial overlap of the non-breeding flocks and the corresponding breeding ranges, alongside the interplay of the social and spatial relationships between seasons, as in a study on great tits (*Parus major*, Firth and Sheldon 2016).

Since food resources appear to be abundant in the Rivelin Valley, further investigation is required to understand what may limit the species' population density. Cold weather has been shown to reduce the birds' survival, indicating they may benefit from the changing climate (Gullett et al., 2014). Furthermore, a study on multiple passerines, including the Rivelin Valley long-tailed tits suggests that when close to the carrying capacity the population density is dependent on mortality (Sæther et al., 2016). Furthermore, at lower densities the population equilibrium is more influenced by stochastic environmental variation driving recruitment (Sæther et al., 2016).

In summary, the studies in this thesis have indicated that long-tailed tits avoid other flocks in the non-breeding season, prefer foraging in the centre

of woodland and in particular types of trees. Moreover, the population level analyses have led to the conclusions and models having predictive capabilities for future data collection. These investigations have led to further questions about seasonal and individual differences in habitat selection, the social and spatial interplay of the population through seasons, and further examination of the avoidance mechanism in the non-breeding season.

5.6 Using these methods to understand other animal species

The mechanistic modelling techniques applied to this specific population of long-tailed tits may also be used to understand the behaviours of further animal species, which I give non-exhaustive examples of here. Perhaps the most obvious species to benefit from these methods are those which are unable to be tagged with GPS devices such as small birds and bats (Kays et al., 2015). In particular, species with conspecific-influenced space use distributions can prosper from the MHRA methods. Furthermore, studies where species are directly observed may be able to uncover behaviours using the iSSA methods by recording data as decisions to move are detected.

The correlation between relatedness and home range structure is also observed in taxomically different species to long-tailed tits, for example bottlenose dolphins (*Tursiops truncatus*, Frère et al., 2010) and giraffes (*Giraffa camelopardalis*, Carter et al., 2013). Understanding the behavioural drivers of these species using MHRA may require quite similar models to those in Chapters 2 and 3. Moreover, the MHRA methods in this thesis demonstrate the flexibility of the models and by altering the taxis term these approaches can be applied to

understand many other home ranging species. Non-territorial species such as polar bears (*Ursus maritimus*, Ferguson et al., 1999) and vultures (Coleman and Fraser, 1989) both live in non-exclusive home ranges which could be understood using MHRA by building an alternative taxis term. For example, instead of movement drivers describing avoidance of other individuals of the same species one could model taxis towards prey or a desirable environment. Vultures are particularly interesting as they are attracted to a central place which is related to their age (Coleman and Fraser, 1989), so an attraction parameter could be introduced which is dependent on age.

Similar to the Rivelin Valley population, long term studies on the apostlebird (*Struthidea cinerea*, Griesser et al. 2009) and fairy wrens (*Malurus elegan*, Brouwer et al. 2014) use direct observations to understand space use of flocks and may benefit from the methods used in this thesis. Locations of animals without GPS tags are further obtained using alternative methods than direct observations, for example using camera traps (Gelardi et al., 2020; McCarthy et al., 2019) or proximity devices (Firth et al., 2018), often for studies on social networks. By using the the spatial locations of these recording devices, the MHRA methods described in this thesis could be used to understand behaviours leading to space use.

Step-selection studies have a range of applications in the literature and many previous models estimate space use using extensive simulations (Osipova et al., 2019; Thurfjell et al., 2014). These studies can take advantage of the method of Potts and Schlägel (2020) by instead obtaining a utilisation distribution using the method of parametrising a diffusion-taxis equation, saving copious computational time. Comparisons of the utilisation distributions obtained from short term simulations and a parametrised habitat selection function

are conducted in Signer et al. (2017). It would be interesting to perform a similar comparison with short term simulations obtained with variable and non-variable step time and the utilisation distribution obtained from parametrising a diffusion-taxis equation using a SSF.

In previous animal tracking experiments, successive animal locations are predominantly recorded over constant time intervals (Tucker et al., 2018). The time variant methods used in Chapter 4 (Munden et al., 2020) demonstrate a simple way to analyse locations recorded as animals make a notable decision to move, influencing more studies to record direct observations in this way. Studies on long distance movements for ringed birds with a long-life expectancy may also benefit (du Feu et al., 2016). Ringed birds are often observed or briefly captured intermittently throughout their life e.g. (Ambrosini et al., 2014; Thorup et al., 2014) and data is recorded in encounter databases such as EURING (du Feu et al., 2016). These individuals may take advantage of the methods in Chapter 4 by treating each successive observation as a step and comparing with alternative large scale habitats.

5.7 Final remarks

The studies in this thesis exemplify how mechanistic modelling can be used to infer the life-history behaviours of animals, given observation data. I presented the first known application of MHRA for a non-territorial species with no central attraction, revealing instead the behaviours of kin and group size led avoidance. Fine scale habitat-selection was explored using iSSA techniques, revealing the preferred foraging trees of long-tailed tits with a novel method of analysing the birds' movement decisions. The models in this thesis have not

only advanced avian biology but additionally illustrate flexible methods for further taxa to readily benefit from these mechanistic techniques.

Glossary

availability kernel a kernel which takes the same form as the movement kernel in step-selection analysis, where parameters fit from the distribution of movement attributes in the data, first = *availability kernel*.

available step a step (linear displacement between two locations) which could have been taken instead of a step in the data. This has the same starting location but a different end location as the step in the data which it corresponds to.

cognitive map a representation of an animal's landscape in the animal's memory.

diffusion the movement of a density from a region of high concentration to a region of low concentration. In this thesis, diffusion describes the movement of the probability density of a utilisation distribution from a high concentration to a low concentration. The process is an approximation a stochastic random walk..

diffusion-taxis equation a partial-differential equation describing the change in a utilisation distribution through time and space with a diffusion term and a taxis term.

habitat location a location at the centre of a 25 by 25m square where the percentage of 22 species of tree were estimated.

habitat-selection function a function describing the selection and distribution of attributes of the available habitat.

home range a finite area of a larger available landscape which an animal chooses to live in as it has all the resources to fulfil its life history needs.

interaction model a system of partial-differential equations where a diffusion-taxis equation describes space use and the taxis is driven by a dynamic cognitive map of interactions.

interaction zone a part of a flock's landscape that it is likely to avoid due to previous interactions.

kinesis the speed of movement of an organism as a response to a stimulus at a location.

long-tailed tit a small European passerine, here they are studied in the Rivelin Valley, Sheffield in non-breeding flocks and breeding pairs.

mechanistic a description of something that is determined by its underlying process or mechanics.

movement attribute calculated movement measurements, for example step length, step time, step speed and step heading.

movement kernel a function describing the movement capabilities of an animal.

path a sequence of successive movements (steps).

perceptual range the maximum distance which an animal can perceive the local habitat where it currently resides.

significant movement the movement of a pair of long-tailed tits (Chapter 4) that is more than 10m from their previously recorded location.

steady-state the point at which the solution to a differential equation stops changing through time.

step the linear displacement between two locations.

step length the distance between two locations in metres.

step speed the step length (distance between two locations) divided by the step time (time difference between two recorded locations).

step time the time difference between two recorded locations in seconds.

taxis the directed movement of an organism as a response to a stimulus at a location.

tree type a general group of tree or shrub species recorded in the study, for example oak, sycamore.

turning angle the angle turned through from the heading of one step to the heading of the next.

used step a step (linear displacement between two locations) recorded in the data.

utilisation distribution a probability density function for the location for an individual or group of individuals at a given region in space and time.

weighting function a function describing the selection and distribution of attributes of the available habitat and movement to be used to fit a step-selection function.

References

Adams, E. S. and Plowes, N. J. (2019). Self-organizing conflicts: Group assessment and the spatio-temporal dynamics of ant territory battles. *Behavioural Processes*, 162:119–129. doi:10.1016/j.beproc.2019.01.009.

Adler, F. R. et al. (2018). Mechanistic models of conflict between ant colonies and their consequences for territory scaling. *American Naturalist*, 192(2):204–216. doi:10.1086/698121.

Allen, M. et al. (2001). Fine-scale habitat selection of foraging bottlenose dolphins Tursiops truncatus near Clearwater, Florida. *Marine Ecology Progress Series*, 222:253–264. doi:10.3354/meps222253.

Ambrosini, R. et al. (2014). Modelling the progression of bird migration with conditional autoregressive models applied to ringing data. *PLoS ONE*, 9(7):e102440. doi:10.1371/journal.pone.0102440.

Angkaew, R. et al. (2019). Nesting near road edges improves nest success and post-fledging survival of White-rumped Shamas (*Copsychus malabaricus*) in northeastern Thailand. *Condor*, 121(1). doi:10.1093/condor/duy013.

Aurenhammer, F. (1991). Voronoi diagrams—a survey of a fundamental geometric data structure. *ACM Computing Surveys (CSUR)*, 23(3):345–405. doi:10.1145/116873.116880.

Avgar, T. et al. (2015). Space-use behaviour of woodland caribou based on a cognitive movement model. *Journal of Animal Ecology*, 84(4):1059–1070. doi:10.1111/1365-2656.12357.

Avgar, T. et al. (2016). Integrated step selection analysis: Bridging the gap between resource selection and animal movement. *Methods in Ecology and Evolution*, 7(5):619–630. doi:10.1111/2041-210X.12528.

Ball, P. (2015). Forging patterns and making waves from biology to geology: a commentary on Turing (1952) 'The chemical basis of morphogenesis'. *Philosophical Transactions of the Royal Society B: Biological Sciences*, 370(1666):20140218. doi:10.1098/rstb.2014.0218.

Bastille-Rousseau, G. et al. (2015). Unveiling trade-offs in resource selection of migratory caribou using a mechanistic movement model of availability. *Ecography*, 38(10):1049–1059. doi:10.1111/ecog.01305.

Bateman, A. W. et al. (2015). Territoriality and home-range dynamics in meerkats, *Suricata suricatta*: A mechanistic modelling approach. *Journal of Animal Ecology*, 84(1):260–271. doi:10.1111/1365-2656.12267.

Benhamou, S. (2011). Dynamic approach to space and habitat use based on biased random bridges. *PLoS ONE*, 6(1):e14592. doi:10.1371/journal.pone.0014592.

Benhamou, S. and Riotte-Lambert, L. (2012). Beyond the Utilization Distribution: Identifying home range areas that are intensively exploited or repeatedly visited. *Ecological Modelling*, 227:112–116. doi:10.1016/j.ecolmodel.2011.12.015.

Benhamou, S. et al. (2014). Movement-based analysis of interactions in African lions. *Animal Behaviour*, 90:171–180. doi:10.1016/j.anbehav.2014.01.030.

Bernstein, J. (2006). Einstein and the existence of atoms. *American Journal of Physics*, 74(10):863–872. doi:10.1119/1.2218357.

Berryman, A. A. (1992). The orgins and evolution of predator-prey theory. *Ecology*, 73(5):1530–1535. doi:10.2307/1940005.

Bhattacharyya, A. (1946). On a measure of divergence between two multinomial populations. *The Indian Journal of Statistics*, 7(4):401–406.

Birkett, P. J. et al. (2012). Animal perception of seasonal thresholds: Changes in elephant movement in relation to rainfall patterns. *PLoS ONE*, 7(6). doi:10.1371/journal.pone.0038363.

Börger, L., Dalziel, B. D. and Fryxell, J. M. (2008). Are there general mechanisms of animal home range behaviour? A review and prospects for future research. *Ecology Letters*, 11(6):637–650. doi:10.1111/j.1461-0248.2008.01182.x.

Bracis, C. et al. (2015). Memory effects on movement behavior in animal foraging. *PLoS ONE*, 10(8). doi:10.1371/journal.pone.0136057.

Brandell, E. E. et al. (2020). Group density, disease, and season shape territory size and overlap of social carnivores. *Journal of Animal Ecology*, pages 1365–2656.13294. doi:10.1111/1365-2656.13294.

Bridge, E. S. et al. (2011). Technology on the move: recent and forthcoming innovations for tracking migratory birds. *BioScience*, 61(9):689–698. doi:10.1525/bio.2011.61.9.7.

Brouwer, L., van de Pol, M. and Cockburn, A. (2014). Habitat geometry does not affect levels of extrapair paternity in an extremely unfaithful fairy-wren. *Behavioral Ecology*, 25(3):531–537. doi:10.1093/beheco/aru010.

Brown, R. (1828). XXVII. A brief account of microscopical observations made in the months of June, July and August 1827, on the particles contained in the pollen of plants; and on the general existence of active molecules in organic and inorganic bodies . *The Philosophical Magazine*, 4(21):161–173. doi:10.1080/14786442808674769.

Bulmer, M. G. (1974). A statistical analysis of the 10-year cycle in Canada. *The Journal of Animal Ecology*, 43(3):701. doi:10.2307/3532.

Burhans, D. E. (2000). Avoiding the nest: responses of field sparrows to the threat of nest predation. *Short Communications The Auk*, 117(3):803–806. doi:10.1093/AUK/117.3.803.

Burt, W. H. (1943). Territoriality and home range concepts as applied to mammals. *Journal of Mammalogy*, 24(3):346. doi:10.2307/1374834.

Carere, C. et al. (2009). Aerial flocking patterns of wintering starlings, *Sturnus vulgaris*, under different predation risk. *Animal Behaviour*, 77(1):101–107. doi:10.1016/j.anbehav.2008.08.034.

Carter, K. D. et al. (2013). Fission-fusion dynamics in wild giraffes may be driven by kinship, spatial overlap and individual social preferences. *Animal Behaviour*, 85(2):385–394. doi:10.1016/j.anbehav.2012.11.011.

Chamberlain, M. J. and Leopold, B. D. (2000). Spatial use patterns, seasonal habitat selection, and interactions among adult gray foxes in Mississippi. *The Journal of Wildlife Management*, 64(3):742. doi:10.2307/3802744.

Chandrasekhar, S. (1943). Stochastic problems in physics and astronomy. *Reviews of Modern Physics*, 15(1):1–89. doi:10.1103/RevModPhys.15.1.

Coleman, B. T. and Hill, R. A. (2014). Living in a landscape of fear: The impact of predation, resource availability and habitat structure on primate range use. *Animal Behaviour*, 88:165–173. doi:10.1016/j.anbehav.2013.11.027.

Coleman, J. S. and Fraser, J. D. (1989). Habitat use and home ranges of black and turkey vultures. *The Journal of Wildlife Management*, 53(3):782. doi:10.2307/3809213.

Cooper, R. L. et al. (2018). An ancient Turing-like patterning mechanism regulates skin denticle development in sharks. *Science Advances*, 4(11):eaau5484. doi:10.1126/sciadv.aau5484.

Cresswell, W. (1994). Flocking is an effective anti-predation strategy in redshanks, *Tringa totanus*. *Animal Behaviour*, 47(2):433–442. doi:10.1006/anbe.1994.1057.

Dahl, F. (2005). Distinct seasonal habitat selection by annually sedentary mountain hares (*Lepus timidus*) in the boreal forest of Sweden. *European Journal of Wildlife Research*, 51(3):163–169. doi:10.1007/s10344-005-0095-y.

Daszak, P., Cunningham, A. A. and Hyatt, A. D. (2000). Emerging infectious diseases of wildlife - Threats to biodiversity and human health. *Science*, 287(5452):443–449. doi:10.1126/science.287.5452.443.

du Feu, C. R. et al. (2016). The EURING Data Bank – a critical tool for continental-scale studies of marked birds. *Ringing & Migration*, 31(1):1–18. doi:10.1080/03078698.2016.1195205.

Dyble, M. et al. (2019). Intergroup aggression in meerkats. *Proceedings. Biological sciences*, 286(1917):20191993. doi:10.1098/rspb.2019.1993.

Einstein, A. (1905). Über die von der molekularkinetischen Theorie der Wärme geforderte Bewegung von in ruhenden Flüssigkeiten suspendierten Teilchen. *Annalen der Physik*, 322(8):549–560. doi:10.1002/andp.19053220806.

Ellis, J., Petrovskaya, N. and Petrovskii, S. (2019). Effect of density-dependent individual movement on emerging spatial population distribution: Brownian motion vs Levy flights. *Journal of Theoretical Biology*. doi:10.1016/j.jtbi.2018.12.016.

Ellison, N. et al. (2020). Mechanistic home range analysis reveals drivers of space use patterns for a non-territorial passerine. *Journal of Animal Ecology*. doi:10.1111/1365-2656.13292.

Elton, C. and Nicholson, M. (1942). The ten-year cycle in numbers of the lynx in Canada. *The Journal of Animal Ecology*, 11(2):215. doi:10.2307/1358.

Emery, N. J. (2006). Cognitive ornithology: The evolution of avian intelligence. *Philosophical Transactions of the Royal Society B: Biological Sciences*, 361(1465):23–43. doi:10.1098/rstb.2005.1736.

Fagan, W. F. et al. (2020). Improved foraging by switching between diffusion and advection: benefits from movement that depends on spatial context. *Theoretical Ecology*, 13(2):127–136. doi:10.1007/s12080-019-00434-w.

Fagan, W. F. et al. (2013). Spatial memory and animal movement. *Ecology Letters*, 16(10):1316–1329. doi:10.1111/ele.12165.

Ferguson, S. H. and Elkie, P. C. (2004). Seasonal movement patterns of woodland caribou (*Rangifer tarandus* caribou). *Journal of Zoology*, 262(2):125–134. doi:10.1017/S0952836903004552.

Ferguson, S. H. et al. (1999). Determinants of home range size for polar bears (*Ursus maritimus*). *Ecology Letters*, 2(5):311–318. doi:10.1046/j.1461-0248.1999.00090.x.

Fick, A. (1855). Ueber Diffusion. *Annalen der Physik*, 170(1):59–86. doi:10.1002/andp.18551700105.

Fieberg, J. and Börger, L. (2012). Could you please phrase "home range" as a question? *Journal of Mammalogy*, 93(4):890–902. doi:10.1644/11-mamm-s-172.1.

Fieberg, J. and Kochanny, C. O. (2005). Quantifying home-range overlap: the importance of the utilization distribution. *The Journal of Wildlife Management*, 69(4):1346–1359. doi:10.2193/0022-541X(2005)69[1346:QHOTIO]2.0.CO;2.

Fieberg, J. R. et al. (2018). Used-habitat calibration plots: a new procedure for validating species distribution, resource selection, and step-selection models. *Ecography*, 41(5):737–752. doi:10.1111/ecog.03123.

Firth, J. A. et al. (2018). Personality shapes pair bonding in a wild bird social system. *Nature Ecology and Evolution*, 2(11):1696–1699. doi:10.1038/s41559-018-0670-8.

Firth, J. A. and Sheldon, B. C. (2016). Social carry-over effects underpin trans-seasonally linked structure in a wild bird population. *Ecology Letters*, 19(11):1324–1332. doi:10.1111/ele.12669.

Fischer, J. and Lindenmayer, D. B. (2007). Landscape modification and habitat fragmentation: A synthesis. *Global Ecology and Biogeography*, 16(3):265–280. doi:10.1111/j.1466-8238.2007.00287.x.

Fisher, R. A. D. (1937). The wave of advantageous genes. *Annals of Eugenics*, 7:355–369. doi:10.1111/j.1469-1809.1937.tb02153.x.

Fleming, C. H. et al. (2015). Rigorous home range estimation with movement data: A new autocorrelated kernel density estimator. *Ecology*, 96(5):1182–1188. doi:10.1890/14-2010.1.

Fokker, A. D. (1914). Die mittlere Energie rotierender elektrischer Dipole im Strahlungsfeld. *Annalen der Physik*, 348(5):810–820. doi:10.1002/andp.19143480507.

Ford, R. G. (1983). Home range in a patchy environment: optimal foraging predictions. *American Society of Zoologists*, 23:315–326.

Forester, J. D., Im, H. K. and Rathouz, P. J. (2009). Accounting for animal movement in estimation of resource selection functions: Sampling and data analysis. *Ecology*, 90(12):3554–3565. doi:10.1890/08-0874.1.

Fortin, D. et al. (2005). Wolves influence elk movements: Behavior shapes a trophic cascade in Yellowstone National Park. *Ecology*, 86(5):1320–1330. doi:10.1890/04-0953.

Frère, C. H. et al. (2010). Home range overlap, matrilineal and biparental kinship drive female associations in bottlenose dolphins. *Animal Behaviour*, 80(3):481–486. doi:10.1016/j.anbehav.2010.06.007.

Fritz, J. (1982). *Partial Differential Equations*. Springer.

Fuller, R. J. and Henderson, A. C. (1992). Distribution of breeding songbirds in bradfield woods, suffolk, in relation to vegetation and coppice management. *Bird Study*, 39(2):73–88. doi:10.1080/00063659209477103.

Gaddis, P. (1980). Mixed flocks, accipiters, And antipredator behavior. *The condor*. doi:10.2307/1367409.

Gaston, A. J. (1973). The ecology and behaviour of the long-lailed tit. *Ibis*, 115(3):330–351. doi:10.1111/j.1474-919X.1973.tb01974.x.

Gaynor, K. M. et al. (2018). The influence of human disturbance on wildlife nocturnality. *Science*, 360(6394):1232–1235. doi:10.1126/science.aar7121.

Gelardi, V. et al. (2020). Measuring social networks in primates: wearable sensors versus direct observations. *Proceedings of the Royal Society A: Mathematical, Physical and Engineering Sciences*, 476(2236):20190737. doi:10.1098/rspa.2019.0737.

Gerisch, A. and Chaplain, M. A. (2006). Robust numerical methods for taxis-diffusion-reaction systems: Applications to biomedical problems. *Mathematical and Computer Modelling*, 43(1-2):49–75. doi:10.1016/j.mcm.2004.05.016.

Giuggioli, L., Potts, J. R. and Harris, S. (2011). Animal interactions and the emergence of territoriality. *PLoS Computational Biology*, 7(3):e1002008. doi:10.1371/journal.pcbi.1002008.

Graham, T. (1833). XIII. Researches on the arseriates, phosphates, and modifications of phosphoric acid. *Philosophical Transactions of the Royal Society of London*, 123:253–284. doi:10.1098/rstl.1833.0015.

Griesser, M. et al. (2009). Influence of winter ranging behaviour on the social organization of a cooperatively breeding bird species, the apostlebird. *Ethology*, 115(9):888–896. doi:10.1111/j.1439-0310.2009.01678.x.

Griffiths, S. W. and Armstrong, J. D. (2002). Kin-biased territory overlap and food sharing among Atlantic salmon juveniles. *Journal of Animal Ecology*, 71(3):480–486. doi:10.1046/j.1365-2656.2002.00614.x.

Gullett, P. et al. (2014). Climate change and annual survival in a temperate passerine: partitioning seasonal effects and predicting future patterns. *Oikos*, 123(4):389–400. doi:10.1111/j.1600-0706.2013.00620.x.

Hansen, N. A. et al. (2019). Predation risk for reptiles is highest at remnant edges in agricultural landscapes. *Journal of Applied Ecology*, 56(1):31–43. doi:10.1111/1365-2664.13269.

Hatchwell, B. (2016). *Cooperative Breeding in Vertebrates: Chapter 3: Long-tailed tits: ecological causes and fitness consequences of redirected helping*. Cambridge University Press. doi:10.1017/CBO9781107338357.

Hatchwell, B. J. et al. (2001a). Social organization of cooperatively breeding long-tailed tits: Kinship and spatial dynamics. *Journal of Animal Ecology*, 70(5):820–830. doi:10.1046/j.0021-8790.2001.00541.x.

Hatchwell, B. J., Gullett, P. R. and Adams, M. J. (2014). Helping in cooperatively breeding long-tailed tits: A test of references. *Philosophical Transactions of the Royal Society B: Biological Sciences*, 369(1642). doi:10.1098/rstb.2013.0565.

Hatchwell, B. J. et al. (2001b). Kin discrimination in cooperatively breeding long-tailed tits. *Proc Biol Sci*, 268(1470):885–890. doi:10.1098/rspb.2001.1598.

Hatchwell, B. J. and Russell, A. F. (1996). Provisioning rules in cooperatively breeding long-tailed tits Aegithalos caudatus: An experimental study. *Proceedings of the Royal Society B: Biological Sciences*, 263(1366):83–88. doi:10.1098/rspb.1996.0014.

Hays, G. C. et al. (2016). Key questions in marine megafauna movement ecology. *Trends in Ecology and Evolution*, 31(6):463–475. doi:10.1016/j.tree.2016.02.015.

Hodgson, P., French, K. and Major, R. E. (2006). Comparison of foraging behaviour of small, urban-sensitive insectivores in continuous woodland and woodland remnants in a suburban landscape. *Wildlife Research*, 33(7):591. doi:10.1071/WR05017.

Holmes, R. T. and Robinson, S. K. (1981). Tree species preferences of foraging insectivorous birds in a northern hardwoods forest. *Oecologia*, (48):31–35.

Hooten, M. B. et al. (2010). Agent-based inference for animal movement and selection. *Journal of Agricultural, Biological, and Environmental Statistics*, 15(4):523–538. doi:10.1007/s13253-010-0038-2.

Horne, J. S. et al. (2007). Analyzing animal movements using Brownian bridges. *Ecology*, 88(9):2354–2363. doi:10.1890/06-0957.1.

Houston, A. I., Prosser, E. and Sans, E. (2012). The cost of disturbance: a waste of time and energy? *Oikos*, 121(4):597–604. doi:10.1111/j.1600-0706.2011.19594.x.

Jetz, W. et al. (2004). The scaling of animal space use. *Science*, 306(5694):266–268. doi:10.1126/science.1102138.

Kass, R. E. and Raftery, A. E. (1995). Bayes factors. *Journal of the American Statistical Association*, 90(430):773–795. doi:10.1080/01621459.1995.10476572.

Kays, R. et al. (2015). Terrestrial animal tracking as an eye on life and planet. *Science*, 348(6240):aaa2478–aaa2478. doi:10.1126/science.aaa2478.

Kernohana, B. J., Gitzen, R. A. and Millspaugh, J. J. (2001). Analysis of animal space use and movements. In *Radio Tracking and Animal Populations*, chapter 5, pages 125–166. Academic Press. doi:10.1016/B978-012497781-5/50006-2.

Kerr, G. D. and Bull, C. M. (2006). Movement patterns in the monogamous sleepy lizard (*Tiliqua rugosa*): effects of gender, drought, time of year and time of day. *Journal of Zoology*, 269(2):137–147. doi:10.1111/j.1469-7998.2006.00091.x.

King, J. A. (1973). The ecology of aggressive behavior. *Annual Review of Ecology and Systematics*, 4(1):117–138. doi:10.1146/annurev.es.04.110173.001001.

Klar, N. et al. (2008). Habitat selection models for European wildcat conservation. *Biological Conservation*, 141(1):308–319. doi:10.1016/j.biocon.2007.10.004.

Knapp, C. R. (2000). Home range and intraspecific interactions of a translocated iguana population (*Cyclura cychlura inornata*). *Caribbean Journal of Science*, 36:250–257.

Kolmogorov, A., Petrovskii, I. and Piskunov, N. (1937). A study of the equation of diffusion with increase in the quantity of matter, and its application to a biological problem. *Translated by V. M. Volosov from Bull. Moscow Univ., Math. Mech.*, 1:1–25.

Krebs, C. J. et al. (2001). What drives the 10-year cycle of snowshoe hares? *BioScience*, 51(1):25–35. doi:10.1641/0006-3568(2001)051[0025:WDTYCO]2.0.CO;2.

Krstic, M. and Smyshlyaev, A. (2008). *Boundary Control of PDEs A Course on Backstepping Designs*. Cambridge University Press.

Kull, K. (1998). On semiosis, Umwelt, and semiosphere. *Semiotica*, 120(3):299–310.

Lack, D. and Lack, E. (1958). The nesting of the long-tailed tit. *Bird Study*, 5(1):1–19. doi:10.1080/00063655809475897.

Leclerc, M. et al. (2016). Quantifying consistent individual differences in habitat selection. *Oecologia*, 180(3):697–705. doi:10.1007/s00442-015-3500-6.

Leedale, A. E. et al. (2018). Fine-scale genetic structure and helping decisions in a cooperatively breeding bird. *Molecular Ecology*, 27(7):1714–1726. doi:10.1111/mec.14553.

Lewis, M. A. and Murray, J. D. (1993). Modelling territoriality and wolf-deer interactions. *Nature*, 366(6457):738–740. doi:10.1038/366738a0.

Lindström, Å. (1989). Finch flock size and risk of hawk predation at a migratory stopover site. *The Auk*, 106(2):225–232. doi:10.1093/AUK/106.2.225.

Liu, Q. X. et al. (2014). Pattern formation at multiple spatial scales drives the resilience of mussel bed ecosystems. *Nature Communications*, 5(1):1–7. doi:10.1038/ncomms6234.

Liu, R. T., Liaw, S. S. and Maini, P. K. (2006). Two-stage Turing model for generating pigment patterns on the leopard and the jaguar. *Physical Review E - Statistical, Nonlinear, and Soft Matter Physics*, 74(1):011914. doi:10.1103/PhysRevE.74.011914.

Lotka, A. (1924). Elements of physical biology. *Baltimore: Williams and Wilkins Co., Inc.*

Macdonald, D. W., Ball, F. G. and Hough, N. G. (1979). The evaluation of home range size and configuration using radio tracking data. In *A Handbook on Biotelemetry and Radio Tracking*, pages 405–424.

Manly, B. F. et al. (2002). *Resource Selection by Animals: Statistical Design and Analysis for Field Studies*. Springer, Dordrecht ; Boston, 2nd editio edition.

McCarthy, M. S. et al. (2019). Camera traps provide a robust alternative to direct observations for constructing social networks of wild chimpanzees. *Animal Behaviour*, 157:227–238. doi:10.1016/j.anbehav.2019.08.008.

McGarigal, K. et al. (2016). Multi-scale habitat selection modeling: a review and outlook. *Landscape Ecology*, 31(6):1161–1175. doi:10.1007/s10980-016-0374-x.

McGregor, H. W. et al. (2014). Landscape management of fire and grazing regimes alters the fine-scale habitat utilisation by feral cats. *PLoS ONE*, 9(10). doi:10.1371/journal.pone.0109097.

Merkle, J. A., Fortin, D. and Morales, J. M. (2014). A memory-based foraging tactic reveals an adaptive mechanism for restricted space use. *Ecology Letters*, 17(8):924–931. doi:10.1111/ele.12294.

Merkle, J. A., Potts, J. R. and Fortin, D. (2017). Energy benefits and emergent space use patterns of an empirically parameterized model of memory-based patch selection. *Oikos*, 126(2). doi:10.1111/oik.03356.

Mitchell, M. S. and Powell, R. A. (2004). A mechanistic home range model for optimal use of spatially distributed resources. *Ecological Modelling*, 177(1-2):209–232. doi:10.1016/j.ecolmodel.2004.01.015.

Mitchell, M. S. and Powell, R. A. (2012). Foraging optimally for home ranges. *Journal of Mammalogy*, 93(4):917–928. doi:10.1644/11-mamm-s-157.1.

Mönkkönen, M. and Forsman, J. T. (2002). Heterospecific attraction among forest birds: a review. 1(1):41–51. doi:10.2326/osj.1.41.

Moorcroft, P. R. (2012). Mechanistic approaches to understanding and predicting mammalian space use: recent advances, future directions. *Journal of Mammalogy*, 93(4):903–916. doi:10.1644/11-mamm-s-254.1.

Moorcroft, P. R. and Barnett, A. (2008). Mechanistic home range models and resource selection analysis: A reconciliation and unification. *Ecology*, 89(4):1112–1119. doi:10.1890/06-1985.1.

Moorcroft, P. R. and Lewis, M. A. (2006). *Mechanistic Home Range Analysis. (MPB-43)*. Princeton University Press.

Moorcroft, P. R., Lewis, M. A. and Crabtree, R. L. (1999). Home range analysis using a mechanistic home range model. *Ecology*, 80(5):1656–1665. doi:10.1890/0012-9658(1999)080[1656:HRAUAM]2.0.CO;2.

Moorcroft, P. R., Lewis, M. A. and Crabtree, R. L. (2006). Mechanistic home range models capture spatial patterns and dynamics of coyote territories in Yellowstone. *Proceedings of the Royal Society B: Biological Sciences*, 273(1594):1651–1659. doi:10.1098/rspb.2005.3439.

Moorman, C. E. et al. (2007). Seasonal diets of insectivorous birds using canopy gaps in a bottomland forest. *Journal of Field Ornithology*, 78(1):11–20. doi:10.1111/j.1557-9263.2006.00081.x.

Moorter, B. V. et al. (2009). Memory keeps you at home: a mechanistic model for home range emergence. *Oikos*, 118(5):641–652. doi:10.1111/j.1600-0706.2008.17003.x.

Morris, D. W. (2003). How can we apply theories of habitat selection to wildlife conservation and management? *Wildlife Research*, 30(4):303–319. doi:10.1071/WR02028.

Morris, L. R., Proffitt, K. M. and Blackburn, J. K. (2016). Mapping resource selection functions in wildlife studies: Concerns and recommendations. *Applied Geography*, 76:173–183. doi:10.1016/j.apgeog.2016.09.025.

Munden, R. et al. (2020). Why did the animal turn? Time-varying step selection analysis for inference between observed turning points in high frequency data. *bioRxiv*, page 2020.08.13.249151. doi:10.1101/2020.08.13.249151.

Murray, J. D. (1993). *Mathematical biology / 2, Spatial models and biomedical applications.* Springer.

Napper, C. J. and Hatchwell, B. J. (2016). Social dynamics in nonbreeding flocks of a cooperatively breeding bird: causes and consequences of kin associations. *Animal Behaviour*, 122:23–35. doi:10.1016/j.anbehav.2016.09.008.

Nathan, R. et al. (2008). A movement ecology paradigm for unifying organismal movement research. *Proceedings of the National Academy of Sciences of the United States of America*, 105(49):19052–19059. doi:10.1073/pnas.0800375105.

Nelder, J. A. and Mead, R. (1965). A simplex method for function minimization. *The Computer Journal*, 7(4):308–313. doi:10.1093/comjnl/7.4.308.

Newmark, W. D. and Stanley, T. R. (2011). Habitat fragmentation reduces nest survival in an Afrotropical bird community in a biodiversity hotspot. *Proceedings of the National Academy of Sciences of the United States of America*, 108(28):11488–11493. doi:10.1073/pnas.1104955108.

Nilsson, J.-A. et al. (2014). Individuality in movement : the role of animal personality. *Animal movement across scales*, pages 90–109. doi:10.1093/acprof:oso/9780199677184.003.0006.

Okubo, A. (1980). *Diffusion and Ecological Problems: Modern Perspectives*.

Oli, M. K., Jacobson, H. A. and Leopold, B. D. (2002). Pattern of space use by female black bears in the White River National Wildlife Refuge, Arkansas, USA. *Journal for Nature Conservation*, 10(2):87–93. doi:10.1078/1617-1381-00010.

Oliveira-Santos, L. G. R. et al. (2016). Incorporating animal spatial memory in step selection functions. *Journal of Animal Ecology*, 85(2):516–524. doi:10.1111/1365-2656.12485.

Osipova, L. et al. (2019). Using step-selection functions to model landscape connectivity for African elephants: accounting for variability across individuals and seasons. *Animal Conservation*, 22(1):35–48. doi:10.1111/acv.12432.

Parton, A. and Blackwell, P. G. (2017). Bayesian inference for multistate 'step and turn' animal movement in continuous time. *Journal of Agricultural, Biological and Environmental Statistics*, 22. doi:10.1007/s13253-017-0286-5.

Patterson, T. A. et al. (2008). State-space models of individual animal movement. *Trends in Ecology and Evolution*, 23(2):87–94. doi:10.1016/j.tree.2007.10.009.

Pearce, F. et al. (2013). Space-use scaling and home range overlap in primates. *Proceedings of the Royal Society B: Biological Sciences*, 280(1751):20122122. doi:10.1098/rspb.2012.2122.

Perrin (1909). Mouvement brownien et grandeurs moléculaires. *Le Radium*, 6(12):353–360. doi:10.1051/radium:01909006012035300.

Philibert, J. (2005). One and a Half Century of Diffusion: Fick, Einstein, before and Beyond. *Diffusion Fundamentals*, 2:1–10.

Pielou, E. C. (1969). *An Introduction to Mathematical Ecology*. Wiley-Interscience. doi:10.4039/ent103288-2.

Planck, M. (1917). *Uber einen Satz der statistischen Dynamik und seine Erweiterung in der Quantentheorie.* Reimer, Berlin.

Port, M., Kappeler, P. M. and Johnstone, R. A. (2011). Communal defense of territories and the evolution of sociality. *The American Naturalist*, 178(6):787–800. doi:10.1086/662672.

Potts, J. R. et al. (2018). Finding turning-points in ultra-high-resolution animal movement data. *Methods in Ecology and Evolution*, 9(10):2091–2101. doi:10.1111/2041-210X.13056.

Potts, J. R. and Lewis, M. A. (2014). A mathematical approach to territorial pattern formation. *The American Mathematical Monthly*, 121(9):754. doi:10.4169/amer.math.monthly.121.09.754.

Potts, J. R. and Lewis, M. A. (2016a). How memory of direct animal interactions can lead to territorial pattern formation. *Journal of the Royal Society Interface*, 13(118):20160059. doi:10.1098/rsif.2016.0059.

Potts, J. R. and Lewis, M. A. (2016b). Territorial pattern formation in the absence of an attractive potential. *Journal of Mathematical Biology*, 72(1-2):25–46. doi:10.1007/s00285-015-0881-4.

Potts, J. R. and Lewis, M. A. (2019). Spatial memory and taxis-driven pattern formation in model ecosystems. *Bulletin of Mathematical Biology*, 81(7):2725–2747. doi:10.1007/s11538-019-00626-9.

Potts, J. R., Mokross, K. and Lewis, M. A. (2014a). A unifying framework for quantifying the nature of animal interactions. *Journal of the Royal Society Interface*, 11(96):20140333. doi:10.1098/rsif.2014.0333.

Potts, J. R. et al. (2014b). Step selection techniques uncover the environmental predictors of space use patterns in flocks of Amazonian birds. *Ecology and Evolution*, 4(24):4578–4588. doi:10.1002/ece3.1306.

Potts, J. R. and Petrovskii, S. V. (2017). Fortune favours the brave: Movement responses shape demographic dynamics in strongly competing populations. *Journal of Theoretical Biology*, 420:190–199. doi:10.1016/j.jtbi.2017.03.011.

Potts, J. R. and Schlägel, U. E. (2020). Parametrising diffusion-taxis equations from animal movement trajectories using step selection analysis. *Methods in Ecology and Evolution, 2020*, pages 00: 1– 14. doi:https://doi.org/10.1111/2041-210X.13406.

Procaccini, A. et al. (2011). Propagating waves in starling, *Sturnus vulgaris*, flocks under predation. *Animal Behaviour*, 82(4):759–765. doi:10.1016/j.anbehav.2011.07.006.

Prokopenko, C. M., Boyce, M. S. and Avgar, T. (2017). Characterizing wildlife behavioural responses to roads using integrated step selection analysis. *Journal of Applied Ecology*, 54(2):470–479. doi:10.1111/1365-2664.12768.

Pulliam, R. and Caraco, T. (1984). Living in groups: is there an optimal group size? In *Behavioural ecology: an evolutionary approach*, pages 122–147. Blackwell, Oxford.

Railsback, S. F. S. F. and Grimm, V. (2011). *Agent-based and individual-based modeling : a practical introduction*. Princeton University Press. doi:doi:10.2307/j.ctt7sns7.

Reiher, W. (1964). Monte Carlo Methods. *Biometrische Zeitschrift*, 8(3):209–209. doi:10.1002/bimj.19660080314.

Rhodes, J. R. et al. (2005). A spatially explicit habitat selection model incorporating home range behavior. *Ecology*, 86(5):1199–1205. doi:10.1890/04-0912.

Riotte-Lambert, L., Benhamou, S. and Chamaillé-Jammes, S. (2015). How memory-based movement leads to nonterritorial spatial segregation. *American Naturalist*, 185(4):E103–E116. doi:10.1086/680009.

Riotte-Lambert, L. and Matthiopoulos, J. (2020). Environmental Predictability as a Cause and Consequence of Animal Movement. *Trends in Ecology and Evolution*, 35(2):163–174. doi:10.1016/j.tree.2019.09.009.

Rockhill, A. P., DePerno, C. S. and Powell, R. A. (2013). The effect of illumination and time of day on movements of bobcats (*Lynx rufus*). *PLoS ONE*, 8(7). doi:10.1371/journal.pone.0069213.

Rosalino, L. M. et al. (2005). Dietary shifts of the badger (*Meles meles*) in Mediterranean woodlands: An opportunistic forager with seasonal specialisms. *Mammalian Biology*, 70(1):12–23. doi:10.1078/1616-5047-00172.

Rosli, Z., Zakaria, M. and Rajpar, M. N. (2018). Edge effects on foraging guilds of upperstory birds in an isolated tropical rainforest of Malaysia. *The J. Anim. Plant Sci*, 28(1):2018.

Russell, A. F. and Hatchwell, B. J. (2001). Experimental evidence for kin-biased helping in a cooperatively breeding vertebrate. *Proceedings of the Royal Society B: Biological Sciences*, 268(1481):2169–2174. doi:10.1098/rspb.2001.1790.

Sæther, B. E. et al. (2016). Demographic routes to variability and regulation in bird populations. *Nature Communications*, 7(1):1–8. doi:10.1038/ncomms12001.

Šálek, M. et al. (2010). Do prey densities determine preferences of mammalian predators for habitat edges in an agricultural landscape? *Landscape and Urban Planning*, 98(2):86–91. doi:10.1016/j.landurbplan.2010.07.013.

Schiesser, W. E. (1991). Numerical method of lines. In *Integration of Partial Differential Equations*, pages 181–204. Academic Press.

Schlägel, U. E. et al. (2016). Robustness of movement models: can models bridge the gap between temporal scales of data sets and behavioural processes? *Journal of Mathematical Biology*, 73:1691–1726. doi:10.1007/s00285-016-1005-5.

Schwarz, G. (1978). Estimating the dimension of a model. *The Annals of Statistics*, 6(2):461–464. doi:10.1214/aos/1176344136.

Scott, D. W. (1992). *Multivariate Density Estimation: Theory, Practice, and Visualization*. Wiley, New York, 1st edition.

Sera, W. E. and Gaines, M. S. (1994). The effect of relatedness on spacing behavior and fitness of female prairie voles. *Ecology*, 75(6):1560–1566. doi:10.2307/1939617.

Sharp, S. P. et al. (2008). Natal dispersal and recruitment in a cooperatively breeding bird. *Oikos*, 117(9):1371–1379. doi:10.1111/j.0030-1299.2008.16392.x.

Sharp, S. P. et al. (2005). Learned kin recognition cues in a social bird. *Nature*, 434(7037):1127–1130. doi:10.1038/nature03522.

Sick, S. et al. (2006). WNT and DKK determine hair follicle spacing through a reaction-diffusion mechanism. *Science*, 314(5804):1447–1450. doi:10.1126/science.1130088.

Siegfried, W. R. and Underhill, L. G. (1975). Flocking as an anti-predator strategy in doves. *Animal Behaviour*, 23(PART 3):504–508. doi:10.1016/0003-3472(75)90126-8.

Signer, J., Fieberg, J. and Avgar, T. (2017). Estimating utilization distributions from fitted step-selection functions. *Ecosphere*, 8(4):e01771. doi:10.1002/ecs2.1771.

Signer, J., Fieberg, J. and Avgar, T. (2019). Animal movement tools (amt): R package for managing tracking data and conducting habitat selection analyses. *Ecology and Evolution*, 9(2):880–890. doi:10.1002/ece3.4823.

Skroblin, A. and Legge, S. (2012). Influence of fine-scale habitat requirements and riparian degradation on the distribution of the purple-crowned fairy-wren (*Malurus coronatus coronatus*) in northern Australia. *Austral Ecology*, 37(8):874–884. doi:10.1111/j.1442-9993.2011.02331.x.

Smith, G. D. (1986). *Numerical Solution Of Partial Differential Equations: Finite Difference Methods*. Oxford University Press, U.S.A., Oxford Oxfordshire : New York, 3 edition edition.

Spiegel, O. et al. (2017). What's your move? Movement as a link between personality and spatial dynamics in animal populations. *Ecology Letters*, 20(1):3–18. doi:10.1111/ele.12708.

Støen, O.-G. et al. (2005). Kin-related spatial structure in brown bears (*Ursus arctos*). *Behav Ecol Sociobiol*, 59:191–197. doi:10.1007/s00265-005-0024-9.

Tellería, J. L., Santos, T. and Telleria, J. L. (1997). Seasonal and interannual occupation of a forest archipelago by insectivorous passerines. *Oikos*, 78(2):239. doi:10.2307/3546290.

Terraube, J. et al. (2016). Forest edges have high conservation value for bird communities in mosaic landscapes. *Ecology and Evolution*, 6(15):5178–5189. doi:10.1002/ece3.2273.

Thorup, K. et al. (2014). Large-scale spatial analysis of ringing and re-encounter data to infer movement patterns: A review including methodological perspectives. *Methods in Ecology and Evolution*, 5(12):1337–1350. doi:10.1111/2041-210X.12258.

Thurfjell, H., Ciuti, S. and Boyce, M. S. (2014). Applications of step-selection functions in ecology and conservation. *Movement Ecology*, 2(1):4. doi:10.1186/2051-3933-2-4.

Tucker, M. A. et al. (2018). Moving in the Anthropocene: Global reductions in terrestrial mammalian movements. *Science*, 359(6374):466–469. doi:10.1126/science.aam9712.

Turchin, P. (1998). *Quantitative analysis of movement measuring and modeling population redistribution in animals and plants*. Sinauer Associates.

Turing, A. M. (1952). The Chemical Basis of Morphogenesis. *Philosophical Transactions of the Royal Society of London. Series B, Biological Sciences*, 237(641):37–72.

Valentine, E. C., Apol, C. A. and Proppe, D. S. (2019). Predation on artificial avian nests is higher in forests bordering small anthropogenic openings. *Ibis*, 161(3):662–673. doi:10.1111/ibi.12662.

van Beest, F. M., Van Moorter, B. and Milner, J. M. (2012). Temperature-mediated habitat use and selection by a heat-sensitive northern ungulate. *Animal Behaviour*, 84(3):723–735. doi:10.1016/j.anbehav.2012.06.032.

van Kampen, N. G. (1981). *Stochastic processes in physics and chemistry*. North-Holland.

Vanak, A. T. et al. (2013). Moving to stay in place: behavioral mechanisms for coexistence of African large carnivores. *Ecology*, 94(11):2619–2631. doi:10.1890/13-0217.1.

VanderWerf, E. A. (1993). Scales of habitat selection by foraging 'elepaio in undisturbed and human-altered forests in Hawaii. *The Condor*, 95(4):980–989. doi:10.2307/1369433.

Vine, I. (1973). Detection of prey flocks by predators. *Journal of Theoretical Biology*, 40(2):207–210. doi:10.1016/0022-5193(73)90127-6.

Virkkala, R. and Liehu, H. (1990). Habitat selection by the siberian tit *Parus cinctus* in virgin and managed forests in northern Finland. *Ornis Fennica*, 67:1–12.

Volpert, V. and Petrovskii, S. (2009). Reaction-diffusion waves in biology. *Physics of Life Reviews*, 6(4):267–310. doi:10.1016/j.plrev.2009.10.002.

Volterra, V. (1926). Variazioni e fluttuazioni del numero d'individui in specie animali conviventi. *Memoria della Reale Accademia Nazionale dei Lincei*, 2:31–113.

Walker, F. M., Taylor, A. C. and Sunnucks, P. (2008). Female dispersal and male kinship-based association in southern hairy-nosed wombats (*Lasiorhinus latifrons*). *Molecular Ecology*, 17(5):1361–1374. doi:10.1111/j.1365-294X.2008.03670.x.

Wangersky, P. J. (1978). Lotka-Volterra Population Models. *Annual Review of Ecology and Systematics*, 9(1):189–218. doi:10.1146/annurev.es.09.110178.001201.

While, G. M., Uller, T. and Wapstra, E. (2009). Family conflict and the evolution of sociality in reptiles. *Behavioral Ecology*, 20(2):245–250. doi:10.1093/beheco/arp015.

Wikelski, M. et al. (2007). Going wild: what a global small-animal tracking system could do for experimental biologists. *The Journal of Experimental Biology*, 210:181–186. doi:10.1242/jeb.02629.

Williams, H. J. et al. (2020). Optimizing the use of biologgers for movement ecology research. *Journal of Animal Ecology*, 89(1):186–206. doi:10.1111/1365-2656.13094.

Winner, K. et al. (2018). Statistical inference for home range overlap. *Methods in Ecology and Evolution*, 9(7):1679–1691. doi:10.1111/2041-210X.13027.

Worton, B. J. (1989). Kernel methods for estimating the utilization distribution in home- range studies. *Ecology*, 70(1):164–168. doi:10.2307/1938423.

Wright, S. (1922). Coefficients of inbreeding and relationship. *The American Naturalist*, 56(645):330–338. doi:10.1086/279872.

Xu, Y., Vest, C. M. and Murray, J. D. (1983). Holographic interferometry used to demonstrate a theory of pattern formation in animal coats. *Applied Optics*, 22(22):3479. doi:10.1364/ao.22.003479.

Zeller, K. A. et al. (2016). Using step and path selection functions for estimating resistance to movement: pumas as a case study. *Landscape Ecology*, 31(6):1319–1335. doi:10.1007/s10980-015-0301-6.

Zwicker, S. M. and Walters, J. R. (1999). Selection of pines for foraging by red-cockaded woodpeckers. *The Journal of Wildlife Management*, 63(3):843. doi:10.2307/3802797.

Appendix A

A.1 A space use model from an individual-based model

I follow the general derivation of Moorcroft et al. (2006) to show how a general individual-based model can be approximated as a diffusion-taxis equation (Chandrasekhar, 1943; Einstein, 1905; Fokker, 1914; Planck, 1917).

The probability of moving from $\mathbf{x}'$ to $\mathbf{x}$ in time δt is described here using the arbitrary individual-based model $p(\mathbf{x}|\mathbf{x}')$, which is a normalised probability density function. The master equation, describing the probability of moving from all possible $\mathbf{x}'$ to $\mathbf{x}$ in small time δt over the landscape Ω has the form

$$u(\mathbf{x}, t+\delta t) = \int_{\Omega} p(\mathbf{x}|\mathbf{x}')u(\mathbf{x}', t)\mathrm{d}\mathbf{x}', \tag{A.1}$$

where $u(\mathbf{x}, t+\delta t)$ describes the overall space use of the individual at time $t+\delta t$. The derivation of a diffusion-taxis equation requires expanding Equation (A.1) as a Taylor series and ignoring small terms as negligible. Therefore, I define the

very small displacement in time δt as $\mathbf{q} = \mathbf{x} - \mathbf{x}'$. Since the location $\mathbf{x}$ depends on $\mathbf{q}$, I define the function

$$\rho(\mathbf{q}|\mathbf{x}') = p(\mathbf{x}|\mathbf{x}'). \tag{A.2}$$

By changing the variable of integration, Equation (A.1) is rewritten as

$$u(\mathbf{x}, t + \delta t) = \int_{\Omega} \rho(\mathbf{q}|\mathbf{x} - \mathbf{q}) u(\mathbf{x} - \mathbf{q}, t) \mathrm{d}\mathbf{q}. \tag{A.3}$$

Expanding Equation (A.3) as a Taylor Series about $\mathbf{x}$ gives

$$\begin{aligned} u(\mathbf{x}, t + \delta t) = \int_{\Omega} \Bigg(& \rho(\mathbf{q}|\mathbf{x}) u(\mathbf{x}, t) - \mathbf{q} \cdot \nabla \rho(\mathbf{q}|\mathbf{x}) u(\mathbf{x}, t) \\ & + \frac{|\mathbf{q}|^2}{4} \nabla^2 \rho(\mathbf{q}|\mathbf{x}) u(\mathbf{x}, t) \ldots \Bigg) \mathrm{d}\mathbf{q}, \end{aligned} \tag{A.4}$$

where the third term is formed by taking a mean-field approximation (covariances in the x and y directions are assumed to be negligible).

Further terms from the Taylor expansion of Equation (A.4) are ignored as $\mathbf{q}$ is small. Since $\rho(\mathbf{q}|\mathbf{x})$ is a probability density function, $\int_{\Omega} \rho(\mathbf{q}|\mathbf{x}) \mathrm{d}\mathbf{q} = 1$. I divide Equation (A.4) through by δt, take the limit as $\delta t \to 0$ and switch the order of differentiation and integration. The diffusion-taxis equation has the form

$$\frac{\partial u}{\partial t} = \nabla^2 \left[D(\mathbf{x}, t) u(\mathbf{x}, t) \right] - \nabla \cdot \left[\mathbf{A}(\mathbf{x}, t) u(\mathbf{x}, t) \right], \tag{A.5}$$

where

$$\begin{aligned}\mathbf{A}(\mathbf{x},t) &= \lim_{\delta t\to 0}\frac{1}{\delta t}\int_{\Omega}\mathbf{q}\rho(\mathbf{q}|\mathbf{x})\mathrm{d}\mathbf{q},\\ &= \lim_{\delta t\to 0}\frac{1}{\delta t}\int_{\Omega}(\mathbf{x}-\mathbf{x}')p(\mathbf{x}'|\mathbf{x})\mathrm{d}\mathbf{x}',\end{aligned} \tag{A.6}$$

$$\begin{aligned}D(\mathbf{x},t) &= \lim_{\delta t\to 0}\frac{1}{4\delta t}\int_{\Omega}|\mathbf{q}|^2\rho(\mathbf{q}|\mathbf{x})\mathrm{d}\mathbf{q},\\ &= \lim_{\delta t\to 0}\frac{1}{4\delta t}\int_{\Omega}|\mathbf{x}-\mathbf{x}'|^2p(\mathbf{x}'|\mathbf{x})\mathrm{d}\mathbf{x}'.\end{aligned} \tag{A.7}$$

where $\nabla = \left(\frac{\partial}{\partial x}, \frac{\partial}{\partial y}\right)$, $\mathbf{A}(\mathbf{x},t)$ and $D(\mathbf{x},t)$ are the Taxis and Diffusion terms respectively.

The solution to Equation (A.5), $u(\mathbf{x},t)$, is a description of space use and depends on the form of probability density function $p(\mathbf{x}|\mathbf{x}')$. The function $D(\mathbf{x},t)$ is the *diffusion* function and $\mathbf{A}(\mathbf{x},t)$ is the *taxis* function.

In the case where $p(\mathbf{x}|\mathbf{x}')$ describes purely random movement directions (the direction is chosen uniformly), the derivation results in the diffusion equation which is equivalent to Equation (A.5) with $\mathbf{A}(\mathbf{x},t) = 0$. In the case where $p(\mathbf{x}|\mathbf{x}')$ models movement in a particular direction, then a pure taxis equation is derived, which takes the form of Equation (A.5) with $D(\mathbf{x},t) = 0$. These results indicate that the diffusion term models movement without a directional bias and the taxis term models directed movement.

Using a similar derivation, a PDE can be derived to approximate space use from an individual-based model on a grid by considering all discrete movements (Moorcroft and Lewis 2006; Turchin 1998) and this is shown in §2.2.2.

A.2 Discrete space and time to continuous

In this section, I use graphical interpretations to explain the redefinitions shown in Equation (2.4), for moving from discrete to continuous space. Fig. A.1 shows two probability density functions in one spatial dimension which must integrate to 1. Integrating the function in Fig. A.1 gives

$$1 = x_0 u_i(x_0) = n_0 U_i(n_0) = n_0 l u_i(x_0)$$
$$U_i(n_0) = l u_i(x_0).$$

Similarly in two spatial dimensions Fig. A.2 shows that

$$1 = x_0 y_0 u_i(x_0, y_0) = n_0 m_0 U_i(n_0, m_0) = n_0 m_0 l^2 u_i(x_0, y_0)$$
$$U_i(n_0, m_0) = l^2 u_i(x_0, y_0),$$

so the utilisation distribution u_i in continuous space must be multiplied by l to the power of the number of spatial dimensions, to equal the discrete form U_i.

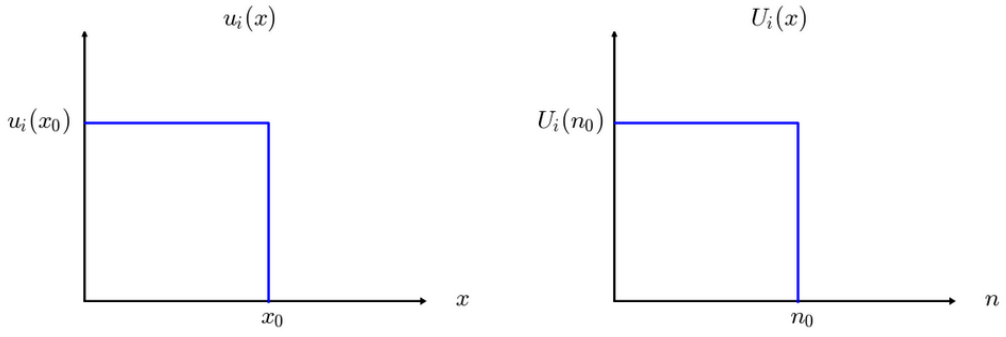

(a) (b)

Fig. A.1. Theoretical examples of 1D probability distributions (a) $u_i(x)$ and (b) $U_i(n)$, where $x = nl$.

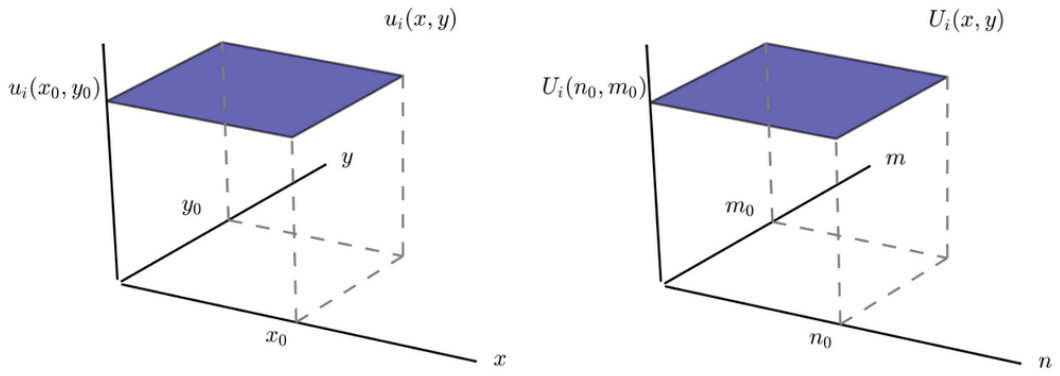

(a) (b)

Fig. A.2. Theoretical examples of 2D probability distributions (a) $u_i(x, y)$ and (b) $U_i(n, m)$ where $x = nl$ and $y = ml$.

A.3 Non-dimensionalisation

Here I define dimensionless parameters for Equations (2.11) and (2.7) in Chapter 2. The parameter L is the length of the domain so

$$\tilde{x} = \frac{x}{L}, \quad \tilde{y} = \frac{y}{L} \tag{A.8}$$

To non-dimensionalise t, u_i and k_i, I introduce new composite parameters T, U and K and define

$$\tilde{t} = \frac{t}{T}, \quad \tilde{u}_i = \frac{u_i}{U}, \quad \tilde{k}_i = \frac{k_i}{K} \tag{A.9}$$

Inserting the definitions (A.8) and (A.9) into space use Equation (2.11) becomes

$$\frac{U}{T}\frac{\partial \tilde{u_i}}{\partial \tilde{t}} = \frac{DU}{L^2}\left(\frac{\partial^2 \tilde{u_i}}{\partial \tilde{x}^2}\right) + \frac{\partial^2 \tilde{u_i}}{\partial \tilde{y}^2} + c\frac{UK}{L^2}\left[\frac{\partial}{\partial \tilde{x}}\left(\tilde{u_i}\frac{\partial \tilde{k_i}}{\partial \tilde{x}}\right) + \frac{\partial}{\partial \tilde{y}}\left(\tilde{u_i}\frac{\partial \tilde{k_i}}{\partial \tilde{y}}\right)\right]. \tag{A.10}$$

Redefining $T = L^2/D$, $K = 1$, $\gamma = c/D$ and omitting the tildes, I obtain

$$\frac{\partial u_i}{\partial t} = \left(\frac{\partial^2 u_i}{\partial x^2}\right) + \frac{\partial^2 u_i}{\partial y^2} + \gamma\left[\frac{\partial}{\partial x}\left(u_i\frac{\partial k_i}{\partial x}\right) + \frac{\partial}{\partial y}\left(u_i\frac{\partial k_i}{\partial y}\right)\right]. \tag{A.11}$$

Substituting the above definitions into the equation for the interaction zone, (2.7), gives

$$\frac{D}{L^2}\frac{d\tilde{k_i}}{d\tilde{t}} = U^2\rho\left(1-\tilde{k_i}\right)\tilde{u_i}\sum_{j\neq i}\tilde{u_i} - \tilde{k_i}\left(\mu + U\beta\tilde{u_i}\right). \tag{A.12}$$

Redefining $U = 1/L$, $a = D/\rho$, $m = \mu L^2/\rho$, $b = \beta L/\rho$ and omitting the tildes, gives

$$a\frac{dk_i}{dt} = \left(1-k_i\right)u_i\sum_{j\neq i}u_j - k_i\left(m + bu_i\right), \tag{A.13}$$

which leads to the full System (2.13)-(2.16) in Chapter 2.

A.4 Numerical techniques

Here I detail the finite difference scheme used to produce numerical solutions to diffusion-taxis equations in this thesis. Examples of solutions can be seen in Fig. 2.1.

The finite difference schemes solve equations over a grid of square cells of length Δx, so that the variables and functions are redefined in a discrete form. The change in time is denoted as Δt, giving $n = (\Delta x)x$, $m = (\Delta x)y$ and $s = (\Delta t)t$. I denote the discrete redefinition of $u_i(\mathbf{x}, t)$ as $U^s_{i,n,m}$, which is the probability of individual i being in space (n, m) at time s. The probability $k_i(\mathbf{x}, t)$ is redefined to give the probability of space (n, m) being in the interaction zone of flock i at time s as $K^s_{i,n,m}$.

I use the following finite difference approximations to describe differential terms

$$\frac{\partial u_i}{\partial t} \approx \frac{1}{\Delta t}\left(U^{s+1}_{i,n,m} - U^s_{i,n,m}\right), \tag{A.14}$$

$$\nabla^2 u_i \approx \frac{1}{(\Delta x)^2}\left(U^s_{i,n+1,m} + U^s_{i,n-1,m} + U^s_{i,n,m+1} + U^s_{i,n,m-1} - 4U^s_{i,n,m}\right), \tag{A.15}$$

$$\begin{aligned}\nabla \cdot (u_i \nabla k_i) \approx \frac{1}{4(\Delta x)^2}\Big[&\left(U^s_{i,n+1,m} - U^s_{i,n-1,m}\right)\left(K^s_{i,n+1,m} - K^s_{i,n-1,m}\right) \\ &+ \left(U^s_{i,n,m+1} - U^s_{i,n,m-1}\right)\left(K^s_{i,n,m+1} - K^s_{n,m-1}\right)\Big] \\ &+ \frac{1}{(\Delta x)^2} U^s_{i,n,m}\left(K^s_{i,n+1,m} + K^s_{i,n-1,m} + K^s_{i,n,m+1} + K^s_{i,n,m-1} - 4K^s_{i,n,m}\right).\end{aligned} \tag{A.16}$$

I use the finite difference approximations (A.14)-(A.16) to form time-stepping equations for the interaction system (2.13)-(2.16). The spatial average $\bar{k}(\mathbf{x}, t)$ from Equation (2.8) is defined as

$$\bar{K}^s_{i,n,m} = \frac{1}{n(P)} \sum_P K^s_{i,n',m'}, \tag{A.17}$$

where P is the set of cells, (n', m'), which is any cell on the landscape where the distance of the centre of the cell from the centre of (n, m) is less than $d = \delta\Delta x$. The distance from $(n, m,)$ to (n', m') is $|\mathbf{n} - \mathbf{n}'| = \sqrt{(n - n')^2 + (m - m')^2}$.

This gives the time-stepping method for each individual i as

$$K^{s+1}_{i,n,m} = K^s_{i,n,m} + \Delta t \left\{ \left(1 - K^s_{i,n,m}\right) U^s_{i,n,m} \sum_{j \neq i} U^s_{j,n,m} - K^s_{i,n,m} \left(m + bU^s_{i,n,m}\right) \right\}, \tag{A.18}$$

$$\begin{aligned} U^{s+1}_{i,n,m} =& U^s_{i,n,m} + \frac{\Delta t}{(\Delta x)^2} \left\{ U^s_{i,n+1,m} + U^s_{i,n-1,m} + U^s_{i,n,m+1} + U^s_{i,n,m-1} - 4U^s_{i,n,m} \right. \\ &+ \frac{\gamma}{4} \left[\left(U^s_{i,n+1,m} - U^s_{i,n-1,m}\right) \left(\bar{K}^s_{i,n+1,m} - \bar{K}^s_{i,n-1,m}\right) \right. \\ &\left. \left. + \left(U^s_{i,n,m+1} - U^s_{i,n,m-1}\right) \left(\bar{K}^s_{i,n,m+1} - \bar{K}^s_{i,n,m-1}\right) \right] \right. \\ &\left. + \gamma U^s_{i,n,m} \left(\bar{K}^s_{i,n+1,m} + \bar{K}^s_{i,n-1,m} + \bar{K}^s_{i,n,m+1} + \bar{K}^s_{i,n,m-1} - 4\bar{K}^s_{i,n,m}\right) \right\}, \end{aligned} \tag{A.19}$$

with zero-flux boundary conditions

$$U^s_{i,0,m} = U^s_{i,2,m} + \gamma U^s_{i,1,m}\left(\bar{K}^s_{i,2,m} - \bar{K}^s_{i,0,m}\right), \tag{A.20}$$

$$U^s_{i,N,m} = U^s_{i,N-2,m} - \gamma U^s_{i,N-1,m}\left(\bar{K}^s_{i,N,m} - \bar{K}^s_{i,N-2,m}\right), \tag{A.21}$$

$$U^s_{i,n,0} = U^s_{i,n,2} + \gamma U^s_{i,n,1}\left(\bar{K}^s_{i,n,2} - \bar{K}^s_{i,n,0}\right), \tag{A.22}$$

$$U^s_{i,n,N} = U^s_{i,n,N-2} - \gamma U^s_{i,n,N-1}\left(\bar{K}^s_{i,n,N} - \bar{K}^s_{i,n,N-2}\right). \tag{A.23}$$

Alongside Equation (A.17), this gives the numerical time-stepping process used to solve System (2.13)-(2.16) in Chapter 2. Initial conditions $u_i(x, y, 0)$ are given within the Chapter. The initial condition for the interaction zone was set to be $k_i(x, y, 0) = 0$ for all i.

Numerical solutions were conducted on a square grid of 50 by 50 cells with timestep $\Delta t = 10^{-5}$. The timestep was chosen such that $\frac{\Delta t}{(\Delta x)^2} < \frac{1}{2}$, which is the von Neumann stability condition for finite difference approximations of PDEs (Smith, 1986). Iterations were stopped when $\max_{n,m}|U^{s+1}_{i,n,m} - U^s_{i,n,m}| < 10^{-10}$ for all i. All analyses and numerical solutions were performed in Python 3.4 and C++ programming languages using an Intel(R) Core(TM) i7-4790T CPU @ 2.70GHz, 2701 Mhz with 8 cores.

Appendix B

B.1 The discrete mathematical form for the woodland attraction

Here I state the discrete mathematical form of each vector field $\mathbf{v}_M$, where $M = 1, \ldots, 4$, corresponding to each of the models described qualitatively in §3.3.1. Each of the models, $M = 1, \ldots, 4$, gives a different kind of attraction to woodland. As the system is solved numerically, I move from continuous space and time to discrete. The discrete landscape used throughout this thesis is square grid of square cells $\mathbf{n} = (n, m)$, each with length l, where $n = xl$ and $m = yl$. For each model I use a discrete mathematical formulation of the vector field, $\mathbf{v}_M(\mathbf{x})$, which I denote as $\mathbf{V}_M(\mathbf{n})$.

Using $l = 34m$, the discrete grid is placed over the satellite image of the Rivelin Valley. Any cell with more than half tree coverage is considered to be in a woodland area. Cells are in a woodland area (connected component) if they are connected in the satellite image that the grid represents, this procedure is described in more detail before $\mathbf{V}_M(n, m)$ for each M.

I created a map of the environment by plotting the discrete landscape grid over a satellite image of the Rivelin Valley. The quantity $l = 34m$ was chosen to be suitable for splitting each section of the landscape that represents a data set, into an integer grid. An example section can be seen in Fig. B.1(a). For each cell on the discrete landscape I also determined whether it was in a woodland area or not and Fig. B.1(b) shows the woodland areas in the study site for the 2011-12 data. Here is the process I followed:

1. For each cell **n** on the landscape, if it is more than half covered by woodland in the satellite image then I define it as being “in woodland". For example, in Fig. B.1(a), cells 560 and 524 would be the only cells in the panel not defined as “in woodland".

2. Next I inspect each of the adjacent cells to **n** and decide whether or not they are also in woodland following the process in Step 1.

3. If an adjacent cell is in woodland and there is woodland over the edge of the **n** and the adjacent cell, then I define them to be in the same woodland area. In Fig. B.1(a) all cells in woodland are in the same woodland area. Fig. B.2(a) shows an example where the cells to the right and below **n** are in the same woodland area. Fig. B.2(b) shows an example where all adjacent cells to **n** are in the same woodland area and **n** is the cell which joins these woodland areas.

4. In the case that two or more cells adjacent to **n** are in a different woodland areas and both have woodland over the edge shared with cell **n**, but the woodlands are not joined inside **n**, cell **n** would belong to the woodland area which covered the larger part of **n**. Fig. B.2(c) shows an example of this where **n** belongs to woodland shown by red text.

The areas for the 2011-12 study site can be visualised in Fig. B.1(b), where each colour represents a different woodland area.

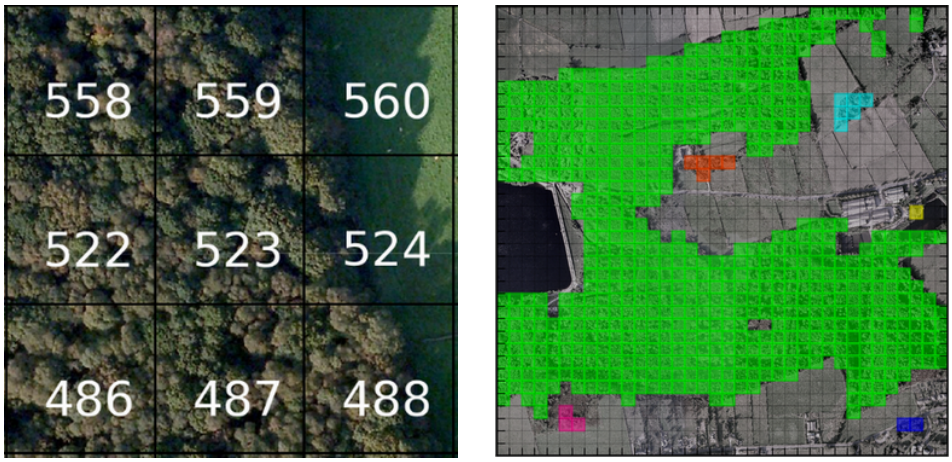

(a) (b)

Fig. B.1. Panel (a) shows a section of the Rivelin Valley study site with the discrete grid plotted over, each square cell is 34m wide. Panel (b) shows the landscape in black and white with the six different woodland areas plotted in colour for the landscape of the 2011-12 data set where each colour (green, pink, orange, blue, yellow and aqua) shows a different woodland area.

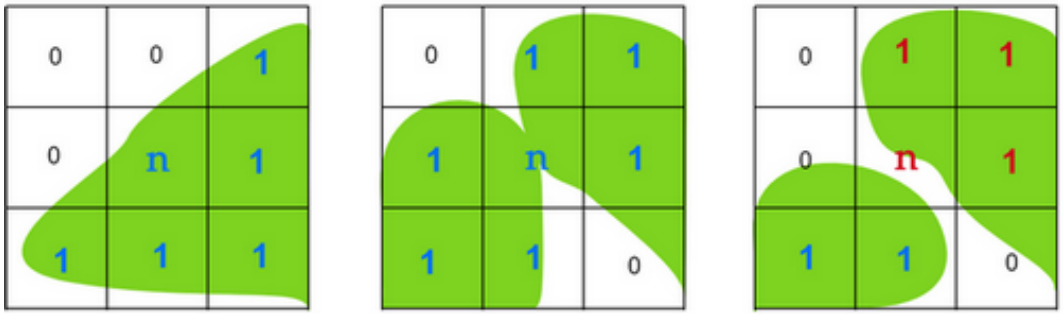

(a) (b) (c)

Fig. B.2. Each panel shows a representation of a section of the Rivelin Valley study site with the discrete grid plotted over. Woodland is shown in green and the different coloured text shows different woodland areas. Panel (a) shows an example where the cell **n** is part of the same woodland as the cells below and to the right of it. Panel (b) shows an example where **n** belongs to the same woodland as all four adjacent cells. Panel (c) shows an example where **n** is connected to both the red and the blue woodland but belongs to the red woodland as this covers a greater area of **n**.

Each of the discrete vector fields defined below can be visualised in Fig. 3.3.

M=1. Taxis into woodland acts solely on the woodland edges, to draw flocks in.

$$\mathbf{V}_M(n,m) = \begin{cases} \hat{\mathbf{r}}, & \text{if } (n,m) \text{ is not in the woodland but adjacent} \\ & \text{to the woodland boundary,} \\ \mathbf{0}, & \text{otherwise,} \end{cases} \tag{B.1}$$

where

$$\mathbf{r}(n,m) = \begin{pmatrix} A(n+1,m)^{\omega_M} - A(n-1,m)^{\omega_M} \\ A(n,m+1)^{\omega_M} - A(n,m-1)^{\omega_M} \end{pmatrix}. \tag{B.2}$$

Here, $A(n,m)$ is the area of the woodland containing (n,m), $\hat{\mathbf{r}} = \frac{\mathbf{r}}{|\mathbf{r}|}$ and ω_M controls the preference for larger woodland areas.

M=2. Taxis into woodland acts both on the woodland edges and within the woodland to draw flocks towards the centre of a connected component.

$$\mathbf{V}_M(n,m) = \begin{cases} \hat{\mathbf{r}}, & \text{if } (n,m) \text{ is not in the woodland but adjacent} \\ & \text{to the woodland boundary,} \\ \hat{\mathbf{d}}, & \text{if } (n,m) \text{ is in the woodland,} \\ \mathbf{0}, & \text{otherwise,} \end{cases} \tag{B.3}$$

where

$$\mathbf{d}(n,m) = \begin{pmatrix} D(n+1,m)^{\omega_M} - D(n-1,m)^{\omega_M} \\ D(n,m+1)^{\omega_M} - D(n,m-1)^{\omega_M} \end{pmatrix}. \tag{B.4}$$

Here $D(n,m)$ is the distance from (n,m) to the nearest woodland edge (measured in number of cells of length l), if cell (n,m) is in the woodland. $D(n,m) = 0$ if cell (n,m) is not in a woodland area.

M=3. Taxis into woodland acts on the woodland edges and all space outside of the woodland areas to draw flocks towards the woodland.

$$\mathbf{V}_M(n,m) = \begin{cases} \hat{\mathbf{w}} & \text{if } (n,m) \text{ is not in the woodland,} \\ \mathbf{0} & \text{otherwise,} \end{cases} \tag{B.5}$$

where

$$\mathbf{w}(n,m) = \sum_{f \in F} \begin{pmatrix} C_f(n+1,m) - C_f(n-1,m) \\ C_f(n,m+1) - C_f(n,m-1) \end{pmatrix},$$

$$C_f(n,m) = \left(\frac{A_f(n,m)}{g_f(n,m)^2} \right)^{\omega_M}, \tag{B.6}$$

where F is the set of all woodlands, f. A_f is the area of woodland f and $g_f(n,m)$ is the distance from (n,m) to the nearest edge of woodland f. The vector $\mathbf{w}$ is the resultant of vectors describing movement towards each woodland f in F and $\hat{\mathbf{w}} = \frac{\mathbf{w}}{|\mathbf{w}|}$.

M=4. Taxis into woodland acts both inside the woodland areas, where flocks are drawn to the centre of a connected component and outside where they are drawn in.

$$\mathbf{V}_M(n,m) = \begin{cases} \hat{\mathbf{w}}, & \text{if } (n,m) \text{ is not in the woodland,} \\ \hat{\mathbf{d}}, & \text{if } (n,m) \text{ is in a woodland area.} \end{cases} \tag{B.7}$$

B.2 Numerical techniques for the MHRA

To solve the system (3.2)-(3.5) for flocks of long-tailed tits I extend the finite difference scheme detailed in Appendix A.4 to include taxis towards the woodland. The involves adding some terms to the iterative equations. When considering taxis along a vector field I redefine continuous space and time (x, y, t) to discrete space and time (n, m, s). I redefine $\mathbf{v}_M(\mathbf{x}) = (v_1, v_2)$ from §3.3.1 to be

$$\mathbf{V}_{n,m} = (V_{1,n,m}, V_{2,n,m})^T, \tag{B.8}$$

where I have omitted the model number M for notational purposes in this section. The iterative equation for space use is equal to Equation (A.19) with the following term added to the right hand side

$$\begin{aligned} &-\frac{\zeta\tau}{2l}\Big\{U^s_{n,m}\left(V_{1,n+1,m} + V_{1,n-1,m} + V_{2,n,m+1} + V_{2,n,m-1}\right) \\ &+ \left(U^s_{i,n+1,m} - U^s_{i,n-1,m}\right)V_{1,n,m} + \left(U^s_{i,n,m+1} - U^s_{i,n,m-1}\right)V_{2,n,m}\Big\}. \end{aligned} \tag{B.9}$$

The boundary conditions are equal to Equations (A.20)-(A.23) with the following terms added to the right hand side respectively

$$- 2l\zeta U^s_{i,1,m} V_{1,1,m}, \tag{B.10}$$

$$+ 2l\zeta U^s_{i,N-1,m} V_{1,N-1,m}, \tag{B.11}$$

$$- 2l\zeta U^s_{i,n,1} V_{2,n,1}, \tag{B.12}$$

$$+ 2l\zeta U^s_{i,n,N-1} V_{2,n,N-1}. \tag{B.13}$$

The time taken to find the best-fit parameters for Equations (2.13)-(2.16) was 13 ± 4 hours (mean $\pm$ 95% CI). These times were calculated by solving each Model 1-4 for the three data sets collected from 2010-13. Example Python and C++ code is provided in the Supporting Information of Ellison et al. (2020).

B.3 Numerical time to real time

The numerical units of space and time can be related to the data so that one can infer the real time of home range pattern formation. The mean square displacement (MSD) is the average amount of space the animal covers per unit of time. I calculate this for the population of flocks of long-tailed tits. The MSD of the data is estimated over time for the using the trajectories of recorded locations. At every 30^{th} point along a recorded trajectory I calculated the MSD after time intervals of 1 minute, 2 minutes, 3 minutes ect and averaged over the displacements calculated for each time interval. These MSD values are shown in Fig. B.3 with a linear fit, MSD$= 1650t$, superimposed over the plot.

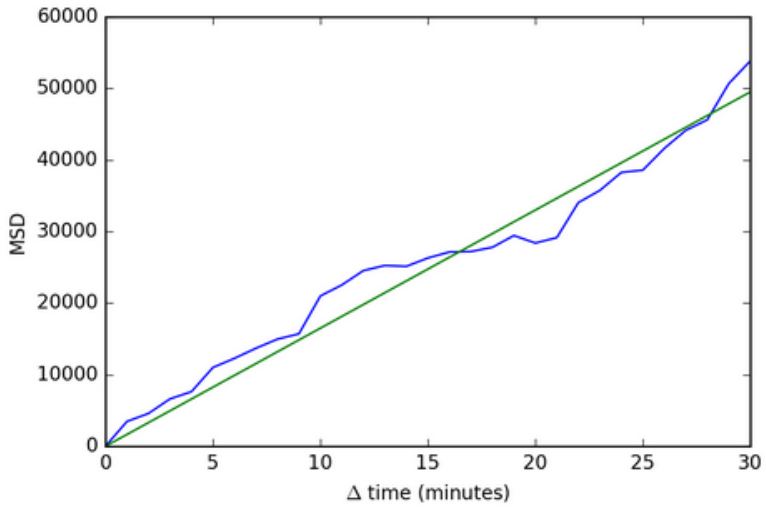

Fig. B.3. Mean squared displacement (MSD) with units m^2, calculated at time intervals Δtime$= 1, \ldots, 30$ minutes and shown in blue. The green line is a linear fit forced through the origin.

The linear fit estimates that for every minute, the mean square displacement is $1650m^2$. In the numerical landscape the area of each cell is equal to $1156m^2$ in the real landscape. I calculate the numerical timestep in minutes using

$$\frac{\Delta x^2}{\Delta t} = \frac{1650}{1} = \frac{1156}{\tau}, \tag{B.14}$$

meaning that each numerical time step is approximately τ =0.7 minutes. The average number of time steps taken to stop the evolution of k_i is 8286 and the average number of time steps taken to evolve u_i is 50375. By assuming the birds are moving for 10 hours per day this means that the birds take around 10 days to decide where the interaction zone is.

B.4 Supplementary results for the MHRA

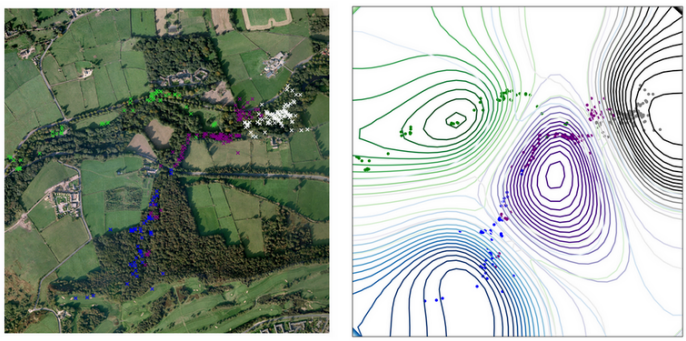

Data

Model 0

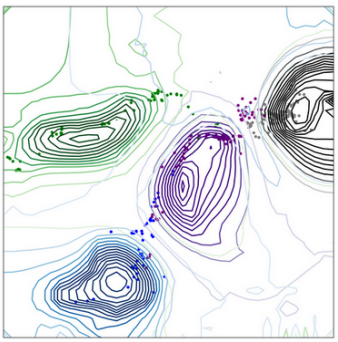

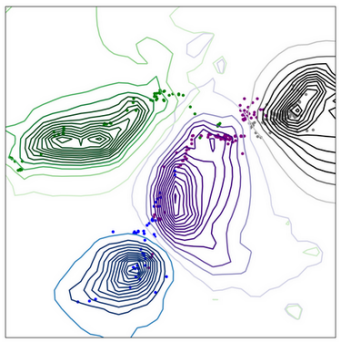

Model 1

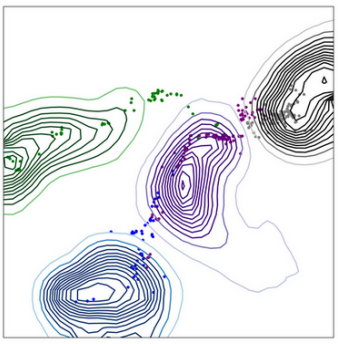

Model 2

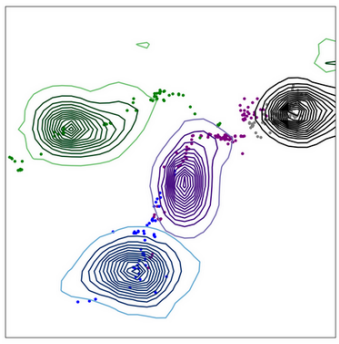

Model 3

Model 4

Model	Parameters	b	γ	δ	ζ	ω	BIC	Difference
0	4	5.95	10.4	0.059			3812	401
1	6	3.5	8.95	0.053	13.7	0.805	3666	255
2	6	3.66	9.53	0.063	13	0.0552	3643	232
3	6	3.08	9.76	0.061	9.44	1.52	3638	227
4	6	1.14	7.96	0.054	12.9	2.05	3411	0

Fig. B.4. Results for the 2010-11 data set

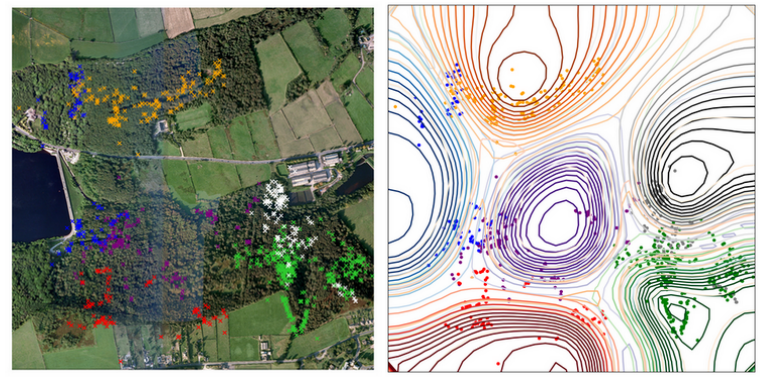

Data

Model 0

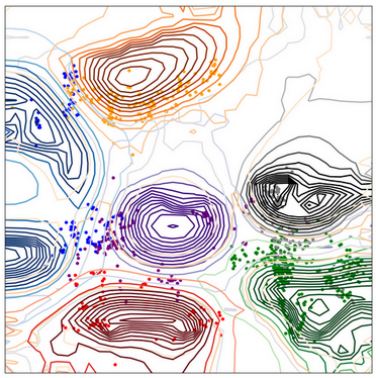

Model 1

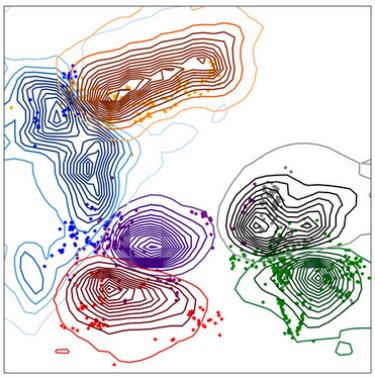

Model 2

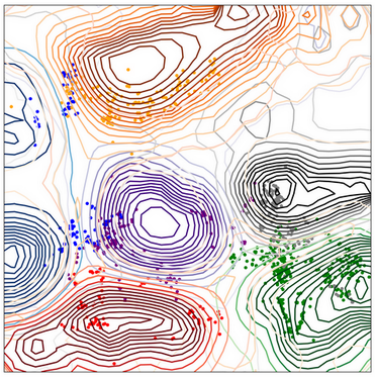

Model 3

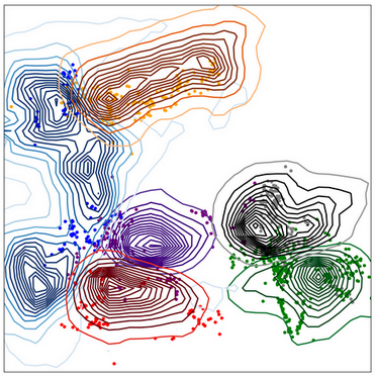

Model 4

Model	Parameters	b	γ	δ	ζ	ω	BIC	Difference
0	4	11.3	10.5	0.048			12244	1155
1	6	8.79	9.16	0.04	25.2	0.844	11859	770
2	6	10.7	9.87	0.065	16.8	0.632	11118	29
3	6	11.8	10.5	0.07	10.7	0.997	11790	701
4	6	13.3	9.6	0.072	18.1	0.51	11089	0

Fig. B.5. Results for the 2011-12 data set

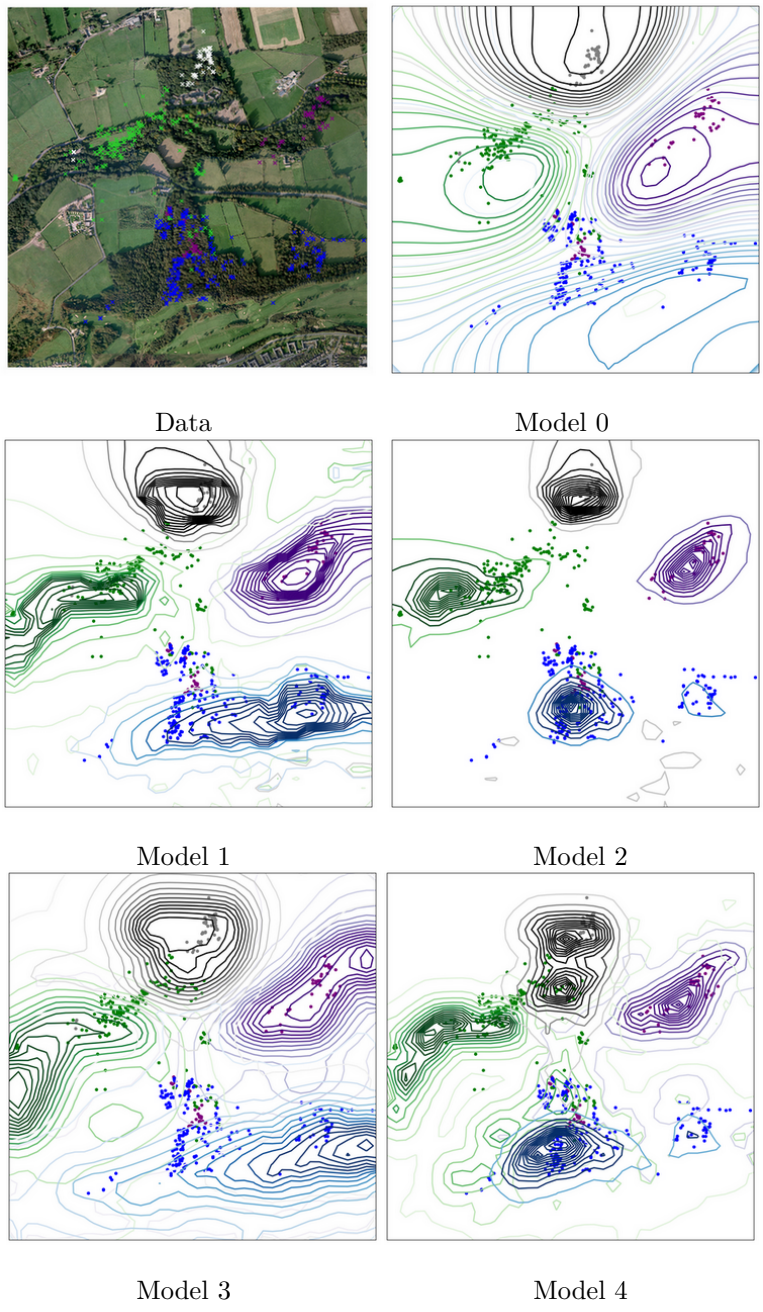

Model	Parameters	b	γ	δ	ζ	ω	BIC	Difference
0	4	8.95	10.9	0.037			7132	733
1	6	3.57	9.3	0.058	30.5	0.786	6746	347
2	6	2.87	10	0.074	19.9	0.741	6399	0
3	6	11.4	10.3	0.054	8.98	1.1	7079	680
4	6	11.2	8.72	0.052	20.5	0.765	6657	258

Fig. B.6. Results for the 2012-13 data set

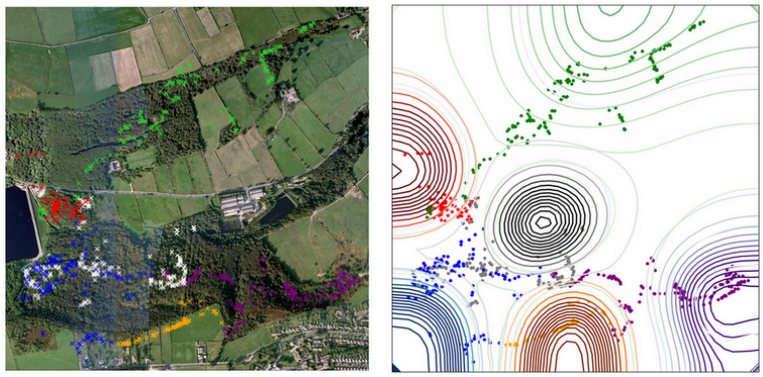

Data

Model 0

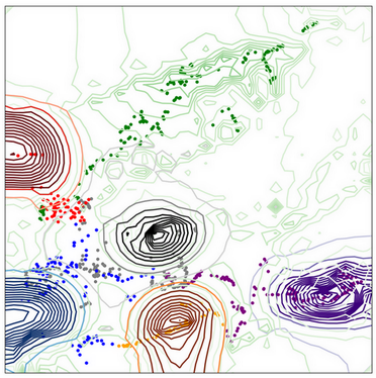

Model 1

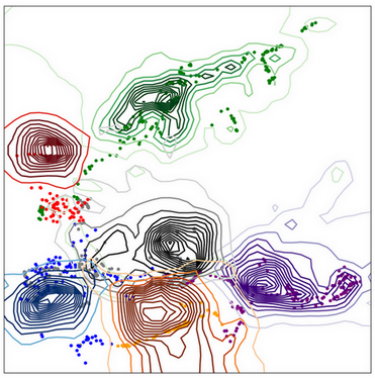

Model 2

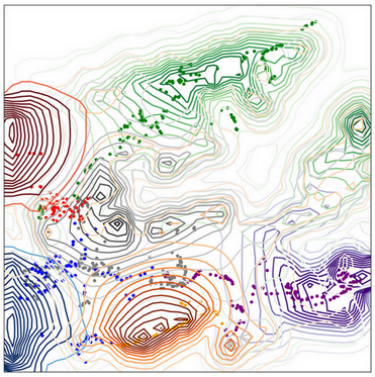

Model 3

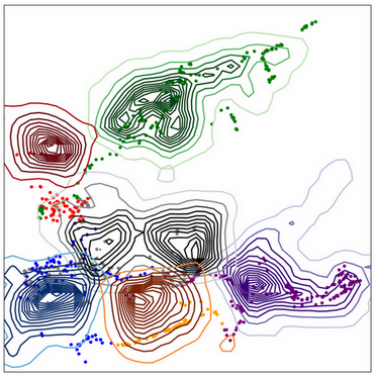

Model 4

Model	Parameters	b	γ	δ	ζ	ω	BIC	Difference
0	4	5.87	9.46	0.062			11690	785
1	6	4.65	8.03	0.048	30.7	0.618	11340	435
2	6	5.11	8.77	0.083	25.7	1.03	11056	151
3	6	11.1	8.06	0.1	25.1	0.873	11210	305
4	6	9.24	9.74	0.096	23.5	0.635	10905	0

Fig. B.7. Results for the 2018-2019$_1$ data set

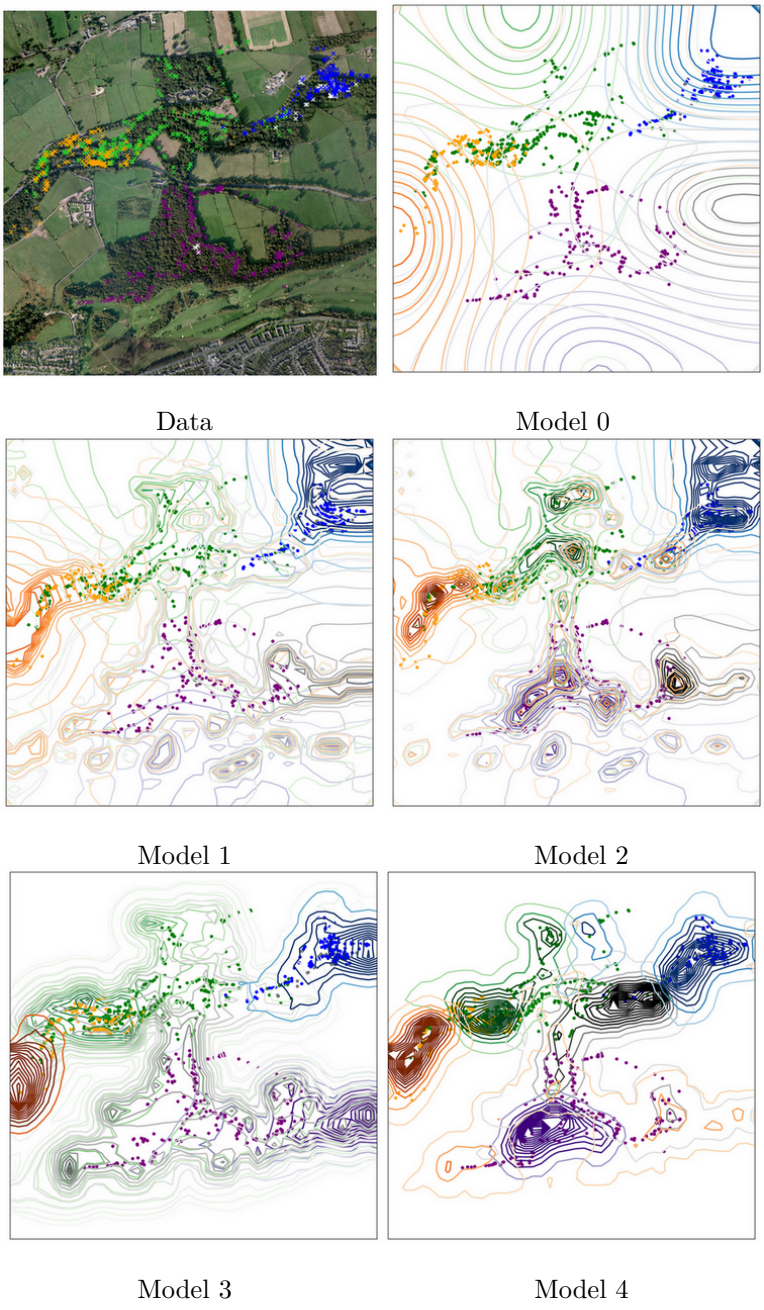

Model	Parameters	b	γ	δ	ζ	ω	BIC	Difference
0	4	15	10.5	0.047			16130	1833
1	6	10.7	7.78	0.098	32.9	1.54	15420	1123
2	6	7.25	8.14	0.098	26.2	2.7	15009	712
3	6	12.3	5	0.066	32.8	1.57	14580	283
4	6	11.7	7.74	0.047	25.9	1.11	14297	0

Fig. B.8. Results for the 2018-2019$_2$ data set

Appendix C

C.1 Probability distributions used to fit movement attributes

Here I give the standard forms for the (a) exponential, (b) half-normal, (c) log-normal and (d) gamma distributions for a random variable y, where $y \in (0, \infty)$ may be step times, step lengths or step speeds (see §4.2.1).

The exponential distribution is defined as:

$$g_a(y) = \lambda \exp(-\lambda y), \tag{C.1}$$

and λ has the units $1/[y]$, where $[y]$ are the units of y.

The half-normal distribution is defined as:

$$g_b(y) = \frac{\sqrt{2}}{\nu\sqrt{\pi}} \exp(-\frac{y^2}{2\nu^2}), \tag{C.2}$$

where ν has the units $[y]$.

The log-normal distribution is defined as:

$$g_c(y) = \frac{1}{\sqrt{2\pi}\sigma y} \exp(-\frac{(\ln(y) - \mu)^2}{2\sigma^2}), \tag{C.3}$$

where σ and μ are dimensionless parameters.

The gamma distribution is defined as:

$$g_d(y) = \frac{y^{k-1}}{\theta^k \Gamma(k)} \exp(-\frac{y}{\theta}), \tag{C.4}$$

where $\Gamma(k) = \int_0^\infty z^{k-1} \exp^{-z} dz$ represents the gamma function, θ has units $[y]$ and k is dimensionless.

For turning angles $z \in (-\pi, \pi)$, the Von-Mises distribution is defined as:

$$g_e(z) = \frac{\exp(\kappa \cos(z - \mu))}{2\pi I_0(\kappa)}, \tag{C.5}$$

where $I_0(\kappa)$ is the modified Bessel function of order 0. The parameters κ and μ are dimensionless.

C.2 Sampling the habitat

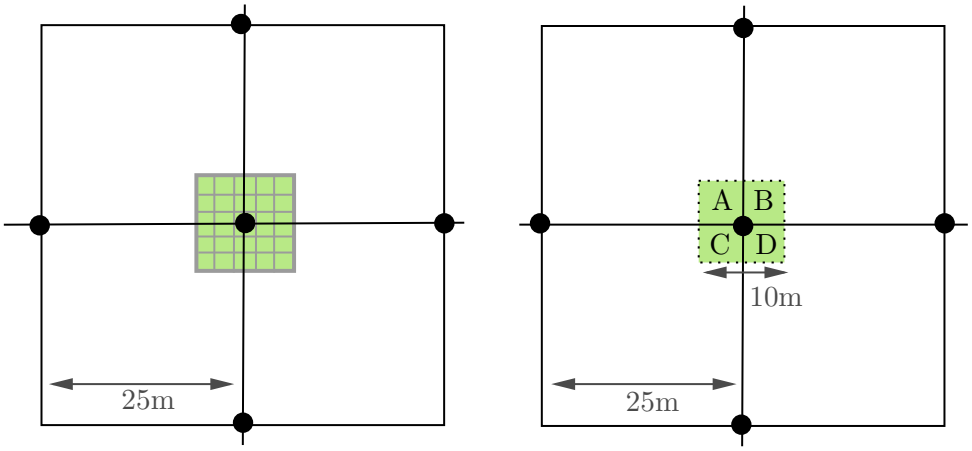

(a) (b)

Fig. C.1. Diagrams to explain collecting habitat data to describe the coverage of different tree types at the canopy layer (>7m) and shrub layer (1-7m). The landscape is split into a 25m by 25m square grid which is shown by the solid black lines. The observer stands at the intersection points of the solid black lines (shown by a black circle) and these are the points where data collection occurs. Panel (a) illustrates the data collection at the canopy layer where the most dominant tree type is estimated for each of the 25 squares. These squares are defined by holding a 25cm by 25cm perspex sheet above the observers head at a constant height and looking at the canopy through this (more than 7m above). An example for a intersection point could be that 8 squares are covered by oak canopy, 10 squares are covered by birch canopy and 7 squares are not covered. Panel (b) shows the data collection at the shrub layer where the dominant tree types are estimated for each quarter A,B,C,D. For example, A may have 10% holly, 80% hawthorn and 10% brambles.

C.3 Correcting for the fit of the availability kernel

Here I give a brief example of correcting an availability kernel (Equation 4.3) to form a corresponding movement kernel (Equation 4.1) using correction functions (Equation 4.9) in the weighting function (Equation 4.8).

Each correction function contains parameters, κ_n corresponding to those in the availability kernel, denoting the magnitude of the corrections. Here I explain this process using the Gamma distribution (Appendix C.1) to represent the distribution of step times τ_j in Equation (4.3). The following distribution would be fit to the step times for the population

$$\tilde{g}_1(\tau_j) = \frac{\tau_j^{k-1}}{\Gamma(k)\theta^k} \exp\left(-\frac{\tau_j}{\theta}\right), \tag{C.6}$$

with shape and scale parameters k and θ, respectively. Since the SSF is eventually normalised and has a log-linear form, it is useful to write Equation (C.6) as

$$\tilde{g}_1(\tau_j) \propto \exp\left((k-1)\ln(\tau_j) - \frac{\tau_j}{\theta}\right). \tag{C.7}$$

The corresponding correction function would have the form

$$C_1(\tau_j) = \kappa_1 \ln(\tau_j) + \kappa_2 \tau_j, \tag{C.8}$$

where κ_1 and κ_2 are inferred alongside the habitat selection parameters $\mathbf{B}$ by fitting Equation (4.8) using CLR.

C.4 Supplementary data

C.4.1 Initial data

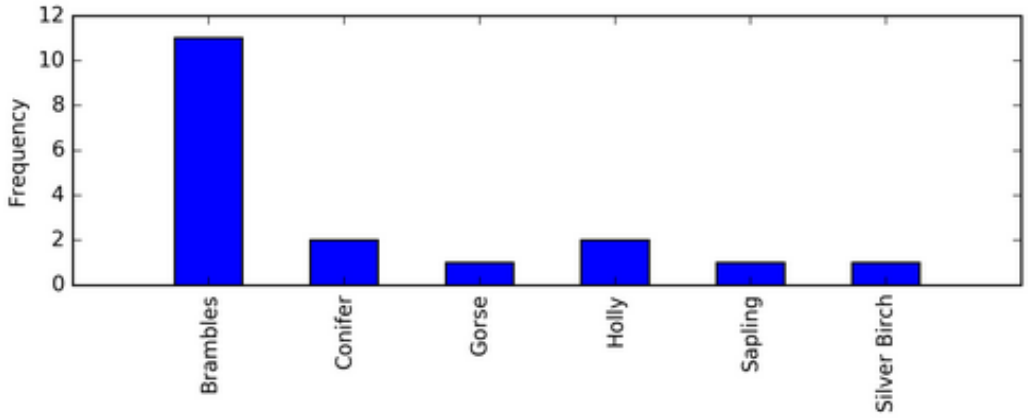

Fig. C.2. Nesting trees of the 18 pairs of long-tailed tits in the season of 2019.

Table C.1. The distribution of tree types across the study site. These values are reported to indicate how accessible each tree type is.

tree type	number of environments recorded in (9 total)	number of pairs accessible to (18 total)	number of habitat locations recorded in (269 total)	mean percentage cover per location
Sycamore	7	16	94	31.7
Oak	9	18	98	29.8
Holly	8	17	78	15.9
Hawthorn	7	16	31	11.9
Birch	6	9	49	32.4
Brambles	4	12	20	7.8
Alder	6	15	22	16.3
Ash	5	12	28	16.0
Lime	3	5	9	20.2
Beech	5	13	36	34.6
Willow	4	12	18	19.1
Hazel	6	15	30	13.4
Elder	6	14	28	7.8
Cherry	3	11	12	19.0
Chestnut	2	4	2	5.0
Cypress	2	4	2	11.5
Elm	5	13	23	19.8
Gorse	1	3	5	17.0
Larch	1	1	6	25.7
Rowan	7	16	33	13.9
Norway spruce	1	1	3	52.7
Sitka spruce	1	1	2	50.0

C.4.2 Splitting the data into two halves

Table C.2. The tree selection analysis reported in Chapter 4, Table 4.4, repeated with the data split into two halves of 25 days. Here all steps to the nest are removed leaving 811 steps.

First 25 days (477 steps)					Second 25 days (334 steps)				
Covariate	$\exp(\beta_n)$	$\text{CI}_{90,L}$	$\text{CI}_{90,H}$	p-value	Covariate	$\exp(\beta_n)$	$\text{CI}_{90,L}$	$\text{CI}_{90,H}$	p-value
Oak	1.006	1.000	1.013	0.056	Oak	1.02	1.009	1.024	$1.\times10^{-5}$
Alder	1.023	1.000	1.047	0.032	Alder	1.024	1.005	1.039	0.009
Elder	1.025	1.000	1.051	0.072	Elder	1.058	1.000	1.129	0.07
Gorse	1.055	1.017	1.095	0.004	Larch	1.019	1.007	1.023	2×10^{-5}
Sycamore	1.007	1.002	1.013	0.012	Hazel	1.031	0.997	1.066	0.069
Birch	1.011	1.001	1.020	0.03					
Brambles	0.901	0.862	0.950	2×10^{-5}					
Cypress	0.917	0.831	1.009	0.075					

C.4.3 Analyses with the first steps of each path removed

In this section I repeat the analyses shown in the Chapter 4, Tables 4.4, 4.5 and 4.6, where the first step of each path is removed from the analysis. This is to reduce observer bias from the first encounter with the birds and this section shows the results stay the same.

Table C.3. The results for fitting to data with the first step of each path removed. Separate covariate functions are fit for each of the 22 types of trees. By indicating which tree type correspond to a p-value less than 0.1. The results show the eight tree types in Table 4.4 are significant and have similar parameter values.

	$\mathbf{C} + Z_{A1} + Z_{B1}$			
Covariate for	$\exp(\beta n)$	$\text{CI}_{95,L}$	$\text{CI}_{95,H}$	p-value
Sycamore	1.010	1.005	1.016	2.3×10^{-4}
Oak	1.010	1.005	1.015	2.4×10^{-4}
Holly	0.999	0.988	1.011	0.977
Hawthorn	1.002	0.986	1.018	0.985
Birch	1.004	0.996	1.013	0.326
Brambles	1.038	1.019	1.056	5.2×10^{-5}
Alder	1.025	1.010	1.039	0.001
Ash	0.997	0.982	1.012	0.537
Lime	1.007	0.991	1.024	0.438
Beech	1.006	0.997	1.015	0.386
Willow	1.010	0.997	1.022	0.207
Hazel	1.019	0.997	1.042	0.082
Elder	1.023	0.997	1.051	0.072
Cherry	1.005	0.987	1.023	0.672
Chestnut	1.113	0.995	1.246	0.073
Cypress	1.032	0.949	1.123	0.401
Elm	1.016	0.994	1.039	0.174
Gorse	1.000	0.967	1.034	0.890
Larch	1.013	1.005	1.021	0.001
Rowan	1.012	1.000	1.023	0.049
Norway Spruce	0.997	0.980	1.014	0.710
Sikta Spruce	0.976	0.888	1.071	0.605

Table C.4. The results for fitting to data with the first step of each path removed and all steps to the nest removed. Separate covariate functions are fit for each of the 22 types of trees. These results show the same eight tree types are significant as indicted by the results shown in Table 4.5 (all 1073 steps) and the parameter values are similar.

	$\mathbf{C}^G + Z_{A1} + Z_{B1}$			
Covariate for	$\exp(\beta_n)$	$\text{CI}_{90,L}$	$\text{CI}_{90,H}$	p-value
Gorse	1.043	0.999	1.088	0.055
Elder	1.036	1.007	1.065	0.013
Alder	1.027	1.012	1.042	3.4×10^{-4}
Larch	1.019	1.010	1.028	2.2×10^{-5}
Oak	1.011	1.005	1.016	1.1×10^{-5}
Birch	1.010	1.002	1.019	0.020
Sycamore	1.009	1.003	1.015	0.003
Brambles	0.942	0.905	0.980	0.003

Table C.5. The results of the model selection with the first step of each path removed. Models 3-8 are fit and compared with Models 0 and 1. The ΔBIC column shows the difference between this BIC value and the lowest BIC value. These show that the same overall results are obtained as using the full 1073 steps shown in Table 4.6.

Model	Covariates	Parameters	BIC	ΔBIC
1	C	4	7033	176
2	C, Z_{A1}	5	6899	42
3	C, Z_{A1}, Z_{B1}	15	6908	51
4	C, Z_{A1}, Z_{B2}	6	6861	4
5	C, Z_{A1}, Z_{B3}	6	6876	19
6	C, Z_{A1}, Z_{B4}	6	6868	11
7	C, Z_{A1} , Z_{B2}, Z_{B3}	7	6864	7
8	C^G, Z_{A1}, Z_{B2}, Z_{B4}	7	6857	0

C.5 Supplementary utilization distributions from the iSSA

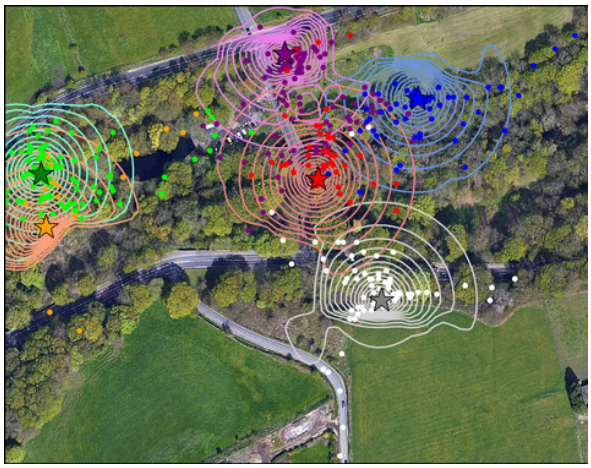

(a)

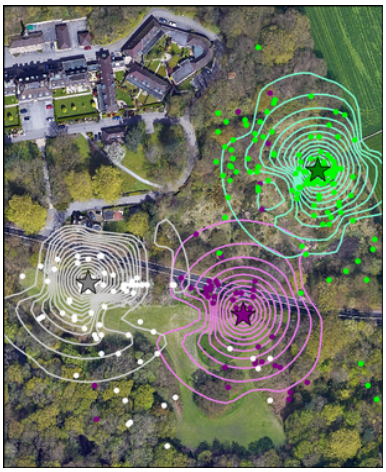

(b)

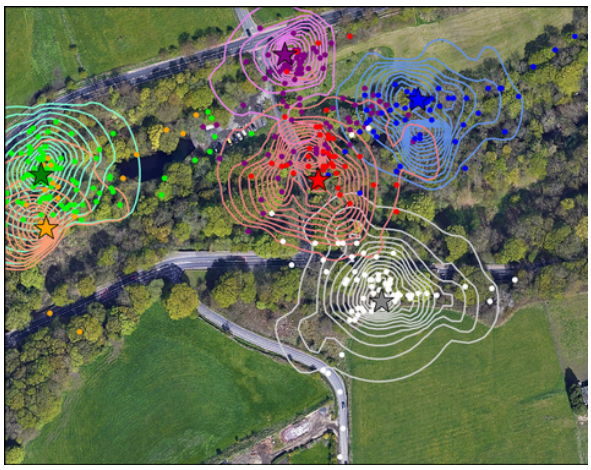

(c)

(d)

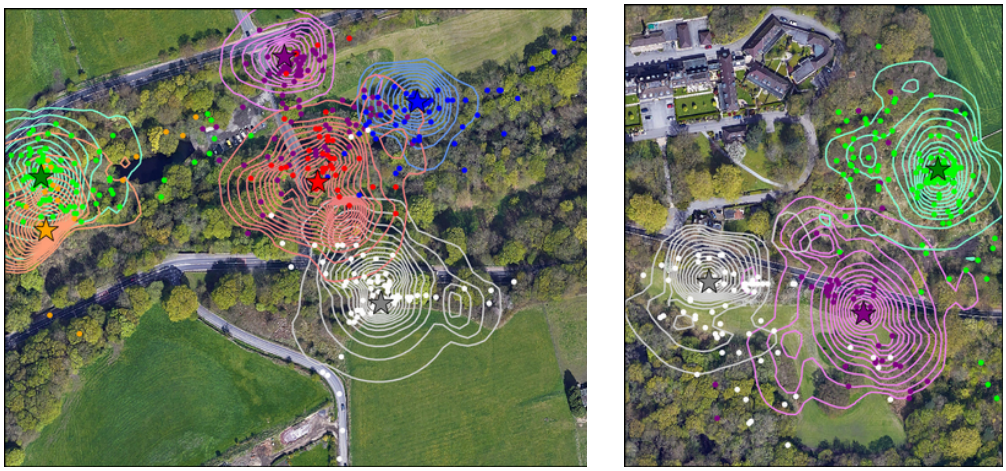

(e) (f)

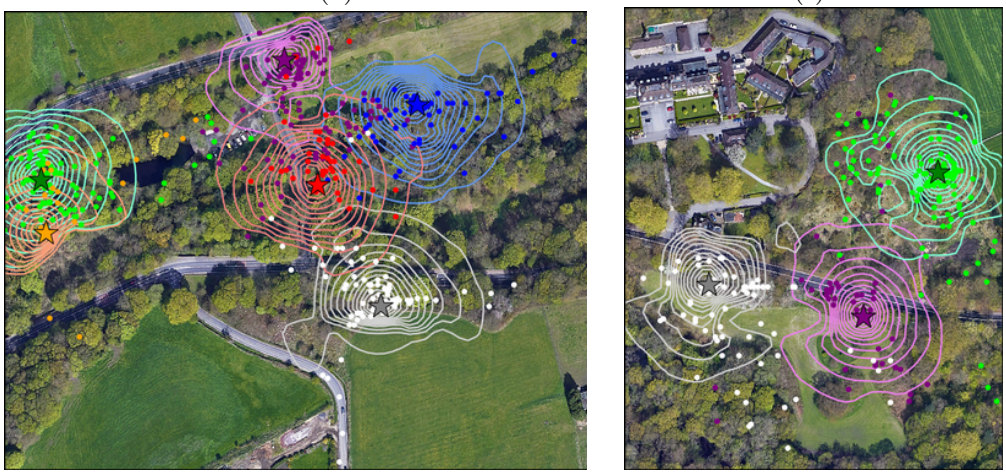

(g) (h)

Fig. C.3. Utilisation distributions for nine pairs of long-tailed tits, calculated using Equation (4.30), where the weighting functions are replaced by those corresponding to each model . Model 4 is shown in panels (a) and (b), Model 5 in panels (c) and (d), Model 6 in panels (e) and (f) and Model 7 in panels (g) and (h).